The Causal Effects of Global Supply Chain Disruptions on Macroeconomic Outcomes: Evidence and Theory*

Xiwen Bai† Jesús Fernández-Villaverde‡ Yiliang Li§

Francesco Zanetti¶

November 9, 2023

Abstract

We study the causal effects and policy implications of global supply chain disruptions on the U.S. economy. We construct a new index of supply chain disruptions from the mandatory Automatic Identification System data of containerships, developing a novel spatial clustering algorithm that determines real-time congestion from the position, speed and heading of containerships in ports around the globe. We develop a new theoretical framework with search frictions between producers and retailers and transportation costs that links spare productive capacity with congestion in the goods market and the responses of output and prices to supply chain shocks. The co-movements of output, prices, and spare capacity yield unique identifying restrictions for supply chain disturbances that allow us to study the causal effects and the changes in the effectiveness of monetary policy amid supply chain disruptions. Structural VAR models with our new index and theoretical restrictions establish that supply chain disruptions significantly: (i) depress real GDP, raise prices, and generate a surge in spare capacity; and (ii) enhance the effectiveness of contractionary monetary policy in taming inflation while reducing the sensitivity of output.

JEL Classification: E32, E58, J64.

Keywords: supply chain disruptions, search-and-matching in the goods market, SVAR, state-dependence of monetary policy.

---

*We are grateful for comments and suggestions from Klaus Adam, Fernando Alvarez, Dennis Bonam, Bjoern Bruegemann, Elena Maria Diaz, Julian di Giovanni, Sebastian Heise, Bo Hu, Callum Jones, George Nikolakoudis, Ekaterina Peneva, Giorgio Primiceri, Omar Rachedi, Ricardo Reis, Karthik Sastry, Frank Smets, Bo Sun, Christian Wolf, Li Yu, Charles Zhang, Yuan Zi, and conference and seminar participants at the NBER Workshop on Methods and Applications for DSGE Models Fall 2023, The ECB-Cleveland Fed Inflation: Drivers and Dynamics Conference 2023, EEA-ESEM Barcelona 2023, AMES Singapore 2023, 11th Shanghai Macroeconomics Workshop at SUFE, AMES China 2023, CEMA 2023, 26th T2M Conference, Leuven Summer Event 2023, 2nd Asia-Pacific SaM Online Workshop, 4th UIBE CCTER Workshop on Transportation Research, Groningen University, and the Tinbergen Institute. Francesco Zanetti gratefully acknowledges financial support from the British Academy.

†Tsinghua University, China. xiwenbai@mail.tsinghua.edu.cn.

‡University of Pennsylvania, U.S. jesusfv@econ.upenn.edu.

§University of International Business and Economics, China. yiliang_li@uibe.edu.cn.

¶University of Oxford, U.K. francesco.zanetti@economics.ox.ac.uk.

1. Introduction

Sudden and large imbalances in the supply and demand for goods, often stemming from disruptions to the supply chain, can lead to protracted deterioration in macroeconomic performance. For instance, the severe disruptions to the flow of goods worldwide during the Covid-19 pandemic led to an unprecedented fall in global trade and a sharp rise in shipping costs and goods prices, culminating in the second-largest recession in U.S. history.[1]

Despite the fundamental role of supply chain disruptions in shaping macroeconomic performance and economic policy, research on this topic is scant, and progress is challenged by two key issues. First, existing indices of supply chain disruptions are often inferred from changes in shipping prices or information from surveys on potential disruptions gleaned from the Purchasing Managers' Index (PMI). These measures are problematic since shipping prices internalize endogenous movements in the demand for goods or expectations that might be unrelated to supply chain disruptions, and surveys of managers are subject to potentially large measurement errors arising from the subjective perceptions of interviewees on supply chain issues, thus providing an imprecise measurement of supply chain disruptions. The ideal measurement of supply chain disruptions requires data that track the disruptions to the regular flows of goods around the globe, which is central to understanding the rationing of supply and the surge in prices during such disruptions.

Second, there is no theoretical framework that studies supply chain disruptions considering the simultaneous rise in spare productive capacity – resulting from increased transportation costs arising from the disruption to the supply chain – with the simultaneous shortage of goods and scarcity of supply in the retail market that exerts upward pressure on prices. Against this backdrop, mounting evidence points to the increase in spare productive capacity and the contemporaneous congestion in the retail market as central drivers of the surge in prices during supply chain disturbances. Furthermore, several policymakers suggest that the trade-offs for the contemporaneous stabilization of prices and output may change amid acute supply chain disruptions.[2]

[1] During the Covid-19 recession (February-April 2020), the decline in GDP from peak to trough was 19.2%. During the Great Depression (August 1929-March 1933), the fall in GDP was 26.7%.

[2] Several articles in the popular press and policy institutions discuss the relevance of disruptions to the

Our paper addresses these issues by developing: (i) a new index of global supply chain disruptions derived from maritime satellite data that tracks the congestion of containerships at ports worldwide, and (ii) a novel theoretical framework that accounts for the coexistence of elevated spare capacity for producers and scarcity of supply in the retail market, and how these affect the responses of output and prices during a disruption to the supply chain. Using our new data and theory, we shed new light on the causal effects of supply chain disruptions on macroeconomic conditions and the implications for the effectiveness of monetary policy.

We study disruptions to the supply chain by examining congestion at container ports around the globe. Container shipment plays a pivotal role in global trade, and approximately 60% of the total value of world seaborne trade passes through container ports (UNCTAD 2019, OECD & EUIPO 2021, Coşar & Demir 2018), implying that even a mild increase in port congestion can significantly impair regular supply chains and generate large imbalances between the supply and demand for tradable goods. Importantly for our analysis, The terms of shipping services for containerships – including itinerary, timing, and conditions of shipment – are typically fixed in advance. These service agreements often extend beyond a year and are rarely modified, as substantial penalties and high switching costs deter changes. Containerships operate on fixed routes – like buses at sea – that remain constant despite the general economic climate or changes in demand. Such a market structure ensures that congestion at a seaport is minimally influenced by the strategic decisions of shipping companies, prevailing economic conditions, or adjustments in capacity across routes to accommodate demand fluctuations.[3] The binding service agreements and fixed routes of containerships allow our measure of port congestion, based on the density of inactive vessels at ports, to be exogenous to the forces of demand that may skew measures of congestion derived from shipment prices and to abstract from the subjective judgment of managers on supply chain issues. Our index provides a precise tracking of the disruptions to the regular flows of goods around the globe, overcoming the two important shortcomings in the measurement of supply chain disruptions.

supply chain for economic performance and macroeconomic policies. See, for instance, Attinasi et al. (2021), Forster van Aerssen et al. (2021), Grimes & Edgecliffe-Johnson (2021), The White House (2021), Dempsey (2022), Lane (2022), World Bank (2022).

[3] In Appendix A, we provide a primer on the containerized shipping industry.

We quantify port congestion using granular shipping data from the Automatic Identification System (AIS), the long-range identification and tracking system on containerships mandated by the International Maritime Organization (IMO) – the specialized agency of the United Nations responsible for regulating the shipping industry worldwide – for major ports around the globe from 2017 to 2022. By developing a novel machine learning clustering algorithm that utilizes the position, speed, and heading of containerships recorded in the AIS data, we construct a new dataset that provides a measure of port congestion in single ports, which we then aggregate across ports to develop the first high-frequency index of Average Congestion Rate (ACR) worldwide. Our ACR index is the first measure of global supply chain disruptions obtained from maritime satellite data of containerships.[4] Unlike alternative metrics, our index indicates that supply chain disruptions and congestion in ports during the Covid-19 pandemic began in the second half of 2020 and remained elevated until the end of our sampling period in the second half of 2022. It shows that the average proportion of containerships experiencing delays in their loading and/or unloading operations upon arrival at ports increased from 17% to 25%, and at the same time, the average duration of such delays rose from four to eight hours by the second half of 2022. Our ACR index provides novel information on the obstructions to the systematic flows of containerships around the globe, resulting in disruptions to the supply chain.

Theoretical framework. To interpret the new data and study the causal effects of supply chain disruptions and the changes in the effectiveness of economic policy, we develop a simple model that accounts for the imbalances between supply and demand for goods resulting from the increase in shipping costs, which generates spare capacity for the producers and scarcity of supply and congestion in the retail market. Our model is based on search and matching frictions between producers and retailers, who are based in different locations and meetings entail search and matching frictions, and the shipment of goods to the retailers requires producers to pay transportation costs. Our model extends the disequilibrium framework of Barro & Grossman (1971), recast in a microfounded framework by Michaillat & Saez

[4]The global nature and the construction of our ACR index account for any changes in port congestion that may result from adjustments in shipping routes, thus preserving the exogeneity of our ACR index when routes are altered. Additionally, since the AIS data has virtually no error in tracking the real-time movements of containerships across the globe, our ACR index is not subject to the large measurement errors that alternative indices based on surveys to purchasing managers on supply chain issues may encounter.

(2015, 2022), and Ghassibe & Zanetti (2022), by separating the locations of producers and retailers, and incorporating transportation costs that generate spare capacity for producers from the reduction in the shipment of goods and the simultaneous scarcity of supply and increased congestion in the retail market.

The presence of search frictions introduces trading externalities – encapsulated by congestion in the exchange of goods – that render prices no longer the only allocative mechanism, since retailers and producers of goods face a probability of failing to match with each other under search frictions. In other words, our framework accounts for rationing in the retail market that cannot be eliminated by price adjustments and is instead determined by the relative number of retailers and producers, which are influenced by search frictions and the increase in transportation costs that curtail the availability of supply in the retail market while simultaneously increasing spare productive capacity amid supply chain disruptions.

Central to the realization of supply chain disruptions, increased transportation costs hinder the free flows of goods between producers and retailers. In our model, each producer draws a random transportation cost in each period and proceeds with the shipment of goods if the drawn cost falls below the threshold for profitable shipments. We assume that a disturbance to the supply chain increases the transportation costs for all producers, as evinced by the large empirical evidence linking supply chain disturbances to higher transportation costs (Alessandria et al. 2023, Dunn & Leibovici 2023). Such a comprehensive rise in transportation costs reduces the number of profitable shipments and curtails the volume of shipped goods, leading to a fall in the supply of goods available to retailers as well as increasing the spare capacity for producers. The shortage of supply to retailers increases the price and intensifies the costs of search frictions between retailers and producers, hence reducing output. Thus, in our framework, the disruption to the supply chain simultaneously increases spare productive capacity for producers and decreases the supply of goods to retailers, fostering high congestion and a surge in prices in the retail market.

Our model demonstrates that the responses of macro aggregates to a supply chain disruption shock differ from those to standard shocks to the demand and supply of goods. Unlike demand shocks, disruptions to the supply chain result in negative co-movements between output and the price of goods. Although traditional supply shocks are also characterized

by negative co-movements between output and the price of goods, disruptions to the supply chain uniquely increase spare capacity for producers due to the reduction in the shipment of goods, whereas traditional supply shocks decrease it. Such a difference is intuitive: higher transportation costs and supply chain disruptions do not change the productive capacity in the goods market; rather, they impede the free flow of goods and effectively limit the supply of goods to retailers, thus giving rise to increased spare capacity and a deficient supply in the retail market. Therefore, the increase in spare capacity, coupled with the rise in prices and the declines in output, enables the unique identification of supply chain disruption shocks.

The causal effects of supply chain disruptions. We apply our theoretical predictions on the responses of endogenous variables to a Structural Vector Autoregression (SVAR) to uniquely identify the shocks to the supply chain and distinguish them from traditional shocks to supply and demand. We estimate the SVAR model using the Bayesian approach, as in Uhlig (2005) and Arias et al. (2018), establishing several key results. First, a disruption shock to the supply chain leads to a large and immediate drop in real GDP, persistently increases inflation and import prices, and generates a surge in unemployment. In addition, similar to a traditional supply shock, the supply chain disruption shock generates a persistent, positive response of inflation, an observation consistent with recent evidence (Bekaert et al. 2020) and Gordon & Clark (2023). As predicted by our model, the traditional supply shock and the supply chain shock differ in their effects on unemployment, which is our empirical proxy for spare capacity. For the supply shock, unemployment transiently falls for less than one quarter, while it persistently increases for the supply chain shock, with the median response reverting to zero slightly after the one-quarter mark.

Second, the historical decomposition shows that the sharp fall in inflation in early 2020 was mainly driven by a significant contraction of aggregate demand that coincided with the first wave of the Covid-19 pandemic across the world. Subsequently, aggregate demand started to rebound, while global supply chain disruptions escalated and explained the bulk of the rise in inflation until the end of 2021. Thereafter, traditional demand, supply, and supply chain shocks jointly drove inflation to its peak during the sample period.

Policy implications. Our analysis shows that supply chain disruptions generate stagflation, characterized by elevated inflation and contracting output, accompanied by a simul-

taneous increase in spare capacity for producers. This higher spare capacity curtails the supply of goods to the retailers and results in a surge in prices, leading to a tighter retail market. We show that prices become highly sensitive to changes in demand while output remains relatively inelastic in response to the shock to the supply chain. Thus, disruptions to the supply chain enhance the effectiveness of contractionary monetary policy in taming inflation while reducing the sensitivity of output to the policy. Our results reinforce the general findings on the state-dependence of the efficacy of monetary policy (Benigno & Ricci 2011, Liu et al. 2019, Eichenbaum et al. 2022, Ikeda et al. 2023).

We test our theoretical prediction on the enhanced effectiveness of monetary policy during supply chain disruptions by developing a Threshold Vector Autoregression (TVAR) model that estimates the statistical differences in the effects of a contractionary monetary policy shock at different levels of the ACR index. Consistent with the theory, we find that an exogenous tightening of monetary policy leads to a significantly larger and more persistent decline in inflation for a given decrease in output during periods of supply chain disruptions. Our results support a more aggressive, yet less contractionary, approach to tightening monetary policy in response to the elevated inflation consequent to supply chain disturbances. This approach aligns with the progressive tightening of monetary policy in the U.S. during the supply chain disruptions following the Covid-19 recession.

Related literature. Our analysis is related to several realms of research. We develop a theoretical framework that maps the mismatch between the supply and demand for goods to changes in prices, real activity, and spare capacity. Our model builds on the disequilibrium framework of Barro & Grossman (1971), incorporating search and matching frictions in the goods market that result in spare capacity, thus extending the theoretical frameworks in Michaillat & Saez (2015, 2022), Ghassibe & Zanetti (2022).

We are also related to studies that focus on the effect of supply chain disturbances on output and inflation, using the amount of spare-labor capacity (Benigno & Eggertsson 2023), shortages in the goods market (Blanchard & Bernanke 2023), capacity constraints (Comin et al. 2023), and a quasi-kinked demand curve for produced goods (Harding et al. 2023). The common finding across these studies is that scarcity of goods during disturbances to the supply chain brings the economy close to capacity constraints, thus generating a non-linear

and strong increase in inflation with a limited effect on output.

We connect to the large empirical literature that develops SVAR models to study the causal effects of shocks (Uhlig 2005, Rubio-Ramirez et al. 2010, Arias et al. 2018), and the studies that focus on the effects of supply chain shocks during the Covid-19 pandemic (Brinca et al. 2021, Finck & Tillmann 2022, Gordon & Clark 2023).

Finally, we relate to studies showing that transportation costs are important for international trade and economic activity (Allen & Arkolakis 2014, Brancaccio et al. 2020, Dunn & Leibovici 2023), infrastructure investment (Fuchs & Wong 2022), asset prices (Smirnyagin & Tsyvinski 2022), inflation expectations (Acharya et al. 2023), the design of new taxes and pricing rules to offset distortionary effects on the transportation network (Brancaccio et al. 2023), and the interlinks between oil shocks and congestion in the supply chain (Bai & Li 2022, Li et al. 2022).

The remainder of our study is organized as follows. Section 2 constructs our ACR index of supply chain disruptions. Section 3 develops our theoretical model and the identifying restrictions. Section 4 presents the baseline estimation results. Section 5 studies the state-dependent effects of monetary policy shocks following supply chain disruptions. Section 6 concludes.

2. Measuring Global Supply Chain Disruptions

In this section, we develop a novel index designed to track global supply chain disruptions by analyzing imbalances between the supply and demand for goods through the lens of containerized trade.

Containerized seaborne trade plays a prime role in transporting goods around the globe and thus facilitating the smooth operation of global supply chains (Notteboom et al. 2022). In the realm of containerized trade, seaports serve as international hubs for freight collection and distribution. A seemingly mild congestion at these ports can significantly impair regular supply chains and trade flows, leading to elevated delay costs and far-reaching consequences for international trade and macroeconomic outcomes.[5] Using satellite data on the positions

[5]Port congestion imposes significant costs on the various stakeholders in the shipping industry. Prior to the

and speeds of containerships, we track congestion in major ports around the world and construct an index of global supply chain disruptions from the aggregation of those granular measures.

2.1. AIS Data

We use satellite data from the AIS, the tracking system mandated by the International Maritime Organization (IMO) for international voyaging vessels larger than 300 gross tonnage (Heiland et al. 2022). The AIS processes over 2,000 reports per minute and updates information as frequently as every two seconds, offering comprehensive coverage of the movements of containerships around the globe from January 2017 to July 2022.[6] Each data entry includes the IMO number, timestamp, current draught, speed, heading, and geographical coordinates of each ship.[7] The precise positioning, speed, and heading of ships allow us to monitor vessel movements within different port zones, enabling the creation of a highly accurate measure of congestion in ports around the globe.

pandemic, waiting times at ports were just a few hours. However, general disruptions related to the Covid-19 pandemic led to extended delays, with waiting times reaching 2-3 days at several major ports worldwide, incurring substantial financial losses. Shippers and freight forwarders faced unexpected delays, compounded by surcharges like the Port Congestion Surcharge (PCS), with charges escalating to USD 1,250 per container in certain cases. Buyers and sellers of goods encountered disruptions in the supply chains, leading to large profit losses, added costs such as demurrage and detention, and challenges in meeting market demands and contractual obligations. Containership owners were directly affected by the PCS, while truckers and terminal operators saw reduced transport efficiency and heightened operational costs. Given that the average value of goods in a 40-foot container is around USD 100,000, the PCS alone accounts for a significant portion of the total value, highlighting the profound economic impact of port congestion on all parties involved in the trade. It is important to note that the delays in ports were not caused by restrictions on the personnel in ports, as these essential workers were exempted from Covid-19 restrictions in several major jurisdictions (e.g., U.S., China, and Europe). For instance, the U.S. Department of Homeland Security identified workers within the transportation and logistics sector, including port workers, as "essential critical infrastructure workers". The essential workers were permitted to continue working despite lockdowns or stay-at-home orders, albeit under new safety guidelines.

[6] Over 99 percent of international container shipments are transported by containerships that exceed 500 gross tonnage.

[7] The draught measures the vertical distance from the bottom of a vessel's keel to the water's surface, indicating how deeply the ship is submerged. While the draught typically reflects a vessel's cargo load (Bai & Li 2022, Li et al. 2022), this measurement can be less indicative for containerships since loading and unloading operations often occur concurrently.

2.2. A Density-Based Spatial Clustering Algorithm

To accurately quantify port congestion, we follow the maritime literature by estimating the likelihood that a vessel will first moor in an anchorage area within the port before docking at a berth (Talley & Ng 2016, Karimi-Mamaghan et al. 2020, Bai et al. 2023).[8] Such estimation requires the precise identification of berth and anchorage areas, a task for which practitioners before us have largely relied on navigational charts and individual knowledge of ports, making it labor-intensive and challenging to generalize to global ports with dynamic arrangements. Hence, we enhance the process by developing an iterative, multi-attribute, density-based spatial clustering algorithm that is both accurate in identifying different areas within ports and applicable to ports with different morphology worldwide.

The algorithm identifies different port areas by focusing on the density of containerships' mooring points recorded in the AIS data, which comprises the full history of visits by containerships to ports around the globe, with each visit containing numerous AIS data points for each location within the port visited by the ship. Our algorithm operates in two layers of clustering. The first layer identifies high-density areas, which are considered potential berth and anchorage areas. The second layer refines these areas by considering additional domain knowledge, such as the headings of ships during mooring, since vessels are observed to dock at berths in an orderly and close fashion, while they moor in the anchorage areas more randomly (Figure 1).[9]

Our algorithm is specifically designed to address two primary challenges inherent in the identification of berth and anchorage areas that existing clustering algorithms struggle with. First is the variability in the density of ships' mooring points *across* ports due to differences in trade volume handled, frequency of vessel visits, and geographical morphology and boundaries. This variability necessitates an adaptive approach to parameter setting for different ports. Our algorithm is designed to automatically iterate and refine its clustering parameters

[8] An anchorage is a location within a port where ships can lower anchors, while a berth is a designated spot within a port where vessels moor to load and unload cargo. If port congestion were not a concern, a ship would dock at a berth immediately upon its arrival in the port to begin loading or unloading cargo.

[9] Appendix B and the paper (Bai et al. 2023) provide details on our clustering algorithm, including pseudo-codes and a case study involving the Port of Ningbo-Zhoushan in China, which illustrates the effectiveness of the methodology in identifying berth and anchorage areas in ports with different morphologies compared to alternative methods.



(a) Headings at a Berth **(b)** Headings at an Anchorage

Figure 1: Information on Headings

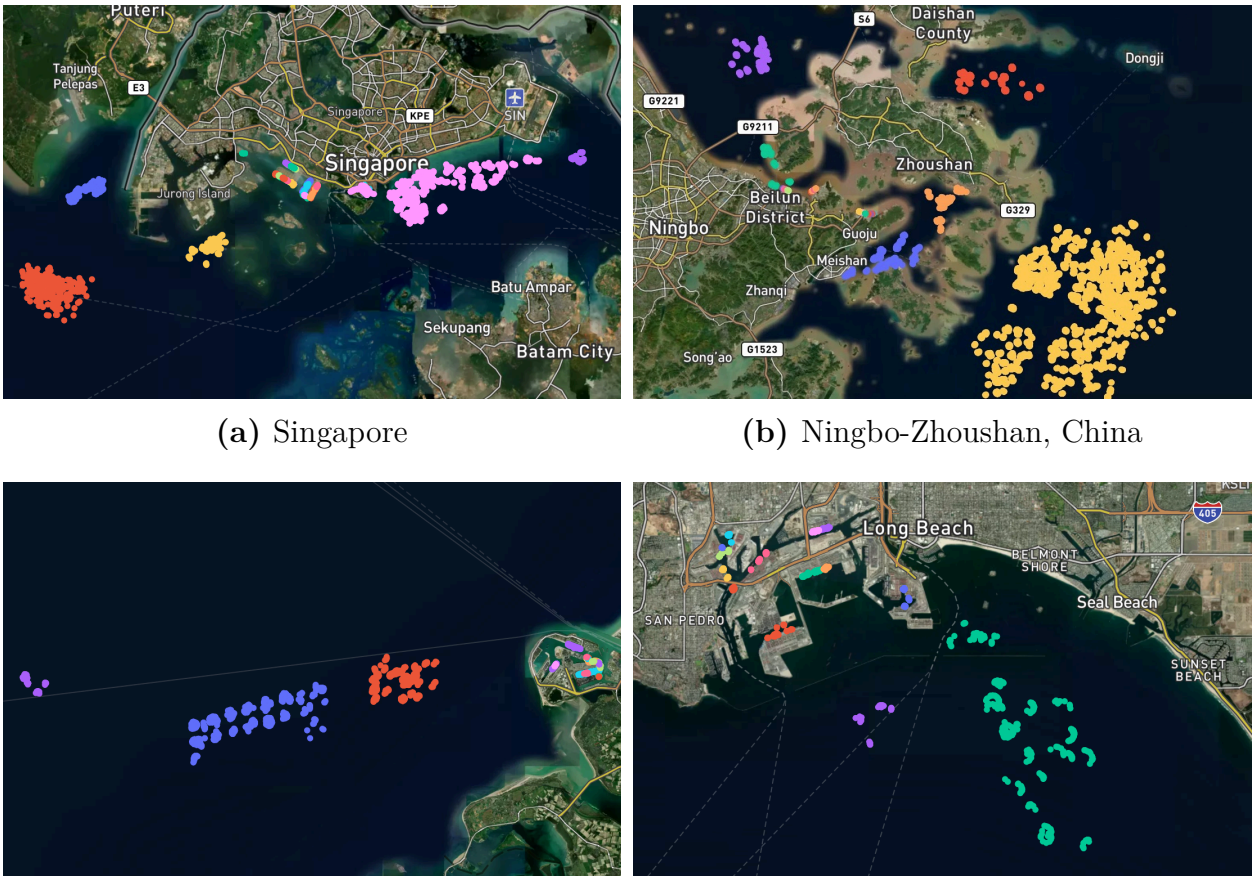
Notes. In both figures, a tip represents the bow of a ship. In (a), the headings are either in the same direction or exactly opposite. As a result, two clusters can be formed with exact opposite headings. In (b), the headings are random, with some of them appearing in a ring shape.

for each individual port, thus accommodating varied and complex port environments. This iterative process streamlines the algorithm, enhancing its generalizability and widening its potential applications. Second, our algorithm accurately distinguishes between berth and anchorage areas *within* ports – a task made challenging by the high density of ships' mooring points that complicates their recognition. The algorithm overcomes this issue by leveraging both the spatial (i.e., geographical coordinates) and non-spatial attributes (i.e., headings of ships) in its two-layer clustering. Our novel approach, based on domain knowledge, significantly enhances the granularity and accuracy of the analysis, making it readily adaptable to other applications.[10]

To illustrate our algorithm, Figures 2a to 2d show the anchorage (colors including red, yellow, blue, purple, pink, cyan, and orange) and berth areas (markers of other colors) in

[10]The identification of berth and anchorage areas in ports with varying morphologies lays the groundwork for a range of granular measures of port performance, such as port handling efficiency and waiting time. While our algorithm is tailored for identifying berth and anchorage areas, its core mechanism – transforming domain knowledge into non-spatial attributes and using them as additional metrics between data points in an iterative clustering process – boasts wider applications. This offers a versatile framework for classifying clusters of varying densities with specific labels in other contexts as well (e.g., identifying disease hotspots, urban planning).

the following major container ports: Singapore (Panel a), Ningbo-Zhoushan in China (Panel b), Rotterdam in the Netherlands (Panel c), and Los Angeles and Long Beach in the U.S. (Panel d). Our algorithm accurately identifies the anchorage and berth areas in each port, despite a broad range of geographical and operational port conditions. Using our algorithm with real-time AIS satellite data, we construct a comprehensive, high-frequency measure of global port congestion, which we discuss in the following section.



(a) Singapore

(b) Ningbo-Zhoushan, China

(c) Rotterdam, Netherlands

(d) Los Angeles and Long Beach, U.S.

Figure 2: Identification of Anchorage and Berth Areas of a Port Using Machine Learning

Notes. The figures depict the identification results for berth and anchorage areas in several representative container ports worldwide: the Port of Singapore, Port of Ningbo-Zhoushan in China, Port of Rotterdam in the Netherlands, and the Ports of Los Angeles and Long Beach in the U.S. We employ various colors to represent different clusters identified by our machine learning clustering algorithm, IMA-DBSCAN (details can be found in Appendix B). Specifically, colors such as red, yellow, blue, purple, pink, cyan, and orange denote clusters identified as anchorages, while other colors symbolize clusters identified as berths. The underlying sample for each figure incorporates the first 50,000 AIS observations of containerships entering each port since 1 January 2020.

2.3. Port Congestion and the Index of Average Congestion Rate

Port congestion arises when ships cannot immediately load and/or unload cargo upon arrival at ports, resulting in the vessels waiting in an anchorage area for an opportunity to dock at a berth and thus experiencing delays in their operations. For the top 50 container ports worldwide, denoted as $\mathscr{P}$, we count the number of delayed ship visits to each port p where the ship first moors in an anchorage before docking at a berth.[11] We then calculate the congestion rate for each port p by dividing the number of delayed ship visits by the total number of ship visits:

$$Congestion_{pt} \equiv \frac{Delayed_{pt}}{Delayed_{pt} + Undelayed_{pt}}, \ \forall p \in \mathscr{P},$$

where $Delayed_{pt}$ and $Undelayed_{pt}$ represent the number of delayed and undelayed ship visits at port p in month t, respectively. We calculate the congestion rate for each port on a monthly basis throughout the sample period.

Figure 3 shows the monthly congestion rates for the top ten container ports worldwide located in China, Singapore, South Korea, and the Netherlands, as well as the Ports of Los Angeles and Long Beach in the U.S., for the period from January 2017 to July 2022 when the AIS data are available. These ports are pivotal to the global supply chain, as they jointly account for more than 30% of the total volume of containerized seaborne trade in the world. Our data shows that the congestion rates for several ports remained largely stable (e.g., Port of Rotterdam, Netherlands) following the onset of the Covid-19 pandemic in March 2020. As the pandemic progressed from October 2020 onwards, congestion increased in the majority of ports, as evidenced by the increase in chromatic intensity in the figure.[12] Such an analysis reveals that containerships faced significant delays in loading and/or unloading operations from October 2020 onwards, leading to acute disruptions to the global distribution of goods.

[11] A ship visit, also known as a port call, refers to the arrival of a ship at a specific port where it docks to load or unload cargo.

[12] By our calculation, in late 2020, approximately 80% of inbound ships at the Port of Los Angeles in the U.S. were unable to dock at a berth immediately upon arrival. This observation aligns with official statistics. According to figures released by the Pacific Merchant Shipping Association, the percentage of containerships at Los Angeles waiting five or more days for unloading surged from 10% in August to 26% in December 2020. Additionally, the Marine Exchange of Southern California reported that the number of vessels anchored in Los Angeles waters also rose from fewer than 20 in August to more than 35 in December 2020.

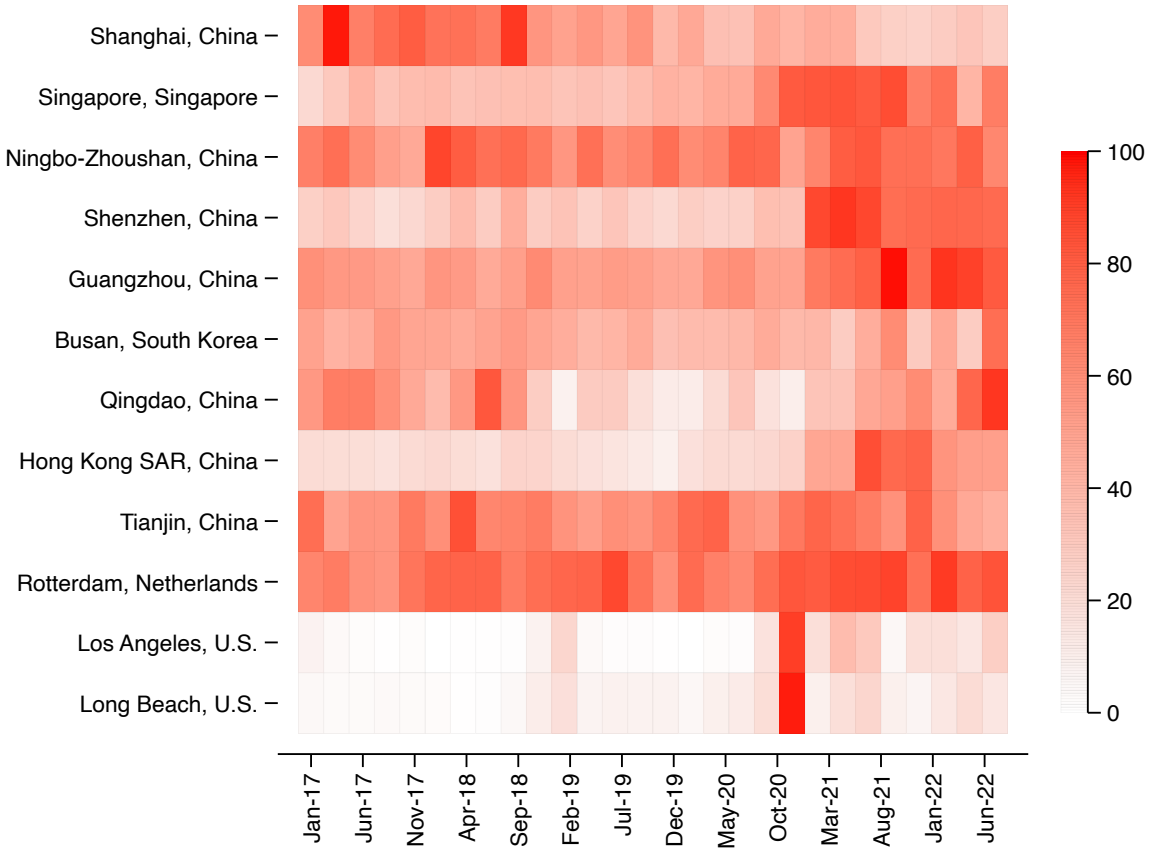


Figure 3: Congestion Rates for the Major Container Ports Worldwide

Notes. The heatmap presents the monthly congestion rates for the top ten global container ports, as well as the Ports of Los Angeles and Long Beach in the U.S., spanning the period from January 2017 to July 2022. Collectively, these ports account for over 30% of the total volume of containerized seaborne trade worldwide. The congestion rate for each port is normalized and expressed as a percentage of its peak value observed within the sample period. Cells in darker shades indicate higher congestion levels for the respective port during the specified month. The congestion rate for a port, as defined in Equation (2.3), represents the proportion of ship visits that experience delays when ships first moor in an anchorage area before docking at a berth.

By normalizing the congestion rate of a port by the number of ship visits to the port, we net out variations in the level of congestion resulting from infrequent but significant changes in demand. While the stringent terms of shipping services for containerships usually render our congestion tracking at seaports independent of general economic conditions and demand fluctuations (as discussed in the introduction), our sample includes the exceptional period of Covid-19. Throughout this period, service agreements might have been canceled, and containership itineraries could have been modified or temporarily suspended, affecting our

assessment of supply chain disruptions inferred from port congestion. For instance, at the onset of the Covid-19 pandemic, shipping companies engaged in active capacity management to accommodate significant declines in demand (Notteboom et al. 2021).[13] Similarly, towards the end of 2021 when the demand for goods skyrocketed, carriers struggled to maintain weekly sailing schedules due to overwhelmed ports and ensuing congestion, and as a result, were forced to implement blank sailings (Sea-Intelligence 2021).[14] These adjustments resulted in significant variations in the number of ship visits to each port, which in turn might influence the level of congestion. As evident in Figure 4, the number of ship visits to major container ports around the globe remained relatively stable until mid-2021. However, there was a substantial decrease thereafter for a number of local ports, notably the Ports of Singapore, Los Angeles, and Long Beach in the U.S.

To construct a time series measure of global supply chain disruptions that minimizes the impact of changes in demand, we define the Average Congestion Rate (ACR) by computing the weighted average of the congestion rates for the top 50 container ports worldwide, with the weights determined by the number of ship visits to each port:

$$ACR_t = \sum_{p \in \mathscr{P}} \left[\frac{Delayed_{pt} + Undelayed_{pt}}{\sum_{p \in \mathscr{P}} \left(Delayed_{pt} + Undelayed_{pt} \right)} \cdot Congestion_{pt} \right].$$

As emphasized earlier, the normalization of the congestion rate ($Congestion_{pt}$) by the number of ship visits ($Delayed_{pt}+Undelayed_{pt}$) serves to minimize the impact of demand changes on port congestion. Furthermore, any infrequent adjustments in shipping capacity across routes, and the subsequent changes in congestion at different ports, are canceled out when we aggregate the congestion rates to construct the ACR index, hence enhancing its exogeneity in measuring global supply chain disruptions. We also use the number of ship visits to each port as weights because they reflect the distinct roles of different ports within the global

[13] In April-May 2020, as lockdowns and economic restrictions in Europe and North America halted industrial manufacturing and led to unprecedented declines in consumer and business demand, shipping carriers reduced their network capacity on primary trade routes by up to 20%. Additionally, they sidelined over 2.7 million twenty-foot equivalent units (TEU) of fleet capacity, equivalent to over 11% of the global container fleet.

[14] Blank sailing, also known as void sailing, refers to situations where a scheduled ship does not sail. This occurs when a carrier or shipping line cancels a vessel's journey, causing it to miss specific ports or its entire intended route.

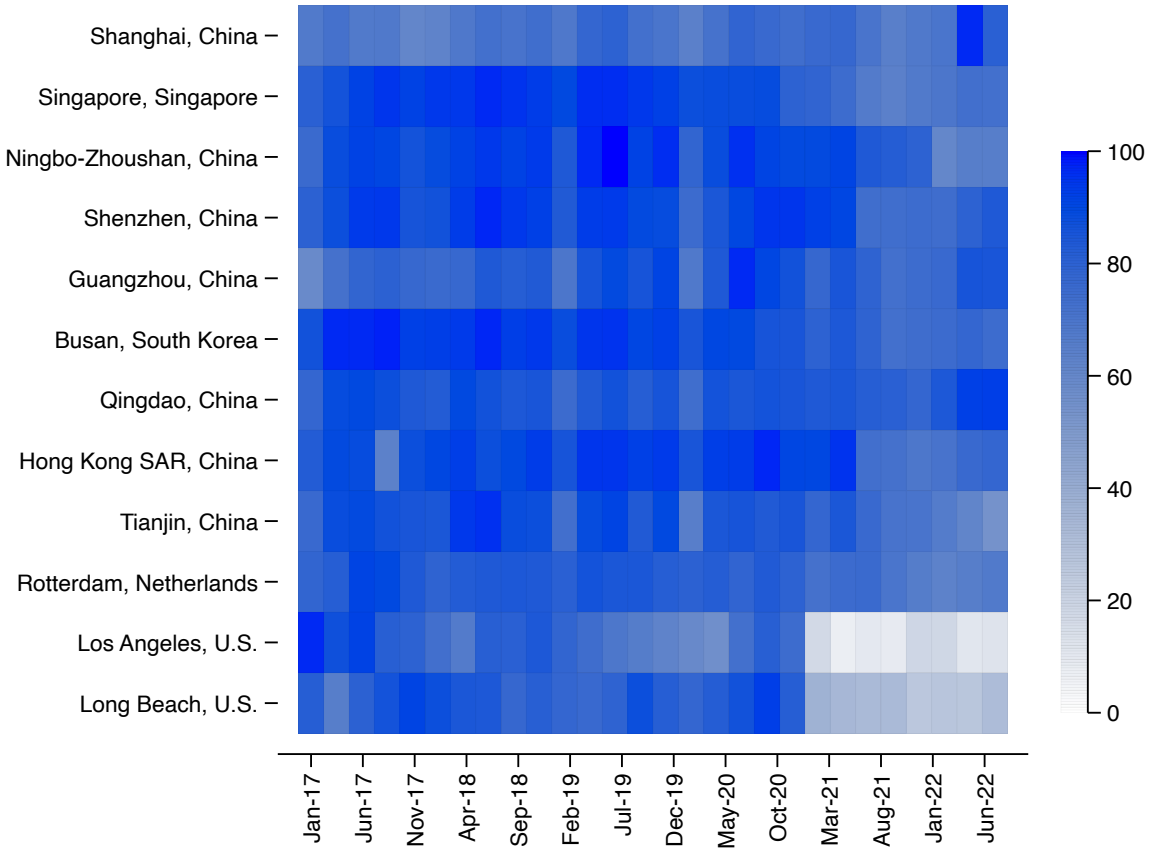


Figure 4: Ship Visits to the Major Container Ports Worldwide

Notes. The heatmap displays the number of ship visits to each of the top ten global container ports, as well as the Ports of Los Angeles and Long Beach in the U.S., covering the period from January 2017 to July 2022. Collectively, these ports represent over 30% of the total volume of containerized seaborne trade worldwide. The number of ship visits to each port is normalized, expressed as a percentage of its peak value observed within the sample period. Cells in darker shades denote a greater number of ship visits to the respective port during the specified month. A ship visit, also known as a port call, refers to the arrival of a ship at a specific port where it docks to load or unload cargo.

supply chain.[15] Figure 5 displays our ACR index. Prior to 2019, the index remained stable around the sample median (17.8%), and it declined to 16% from early 2019 to mid-2020. Subsequently, the index consistently rose, reaching its peak at 25% in June 2021, indicative of the significant disruptions to the supply chain related to the Covid-19 pandemic.[16]

[15]The weighting considers the differential impact on global supply chain disruptions resulting from changes in the congestion rates at different ports. For instance, a slight increase in the congestion rate at the Port of Hong Kong in China would likely have triggered a more pronounced global supply chain disruption than a significant increase at the Port of Manila in the Philippines.

[16]In Appendix F, we compare our ACR index to other indices of supply chain disruptions in the literature, notably the Harper Peterson Time Charter Rates Index (HARPEX), New York Fed's Global Supply Chain

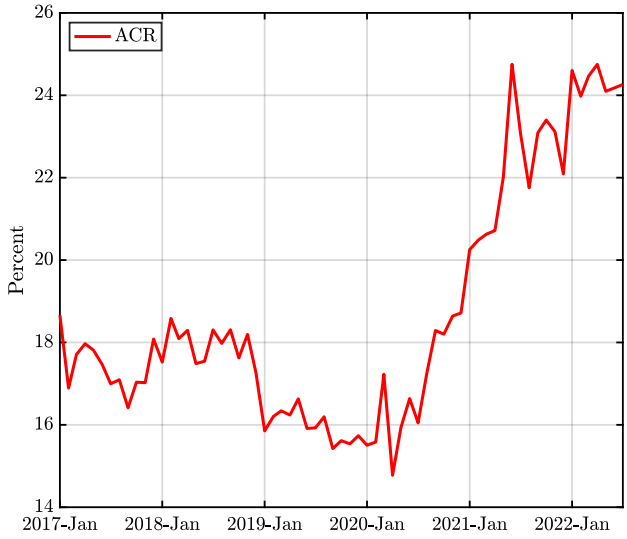


Figure 5: ACR Index of Global Supply Chain Disruptions

Notes. The ACR index of global supply chain disruptions is derived by taking a weighted average of the congestion rates for the top 50 global container ports, with the number of ship visits used as the weight for each port. The index is presented in percentage terms and has been seasonally adjusted. For the complete ranking of container ports, see https://www.worldshipping.org/top-50-ports (Accessed June 15, 2022).

3. A Model of Congestion and Spare Capacity

In this section, we develop our model featuring search and matching frictions in the goods market, similar to the framework in Michaillat & Saez (2015, 2022) and Ghassibe & Zanetti (2022). Our model incorporates transportation costs that prevent the shipment of full productive capacity to retailers and result in supply chain disruptions by curtailing the supply of goods. Search frictions and transportation costs hinder the allocative mechanism of prices in clearing the quantity of goods sold by producers to retailers.[17] Our model links disruptions in the supply chain arising from increased transportation costs to search frictions and the resulting changes in spare capacity, prices, and output. It outlines the relevance of the

Pressure Index (GSCPI), and the Supply Disruptions Index (SDI) compiled by Smirnyagin & Tsyvinski (2022), among others. We show that there are significant differences between the indices that influence the interpretations of supply chain disruptions and their causal effects on the macro aggregates of interest, such as inflation. Additionally, in Appendix G, we construct an alternative measure of port congestion – the Average Congestion Time (ACT) – using AIS data and IMA-DBSCAN. Unlike the ACR index, the ACT index measures the average number of hours a containership waits in an anchorage area of a port before docking at a berth, weighted by the number of ship visits. We show that using the ACT index in the causality assessment delivers quantitatively similar results to those obtained with the ACR index.

[17] Appendix C discusses the evidence of search and matching frictions in the goods market and the relevance of transportation costs for the severance of commercial trade.

co-movement of spare capacity with prices and output in identifying the causal effects of supply chain disruptions (Section 4) and connects these disruptions to the effectiveness of monetary policy in controlling inflation (Section 5).

The economy comprises maximizing firms and households. Firms can be either producers or retailers. Producers manufacture goods using a fixed amount of labor supplied by households and incur transportation costs when selling the goods to retailers. Retailers purchase goods from producers but face search frictions that prevent the free flow of meetings with these producers. They then sell the goods to households in exchange for money, which is the numeraire of the economy.[18]

We begin by studying the distinct problems of producers and retailers, who face transportation and visiting costs, respectively. The magnitude of these costs jointly determines the supply of goods in the retail market. We then examine the optimal choices of households, who determine aggregate demand. Subsequently, we show that in an equilibrium where supply meets demand, search frictions and transportation costs together determine the spare productive capacity that producers cannot transfer to the retailers. This leads to a supply shortage in the retail market, and the adjustment of this shortage is pivotal to changes in prices and sales of goods in response to disruptions in the supply chain.

3.1. Firms

Firms in the economy comprise producers and retailers. Producers manufacture goods with a capacity determined by the inelastic labor inputs $l > 0$. They sell these goods to retailers in a frictional goods market that prevents the sale of the full capacity. Each unmatched retailer (identified by the subscript U) makes visits i_U to unmatched producers at a unitary cost $\rho > 0$, and upon a successful trade, resells the purchased goods to households at the price p.

Matching process. In each period, a constant-returns-to-scale matching function encapsulates the search frictions in the product market, determining the number of meetings (m) between

[18] Our approach is similar to the standard assumption that firms require intermediate goods for the production of final goods. See, for instance, Costinot et al. (2013), Kasahara & Lapham (2013), Ramondo & Rodríguez-Clare (2013).

unmatched producers and retailers according to:

$$\mathscr{m} = (x_U^{-\xi} + i_U^{-\xi})^{-\frac{1}{\xi}}, \tag{1}$$

where x_U and i_U are the number of unmatched producers and retailers, respectively, and the parameter ξ is the elasticity of substitution between the inputs of the matching function. We assume $\xi > 0$, such that $\mathscr{m} \leq \min\{x_U, i_U\}$.

We define the product market tightness θ as the ratio between the number of visits by the unmatched retailers and the number of unmatched producers, such that $\theta \equiv i_U/x_U$. Given the Law of Large Numbers, product market tightness is taken as given by individual producers and retailers. It determines the probabilities that producers and retailers meet each other, given the constant returns to scale in the matching function. Specifically, the probability for a producer to meet a retailer is:

$$f(\theta) = \frac{\mathscr{m}}{x_U} = (1 + \theta^{-\xi})^{-\frac{1}{\xi}}, \tag{2}$$

and the probability for a retailer to meet a producer with probability:

$$q(\theta) = \frac{\mathscr{m}}{i_U} = (1 + \theta^{\xi})^{-\frac{1}{\xi}}. \tag{3}$$

The function $f(\theta)$ is smooth and strictly increasing in the domain $[0, +\infty)$, with $f(0) = 0$, $\lim_{\theta\to+\infty} f(\theta) = 1$, and $f'(\theta) > 0$, whereas the function $q(\theta)$ is smooth and strictly decreasing in the same domain $[0, +\infty)$, with $q(0) = 1$, $\lim_{\theta\to+\infty} q(\theta) = 0$, and $q'(\theta) < 0$. Two properties that will be useful later are that $f(\theta)/q(\theta) = \theta$ and $df(\theta)/d\theta = q(\theta)^{1+\xi}$.

Transportation cost. Producers pay an idiosyncratic transportation cost to ship goods to retailers.[19] In each period, producers draw a transportation cost z from the log-normal distribution $G(z)$ with the scale parameter γ and the shape parameter σ, i.e., $G(z) \equiv \Phi\big[(\log z - \gamma)/\sigma\big]$, where $\Phi(\cdot)$ is the standard normal cumulative density function.[20] As we

[19] Our results continue to hold if the transportation cost is borne by retailers instead of producers. This is because the match separation condition (12) is invariant to such a modeling choice.

[20] We could also apply a more general setup that each producer maintains its previous draw of transportation cost with probability $1 - \varphi$, and with probability φ, the producer draws a new transportation cost from $G(z)$. This setup is often found in the traditional labor search and matching theory that studies the labor market outcomes following a rise in economic turbulence (den Haan et al. 2005, Fujita 2018, Pizzinelli et al. 2020). Despite more involved algebra, our main results still hold.

discuss later, there exists a reservation level of transportation cost $\bar{z}$, above which matches are unprofitable and therefore severed. Consequently, the matches with a draw of transportation cost higher than the reservation level ($z > \bar{z}$) are optimally severed, whereas they continue otherwise ($z \leq \bar{z}$).

Recursive value functions. At the beginning of each period, the matched producers sell the manufactured goods to retailers and pay the transportation costs, while the matched retailers sell their purchased goods to households and pay the wholesale price of goods to the producers. The unmatched producers and retailers search to form a match with each other. At the beginning of the next period, each producer draws a new transportation cost, and the match continues if the new cost is sufficiently low to retain the profitability of the match (we describe the match separation decision later in the section).

Four recursive value functions describe the values for the different status of producers and retailers. The value for a matched producer (identified by the subscript M), $X_M(z)$, is equal to:

$$X_M(z) = r(z) - z + \beta \mathbb{E}_{z'}\big[\max\big(X_M(z'), X_U\big)\big], \tag{4}$$

where $r(z)$ stands for the wholesale price of the goods that is endogenously determined, z for the cost of transportation, β for the discount factor, and z' for the draw of transportation cost at the beginning of the next period. Equation (4) shows that the present value of being a matched producer is the profit margin $r(z) - z$, plus the continuation value which depends on whether it endogenously separates from the match. Such a decision is determined by z', and hence the max operator characterizes the optimal continuation/separation decision.

The value for an unmatched producer, X_U, is:

$$X_U = \beta f(\theta) \mathbb{E}_{z'}\big[\max\big(X_M(z'), X_U\big)\big] + \beta\big(1 - f(\theta)\big) X_U. \tag{5}$$

With probability $f(\theta)$, the unmatched producer meets a retailer and then decides whether to endogenously separate if the given draw of transportation cost makes the match unprofitable. With probability $1 - f(\theta)$, the producer forgoes a successful match with a retailer and remains unmatched at the beginning of the next period.

The value for a matched retailer, $I_M(z)$, is:

$$I_M(z) = p - r(z) + \beta \mathbb{E}_{z'}\big[\max\big(I_M(z'), I_U\big)\big]. \tag{6}$$

The retailer earns the price p by reselling the purchased goods to the households and it pays the wholesale price $r(z)$ to the producer. The max operator characterizes the optimal continuation/separation decision conditional on the draw of transportation cost at the beginning of the next period. If the drawn transportation cost makes the match unprofitable, the retailer endogenously separates from the match and hence starts the next period with a value equal to:

$$I_U = -\rho + \beta q(\theta) \mathbb{E}_{z'}\big[\max\big(I_M(z'), I_U\big)\big] + \beta\big(1 - q(\theta)\big) I_U, \tag{7}$$

where ρ is a fixed cost that the retailer pays per visit to the producer. We assume free-entry into the retail market that drives the value for an unmatched retailer to zero in equilibrium, i.e., $I_U = 0$.

Nash bargaining. Nash bargaining splits the total surplus from the matching between the producer and the retailer. The total surplus from matching is equal to:

$$S(z) = X_M(z) - X_U + I_M(z) - I_U. \tag{8}$$

The producer earns a constant share η of the total surplus, and the retailer earns the remaining share $1 - \eta$, which in equilibrium yields:

$$\eta\big(I_M(z) - I_U\big) = (1 - \eta)\big(X_M(z) - X_U\big). \tag{9}$$

Given the equilibrium rule (9), the value functions (4), (5), (6), and the free-entry condition $I_U = 0$, the wholesale price that splits the surplus is equal to:

$$r(z) = \eta(p + \rho\theta) + (1 - \eta)z. \tag{10}$$

Equation (10) shows that the bargaining power η is central to the determination of the wholesale price. When the producers have significant bargaining power ($\eta \to 1$), they earn the total surplus accrued to the retailers from selling the goods to the household $(p + \rho\theta)$.

On the other hand, when the bargaining power of the producer is low ($\eta \to 0$), the wholesale price is close to the cost of transportation (z). Intermediate values for the bargaining parameter proportionally split the total surplus between producers and retailers, with the share of surplus determined by the bargaining parameter. Important to our analysis, congestion in the matching process, captured by tightness in the product market, worsens the bargaining position of retailers by lowering their matching probability consequent to the scarcity of supply of goods, thus increasing the wholesale price they pay to purchase goods from producers.

Match separation. Since the total value for a matched producer and a matched retailer, i.e., $X_M(z) + I_M(z)$, strictly decreases with the cost of transportation z, there exists a cut-off transportation cost $\bar{z}$, above which the costs are too high, making the matches unprofitable and consequently severed. This cut-off makes the total surplus in Equation (8) equal to zero:

$$S(\bar{z}) = 0. \tag{11}$$

By substituting the value functions (4), (5), (6), and the free-entry condition $I_U = 0$ into Equation (11), we can express the match separation condition as a function of price p, reservation transportation cost $\bar{z}$, and product market tightness θ, defined for all $p \in (0, +\infty)$, $\bar{z} \in (0, +\infty)$, and $\theta \in [0, +\infty)$, satisfying:

$$\mathbb{F}(p, \bar{z}, \theta) = p - \bar{z} + \big(1 - \eta f(\theta)\big)\beta \mathbb{E}_{z'} S(z') = 0, \tag{12}$$

where the expected surplus is defined by $\mathbb{E}_{z'} S(z') = \int_0^{\bar{z}} S(z') dG(z')$.

Match creation. Using the value function for an unmatched retailer (7) and the free-entry condition $I_U = 0$, we define the match creation condition as a function of reservation transportation cost $\bar{z}$ and product market tightness θ, defined for all $\bar{z} \in (0, +\infty)$ and $\theta \in [0, +\infty)$, satisfying:

$$\mathbb{H}(\bar{z}, \theta) = \frac{\rho}{q(\theta)} - (1 - \eta)\beta \mathbb{E}_{z'} S(z') = 0. \tag{13}$$

Aggregate supply. The aggregate supply in the economy results from the equilibrium in the product market, which is defined as:

Definition 1. *The equilibrium in the product market consists of a price* $p \in (0, +\infty)$*, a reservation transportation cost* $\bar{z} \in (0, +\infty)$*, and a product market tightness* $\theta \in [0, +\infty)$ *such that the conditions for match separation* (12) *and match creation* (13) *simultaneously hold:*

$$\mathbb{F}(\bar{z}, \theta, p) = \mathbb{H}(\bar{z}, \theta) = 0.$$

Definition 1 indicates that the equilibrium product market tightness is a function of both the price and the reservation transportation cost. Such a relationship is governed by the conditions for match separation and creation, as outlined in Equations (12) and (13), respectively. The following proposition summarizes this relationship.

Proposition 1. *In equilibrium, the price* p*, reservation transportation cost* $\bar{z}$*, and product market tightness* θ *satisfy the relationship:*

$$\theta(p, \bar{z}) = \frac{1-\eta}{\eta\rho}\big(p - \bar{z} + \beta \int_0^{\bar{z}} G(z')dz'\big), \tag{14}$$

where $G(.)$ *is the log-normal cumulative density function. Hence, the product market tightness* θ *has the following properties:*

1. $\theta(p^{min}, \bar{z}) = 0$ *and* $\lim_{p\to+\infty} \theta(p, \bar{z}) = +\infty$*, where* p^{min} *satisfies:*

$$p^{min} - \bar{z} + \beta \int_0^{\bar{z}} G(z')dz' = 0;$$

2. $\theta(p, \bar{z})$ *is strictly increasing on* $[p^{min}, +\infty)$*;*

3. $\theta(p, \bar{z})$ *is linear on* $[p^{min}, +\infty)$*;*

4. $\lim_{\bar{z}\to 0^+} \theta(p, \bar{z}) = (1-\eta)p/(\eta\rho)$ *and* $\theta(p, \bar{z}^{max}) = 0$*, where* $\bar{z}^{max}$ *satisfies:*

$$p - \bar{z}^{max} + \beta \int_0^{\bar{z}^{max}} G(z')dz' = 0;$$

5. $\theta(p, \bar{z})$ *is strictly decreasing on* $(0, \bar{z}^{max}]$*; and*

6. $\theta(p, \bar{z})$ *is convex on* $(0, \bar{z}^{max}]$.

Proof. See Appendix D.1. ■

Proposition 1 establishes that the product market tightness strictly increases with the price of goods and decreases with the reservation transportation cost. These properties are intuitive. When the total surplus rises due to an elevated price, retailers are incentivized to visit more producers, leading to increased tightness. Conversely, a rise in the reservation transportation cost diminishes the total surplus shared between producers and retailers at the margin. As a result, this dampens the incentives for retailers to visit producers, causing a more slack product market.[21]

Next, the aggregate supply comprises the quantity of goods traded by the retailers and producers that survive separation for a given productive capacity l. To determine the equilibrium number of matched producers, we consider the law of motion for the number of matched producers at the beginning of the next period:

$$x'_M = G(\bar{z})x_M + f(\theta)G(\bar{z})x_U,$$

and that for the number of unmatched producers at the beginning of the next period:

$$x'_U = \big[1 - f(\theta) + f(\theta)\big(1 - G(\bar{z})\big)\big]x_U + \big(1 - G(\bar{z})\big)x_M.$$

By focusing on the steady-state equilibrium and normalizing the total number of matched and unmatched producers to one, i.e., $x_M + x_U = 1$, we derive the equilibrium number of matched producers x_M^{eqm} equal to:

$$x_M^{eqm}(\bar{z}, \theta) = \frac{f(\theta)G(\bar{z})}{1 - G(\bar{z}) + f(\theta)G(\bar{z})}.$$

The aggregate supply in the economy is thus equal to the quantity of goods supplied by matched producers for the given productive capacity l:

$$c_s(\bar{z}, \theta) = x_M^{eqm}(\bar{z}, \theta) \cdot l = \frac{f(\theta)G(\bar{z})}{1 - G(\bar{z}) + f(\theta)G(\bar{z})} l. \tag{15}$$

By substituting the expressions for $f(\theta)$ and θ from Equations (2) and (14) into Equation (15), we express the aggregate supply in the economy as a function of price and reservation

[21] An increase in the reservation transportation cost raises the expected total surplus $\beta \mathbb{E}_{z'} S(z')$, since matches are less likely to dissolve in the subsequent period. However, this positive effect is outweighed by the decrease in the profit margin $p - \bar{z}$, resulting in a net negative impact on the total surplus.

transportation cost, as stated in the next definition.

Definition 2. *The aggregate supply c_s, expressed as a function of price p and reservation transportation cost $\bar{z}$, is equal to:*

$$c_s(p,\bar{z}) = \frac{\left\{1+\left[\frac{1-\eta}{\eta\rho}\left(p-\bar{z}+\beta\int_0^{\bar{z}}G(z')dz'\right)\right]^{-\xi}\right\}^{-\frac{1}{\xi}}G(\bar{z})}{1-G(\bar{z})+\left\{1+\left[\frac{1-\eta}{\eta\rho}\left(p-\bar{z}+\beta\int_0^{\bar{z}}G(z')dz'\right)\right]^{-\xi}\right\}^{-\frac{1}{\xi}}G(\bar{z})}l, \tag{16}$$

for all $(p,\bar{z}) \in (0,+\infty)\times(0,+\infty)$ satisfying:

$$p-\bar{z}+\beta\int_0^{\bar{z}}G(z')dz' \geq 0. \tag{17}$$

Since the aggregate supply in Equation (16) is determined by two endogenous variables, there exist infinite combinations of price and reservation transportation cost that yield the same aggregate supply, as long as they satisfy the constraint (17).[22] We resolve the indeterminacy by selecting the equilibrium where the reservation transportation cost remains fixed at an arbitrary level τ, and price moves to satisfy the aggregate supply condition. By considering the equilibrium with freely adjusting prices, we can study the responses of prices to the distinct disturbances to aggregate demand, productive capacity, and the supply chain respectively, and then use the co-movements across variables to formulate unique identifying restrictions to estimate the causal effects of supply chain disturbances in our SVAR model developed in Section 4.

Consequently, Definition 2′ recasts the original Definition 2 of aggregate supply as a function of price p for an arbitrary reservation transportation cost τ.

Definition 2′. *For an arbitrary reservation transportation cost $\tau \in (0,+\infty)$, the flexible-price aggregate supply c_s^{flex} is the function of price p defined by:*

$$c_s^{flex}(p) = \frac{\left\{1+\left[\frac{1-\eta}{\eta\rho}\left(p-\tau+\beta\int_0^{\tau}G(z')dz'\right)\right]^{-\xi}\right\}^{-\frac{1}{\xi}}G(\tau)}{1-G(\tau)+\left\{1+\left[\frac{1-\eta}{\eta\rho}\left(p-\tau+\beta\int_0^{\tau}G(z')dz'\right)\right]^{-\xi}\right\}^{-\frac{1}{\xi}}G(\tau)}l, \tag{18}$$

[22] The indeterminacy of the equilibrium is standard in search models. For instance, it arises in Michaillat & Saez (2015), where either the price or tightness must be assumed fixed to select an equilibrium. Our model also does not allow for an equilibrium in which both the price and reservation transportation cost can be determined simultaneously. The reason is similar: each retailer-household pair decides the price in a situation of bilateral monopoly. Since the solution to the bilateral monopoly problem is indeterminate (Howitt & McAfee 1987, Hall 2005), it cannot be used to impose a condition on the price.

for all $p \in [p^{min}, +\infty)$*, where* p^{min} *satisfies:*

$$p^{min} - \tau + \beta \int_0^{\tau} G(z')dz' = 0.$$

The next proposition outlines the properties of the aggregate supply when the price adjusts to satisfy the aggregate supply condition.[23]

Proposition 2. *The flexible-price aggregate supply* c_s^{flex} *has the following properties:*

1. $c_s^{flex}(p^{min}) = 0$ *and* $\lim_{p\to+\infty} c_s^{flex}(p) = G(\tau)l$*;*
2. $c_s^{flex}(p)$ *is strictly increasing in* p *on* $[p^{min}, +\infty)$*; and*
3. $c_s^{flex}(p)$ *is concave on* $[p^{min}, +\infty)$*.*

Proof. See Appendix D.2. ■

The aggregate supply $c_s^{flex}(p)$ represents the quantity of goods traded that satisfies Equation (18) for a given transportation cost τ. Therefore, the dynamics of the aggregate supply are uniquely determined by the interaction between the price and tightness in the product market. A higher price initially leads to a greater total surplus by increasing the value for the matched retailer. This, in turn, enhances the incentives for retailers to visit producers, resulting in increased product market tightness and a higher probability for a producer to match with a retailer. More matches are created, leading to an increase in aggregate supply. Thus, while transportation costs and matching frictions reduce the aggregate supply of goods to retailers, and the economy entails spare capacity, the model retains the standard positive relationship between the price and the aggregate supply.

Figure 6 shows the aggregate supply in the quantity-price (Q,p) space. For a given capacity of the economy l (brown line), transportation costs limit the production to $G(\tau)l$ (green line). Search frictions further reduce the aggregate supply to the level $c_s^{flex}(p)$ (blue line), which, as in standard models, increases with the price. The spare capacity, represented by the difference between the capacity of the economy and the actual production (i.e., $l -$

[23] Appendix D.8 discusses the alternative pricing mechanism in which the price of goods remains fixed while the reservation transportation cost can vary. In addition to deriving its key analytical properties, we use numerical methods to approximate this fixed-price aggregate supply and illustrate its properties across different values of the reservation transportation cost.

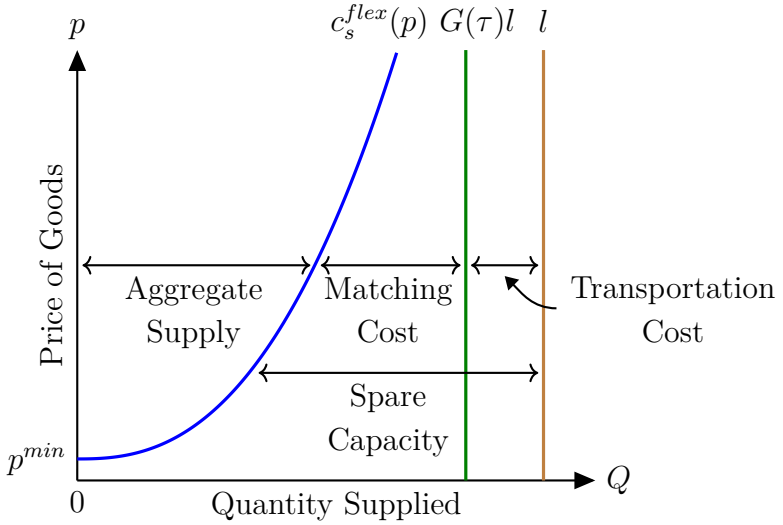


Figure 6: Supply Side of the Economy With Flexible Price of Goods

$c_s^{flex}(p)$), arises from both the transportation and matching costs. It is worth noting that in our model, the spare capacity is equivalent to unemployment in the labor market, as it represents the difference between the supply of labor linked to the capacity of the economy and the demand for labor associated with actual production.

3.2. Households

The representative household derives utility from consuming goods and holding real money balances.[24] The household's utility is given by:

$$u\big(c, \frac{m}{p}\big) = \frac{\chi}{1+\chi} c^{\frac{\epsilon-1}{\epsilon}} + \frac{1}{1+\chi}\big(\frac{m}{p}\big)^{\frac{\epsilon-1}{\epsilon}},$$

where c denotes consumption, m is the nominal money balance, p is the price, the parameter $\chi > 0$ represents the taste for consumption relative to holding money, and the parameter $\epsilon > 1$ is the elasticity of substitution between consumption and real money balances.

Taking the price as given, the representative household chooses consumption and nominal money balances to maximize utility, subject to the budget constraint. The household, with an endowment $\mu > 0$ of nominal money, purchases c goods at price p from retailers and holds

[24] We borrow the money in the utility function directly from Michaillat & Saez (2015) to ensure that aggregate demand plays an instrumental role in driving the macro aggregates. The presence of money is convenient for studying the state-dependent effects of a contractionary monetary policy shock (Section 5).

m units of nominal money balances. This leads to the following budget constraint:

$$pc + m \leq \mu.$$

Solving the utility-maximization problem yields the optimal condition for the household:

$$\frac{\chi}{1+\chi} c^{-\frac{1}{\epsilon}} = \frac{1}{1+\chi} \left(\frac{m}{p}\right)^{-\frac{1}{\epsilon}}, \tag{19}$$

implying that she is indifferent between consumption and holding money at the margin.

Aggregate Demand. The aggregate demand in the economy is equal to the level of consumption that maximizes utility at a given price when all resources are consumed.[25]

Definition 3. *The aggregate demand c_d for a given price $p \in (0, +\infty)$ equals:*

$$c_d(p) = \frac{\chi^\epsilon}{1+\chi^\epsilon} \frac{\mu}{p}. \tag{20}$$

Proposition 3. *$c_d(p)$ is strictly decreasing and convex on $(0, +\infty)$.*

Proof. Direct proof from Equation (20). ■

Figure 7 in the next section shows the aggregate demand, which is downward sloping in the (c, p) plane. Since a higher price leads to lower real money balances, the households' indifference between consumption and holding money implies that they would behave optimally and desire lower consumption when the price is higher. Hence, the aggregate demand in the economy decreases with the price.

3.3. Flexible-Price Equilibrium

For a given reservation transportation cost τ, the flexible-price equilibrium is defined in Definition 4, and its existence is demonstrated in Proposition 4.

Definition 4. *Fixing the reservation transportation cost $\bar{z}$ to an arbitrary value $\tau > 0$, the flexible-price equilibrium consists of a price p that equates aggregate supply and aggregate*

[25] Equation (19) implies that $m = pc/\chi^\epsilon$. By substituting this into the budget constraint, we obtain $pc(1 + 1/\chi^\epsilon) = \mu$. This can then be rearranged to derive the aggregate demand as given in Equation (20).

demand, $c_s^{flex}(p) = c_d(p)$*, yielding:*

$$\frac{f\big(\theta(p)\big)G(\tau)}{1-G(\tau)+f\big(\theta(p)\big)G(\tau)}l = \frac{\chi^\epsilon}{1+\chi^\epsilon}\frac{\mu}{p}, \tag{21}$$

where the product market tightness θ *is given by:*

$$\theta(p) = \frac{1-\eta}{\eta\rho}\big(p-\tau+\beta\int_0^\tau G(z')dz'\big), \tag{22}$$

Proposition 4. *For any* $\tau > 0$*, there exists a unique flexible-price equilibrium that features positive price and consumption.*

Proof. See Appendix D.3. ■

Figure 7 shows the aggregate supply, aggregate demand, and the resulting flexible-price equilibrium. The equilibrium price, p_0, is where the aggregate supply and demand intersect on the (Q, p) plane. Both the maximum quantity of goods that could be supplied when the matching process between producers and retailers becomes frictionless, and the productive capacity, are also plotted on the figure for comparison.

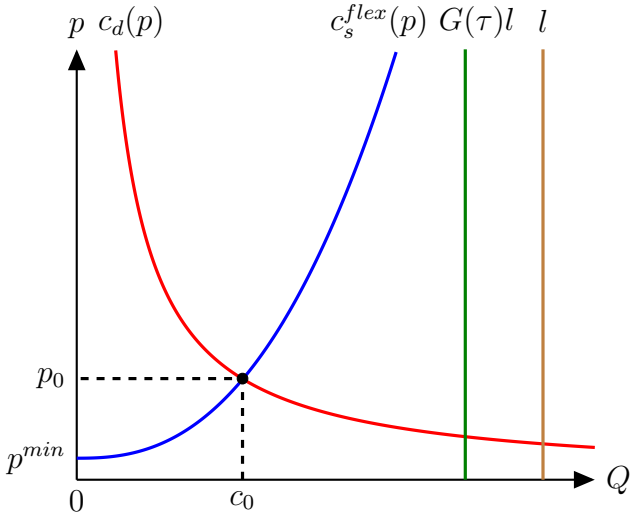


Figure 7: Aggregate Supply, Aggregate Demand, and Flexible-Price Equilibrium

3.4. Comparative Statics

We use comparative statics to study the responses of the macro aggregates to adverse shocks to aggregate demand, productive capacity, and the supply chain, respectively. These re-

sponses will offer unique identifying restrictions for studying the causal effects of supply chain disturbances in the SVAR model in the subsequent section.

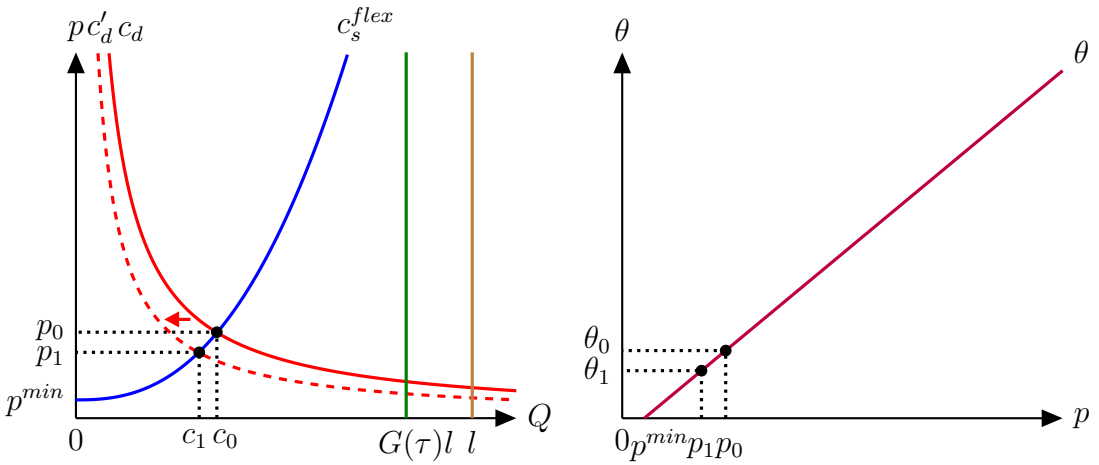
In our model, an adverse shock to aggregate demand can manifest as either a decrease in the money supply, μ, or a decline in the preference for consuming goods, χ. An adverse shock to productive capacity corresponds to a negative disturbance to the inelastic labor supply, l. An adverse shock to the supply chain involves an increase in the distribution of transportation costs, which is characterized by a rise in γ, the scale parameter of the log-normal distribution of transportation costs. *Ceteris paribus*, an increase in γ indicates a higher average transportation cost for producers, i.e., $exp(\gamma + \sigma^2/2)$. Proposition 5 summarizes the responses of the key macroeconomic variables to these specific shocks.[26]

Proposition 5. *In equilibrium:*

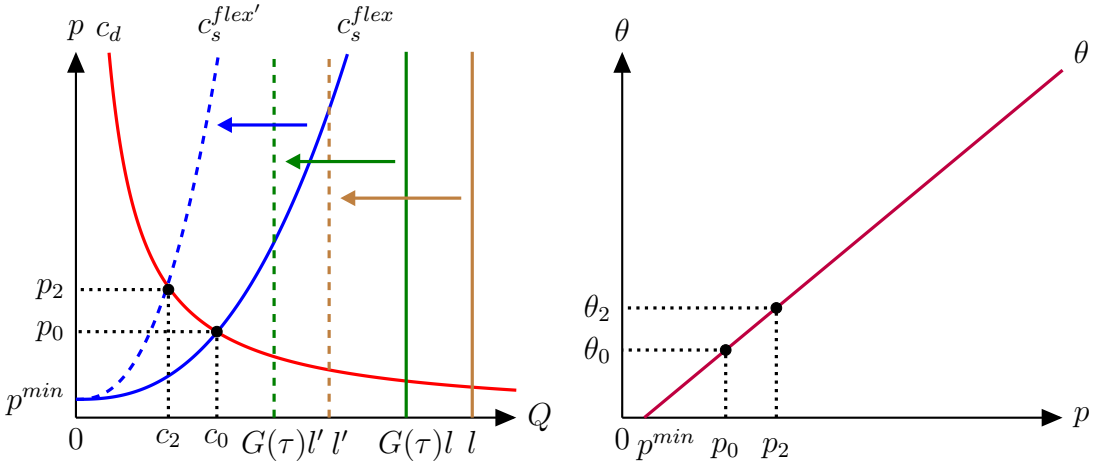
- ***An adverse shock to aggregate demand*** *increases matching cost and spare capacity (or equivalently, unemployment), while it decreases consumption (or equivalently, output), price, product market tightness, and wholesale price.*
- ***An adverse shock to productive capacity*** *increases price, product market tightness, and wholesale price, while it decreases consumption (or equivalently, output), matching cost, and spare capacity (or equivalently, unemployment).*
- ***An adverse shock to supply chain*** *increases price and spare capacity (or equivalently, unemployment), while it decreases consumption (or equivalently, output). The responses of product market tightness, wholesale price, and matching cost are undetermined.*

Proof. See Appendix D.4. ■

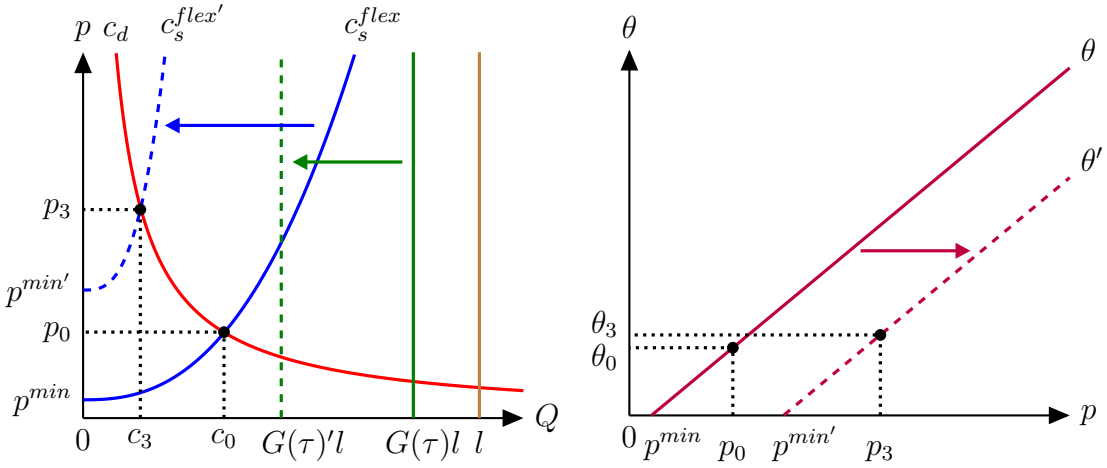
Figure 8 plots the comparative statics (left panels) alongside the corresponding equilibrium conditions between product market tightness and price (right panels) from Equation (22), which describes the optimal response of product market tightness to a change in price. Table 1 summarizes the signs of the responses of the endogenous variables to the three different shocks respectively.



(a) An Adverse Shock to Aggregate Demand, i.e., $\mu \downarrow$ or $\chi \downarrow$



(b) An Adverse Shock to Productive Capacity, i.e., $l \downarrow$



(c) An Adverse Shock to Supply Chain, i.e., $\gamma \uparrow$

Figure 8: Graphical Representation of Comparative Statics

Table 1: Comparative Statics for Adverse Shocks to Aggregate Demand, Productive Capacity, and the Supply Chain

Adverse Shock To:	**Effects On:**					
	Consumption (or Output) c	Price p	Product Market Tightness θ	Wholesale Price r	Matching Cost $G(\tau)l - c$	Spare Capacity (or Unemployment) $l - c$
Aggregate Demand	$-$	$-$	$-$	$-$	$+$	$+$
Productive Capacity	$-$	$+$	$+$	$+$	$-$	$-$
Supply Chain	$-$	$+$	Undetermined	Undetermined	Undetermined	$+$

Notes. The table summarizes the comparative statics in Proposition 5. An adverse shock to aggregate demand is either a decrease in the money supply, μ, or a decline in the preference for consuming goods, χ. An adverse shock to productive capacity is a decrease in the labor supply, l. An adverse shock to the supply chain is an increase in the scale parameter of the log-normal distribution of transportation costs, γ.

Panel (a) in Figure 8 shows the response of the system to a decline in aggregate demand. The aggregate demand curve shifts inwards from c_d to c'_d, driven by the preference for lower consumption by households, either because they hold less money or prefer to decrease consumption. In equilibrium, the price decreases to clear the market. As the price decreases and the profits from sales to the households fall, retailers visit fewer producers to participate in trade, hence lowering product market tightness. The declines in price and product market tightness then contribute to a lower wholesale price, since not only the sale of goods is less profitable, but also the probability of establishing a match with producers increases, given the decreased tightness in the product market. Consequently, producers sell a lower fraction of their productive capacity to retailers, resulting in a decrease in consumption (or equivalently, output). This leads to an increase in matching cost and spare capacity (or equivalently, unemployment) in reaction to a decline in aggregate demand.

Panel (b) in Figure 8 shows the response of the system to a negative supply shock that decreases productive capacity from l to l'. The negative capacity shock causes the aggregate supply curve to rotate inwards while leaving p^{min} unchanged (since the distribution of transportation costs remains the same, and thus the minimum price for profitable transactions). The price increases to clear the market, and consumption (or equivalently, output) decreases as the economy moves upwards along the aggregate demand curve to reach the new equilib-

[26] Unlike Michaillat & Saez (2015), where there exists a matching cost that differentiates consumption from output, consumption and output are equivalent in our model.

rium. The increase in price attracts more retailers to enter the market, which raises product market tightness. The simultaneous rise in price and product market tightness leads to a higher wholesale price. Along with the contraction in productive capacity, matching costs and spare capacity (or equivalently, unemployment) also fall.

Panel (c) in Figure 8 shows the response of the system to an increase in transportation costs corresponding to a negative supply chain shock, encapsulated by an increase in the scale parameter γ of the log-normal distribution of transportation costs. Such an increase in the scale parameter generates a higher mean transportation cost, increasing the probability for producers to draw a transportation cost above the fixed reservation threshold. As a result, the number of unprofitable trades increases, curtailing the supply of goods available to households, and the price of goods increases to clear the market. Thus, the price rises while consumption (or equivalently, output) falls. Graphically, this process is represented by an inward shift of the aggregate supply curve from c_s^{flex} to $c_s^{flex'}$, together with an increase in p^{min} (unlike with the negative capacity shock, the higher transportation costs increase the minimum price necessary for producers to trade profitably). Since the productive capacity (or equivalently, labor supply) remains unchanged while the number of successful trades falls, spare capacity (or equivalently, unemployment) increases.

The disturbance to the supply chain can either tighten or loosen product market tightness, depending on the extent to which the price rise compares to the fall in expected profits due to higher transportation costs. To consider these countervailing forces more explicitly, we revisit the equilibrium condition for product market tightness in Equation (22):

$$\theta(\gamma) = \frac{1-\eta}{\eta\rho}\Big[\underbrace{p(\gamma)-\tau}_{\text{Profit Margin }\uparrow} + \underbrace{\beta\int_0^{\tau}\Phi\Big(\frac{\log z'-\gamma}{\sigma}\Big)dz'}_{\text{Expected Total Surplus }\downarrow}\Big].$$

This equation illustrates that the sensitivity of price to transportation costs determines the "profit margin", which incentivizes retailers to search for producers, thereby increasing tightness in the product market. Conversely, higher transportation costs decrease the "expected total surplus" from trading, which can deter retailers from searching for producers. The net change in product market tightness resulting from a supply chain disruption is determined by the interplay of these two opposing forces on retailers' behavior.

Important to our analysis in Section 5 on the effectiveness of monetary policy in controlling inflation and output, changes in product market tightness also have significant implications for the sensitivity of goods supply to price variations following an adverse shock to the supply chain. Suppose the price increase is sufficiently large that, at the new equilibrium, the rise in visits made by unmatched retailers significantly outpaces the increase in the number of unmatched producers (i.e., the goods market is congested on the retailers' side). While this imbalance leads to a tighter product market and increases the likelihood of a producer participating in trade, an additional retailer has only a limited impact on the producer's probability of forming a match. To see even a slight further increase in such a probability, prices would need to rise considerably more, due to the diminishing returns to searching inherent in the constant-return-to-scale matching function (see Equation (1)). Consequently, the number of matches, and therefore, the supply of goods becomes less sensitive to price changes resulting from supply chain disruptions when the goods market is tight. Graphically, this change in the sensitivity of output to price fluctuations is represented by a steeper slope of the aggregate supply curve at the new equilibrium, as depicted in Panel (c) of Figure 8.[27]

Lastly, Appendix D.4 demonstrates that the changes in the wholesale price and matching cost depend on the responses of product market tightness and price to the supply chain shock.

4. The Causal Effects of Supply Chain Disruptions

In this section, we study the causal effects of supply chain disruptions by developing an SVAR model that utilizes our ACR index and constrains the responses of the macro aggregates to three distinct shocks, in line with our theoretical results. Our empirical model is based on Rubio-Ramirez et al. (2010), Arias et al. (2018):

$$\boldsymbol{y}_t'\boldsymbol{A}_0 = \sum_{l=1}^{L} \boldsymbol{y}_{t-l}'\boldsymbol{A}_l + \boldsymbol{\omega}_t'\boldsymbol{C} + \boldsymbol{\epsilon}_t', \quad 1 \leq t \leq T, \tag{23}$$

[27] In Appendix D.5, we demonstrate that the slope of the aggregate supply curve is inversely related to product market tightness. Specifically, the aggregate supply curve becomes steeper in the (Q, p) plane as product market tightness increases. Additionally, in Figure D.1, we illustrate the alternative scenario where the price increase is insufficient to raise the product market tightness at the new equilibrium.

where $\boldsymbol{y}_t$ is an $n \times 1$ vector of endogenous variables, $\boldsymbol{\omega}_t = [1, t]'$ is a 2×1 vector of a constant and a linear trend, $\boldsymbol{\epsilon}_t$ is an $n \times 1$ vector of structural shocks, $\boldsymbol{A}_l$ is an $n \times n$ matrix of structural parameters for $0 \leq l \leq L$ with $\boldsymbol{A}_0$ invertible, $\boldsymbol{C}$ is a $2 \times n$ matrix of parameters, L is the lag length, and T is the sample size. The vector $\boldsymbol{\epsilon}_t$, conditional on past information and the initial conditions $\boldsymbol{y}_0, \ldots, \boldsymbol{y}_{1-L}$ is Gaussian with mean zero and covariance matrix $\mathbf{1}_{n \times n}$, i.e., the $n \times n$ identity matrix. The SVAR described in Equation (23) can be written compactly as:

$$\boldsymbol{y}_t' \boldsymbol{A}_0 = \boldsymbol{x}_t' \boldsymbol{A}_+ + \boldsymbol{\epsilon}_t', \quad 1 \leq t \leq T, \tag{24}$$

where $\boldsymbol{A}_+' = [\boldsymbol{A}_1' \ \ldots \ \boldsymbol{A}_L' \ \boldsymbol{C}']$ and $\boldsymbol{x}_t' = [\boldsymbol{y}_{t-1}' \ \ldots \ \boldsymbol{y}_{t-L}' \ \boldsymbol{\omega}_t']$ for $1 \leq t \leq T$. The dimension of $\boldsymbol{A}_+$ is $m \times n$, where $m = nL + 2$. The reduced-form representation implied by Equation (24) is given by:

$$\boldsymbol{y}_t' = \boldsymbol{x}_t' \boldsymbol{B} + \boldsymbol{u}_t', \quad 1 \leq t \leq T,$$

where $\boldsymbol{B} = \boldsymbol{A}_+ \boldsymbol{A}_0^{-1}, \boldsymbol{u}_t' = \boldsymbol{\epsilon}_t' \boldsymbol{A}_0^{-1}$, and $\mathbb{E}(\boldsymbol{u}_t \boldsymbol{u}_t') = \boldsymbol{\Sigma} = (\boldsymbol{A}_0 \boldsymbol{A}_0')^{-1}$. The matrices $\boldsymbol{B}$ and $\boldsymbol{\Sigma}$ are the reduced-form parameters, while $\boldsymbol{A}_0$ and $\boldsymbol{A}_+$ are the structural parameters.

We estimate the model using the monthly U.S. series for real GDP, Personal Consumption Expenditures (PCE) goods price, unemployment, retail market tightness, import price as well as our ACR index over the period from January 2017 to July 2022, with all series being seasonally adjusted. Note that the import price is used as a proxy for the wholesale price in order to capture the international sourcing strategies of U.S. retailers, particularly during the pandemic period. All variables are retrieved directly or constructed using available data from the Federal Reserve Economic Data (FRED), maintained by the Federal Reserve Bank of St. Louis.[28] The real GDP, PCE goods price, retail market tightness, and import price

[28] The mnemonics of the variables that we use in the SVAR estimation are: `GDPC1` (real GDP), `INDPRO` (industrial production), `DGDSRG3M086SBEA` (PCE goods price), `UNRATE` (unemployment), `RETAILIMSA` (retailers' inventories), `RETAILIRSA` (retailers' inventories to sales ratio), `MNFCTRIMSA` (manufacturers' inventories), and `IREXFDFLS` (import price). The monthly time series for real GDP is constructed using interpolation of the corresponding quarterly series, as in Bernanke & Mihov (1998) and Arias et al. (2019). Specifically, we apply the Chow-Lin method for temporal disaggregation (Chow & Lin 1971) to interpolate the real GDP based on the industrial production index. The monthly time series for retail market tightness is constructed by dividing the new orders made by retailers by the inventories held by manufacturers, where the retailers' new orders ($Order_t$) are approximated using the following relationship:

$$Order_t = (Inventory_t - Inventory_{t-1}) + Sale_t,$$

where $Inventory_t$ and $Sale_t$ represent the U.S. retailers' inventories and sales in month t. The monthly

enter the SVAR in log percent, while the unemployment and ACR enter in percent. We set the number of lags to two in the baseline specification, but the results are robust to considering longer lags.[29,30]

Our identification scheme applies the sign restrictions from our theoretical model, which are summarized in Table 1, as well as the zero restrictions on the responses of the ACR index to adverse shocks to aggregate demand and productive capacity. We impose the zero restrictions to sharpen our identification of the supply chain shock, and the results are robust to removing them in the estimation (see Appendix E.1). We estimate the SVAR using a Bayesian approach as in Arias et al. (2018, 2019, 2023) with restrictions on the first period of response (i.e., $k = 1$), thus imposing a minimal structure as in Mumtaz & Zanetti (2012, 2015).[31] More concretely, we impose the following restrictions:

Restriction 1. ***An adverse shock to aggregate demand*** *leads to a negative response of real GDP, PCE goods price, retail market tightness, and import price, as well as to a positive response of unemployment at $k = 1$. ACR does not respond at $k = 1$.*

Restriction 2. ***An adverse shock to productive capacity*** *leads to a negative response of real GDP and unemployment, as well as to a positive response of PCE goods price, retail market tightness, and import price at $k = 1$. ACR does not respond at $k = 1$.*

Restriction 3. ***An adverse shock to supply chain*** *leads to a negative response of real GDP, as well as to a positive response of PCE goods price, unemployment, and ACR at $k = 1$.*

series for the PCE goods price and unemployment are raw series directly taken from FRED, while the series for import price is seasonally adjusted using the X-13ARIMA-SEATS algorithm.

[29] Appendix E.2 demonstrates the robustness of our baseline results when considering different lag structures (i.e., one, three, or four lags).

[30] We also check the robustness of our baseline results by replacing real GDP with real PCE of goods, unemployment with spare capacity, and manufacturers' inventories with merchant wholesalers' inventories (in the construction of the retail market tightness), respectively. The monthly time series for spare capacity is constructed by subtracting the capacity utilization rate from one. As shown in Appendix E.3, the baseline results remain consistent.

[31] We impose a normal-generalized-normal (NGN) prior distribution over the structural parameters $\boldsymbol{A}_0$ and $\boldsymbol{A}_+$. The NGN prior is a conjugate prior characterized by four parameters $(\nu, \boldsymbol{\Phi}, \boldsymbol{\Psi}, \boldsymbol{\Omega})$. The parameters ν and $\boldsymbol{\Phi}$ govern the marginal prior distribution of $vec(\boldsymbol{A}_0)$, while the remaining parameters $\boldsymbol{\Psi}$ and $\boldsymbol{\Omega}$ govern the prior distribution of $vec(\boldsymbol{A}_+)$, conditional on $\boldsymbol{A}_0$. Our choice of the prior density parameterization is $\nu = 0, \boldsymbol{\Phi} = \boldsymbol{0}_{n\times n}, \boldsymbol{\Psi} = \boldsymbol{0}_{m\times n}$, and $\boldsymbol{\Omega}^{-1} = \boldsymbol{0}_{m\times m}$. This parameterization generates prior densities that are equivalent to those in Uhlig (2005). Our results are robust to using the prior robust approach in Giacomini & Kitagawa (2021), as illustrated in Appendix E.4.

Note that we leave the responses of retail market tightness and import price unrestricted when estimating the causal effects of a supply chain disruption shock, consistent with our theoretical model.

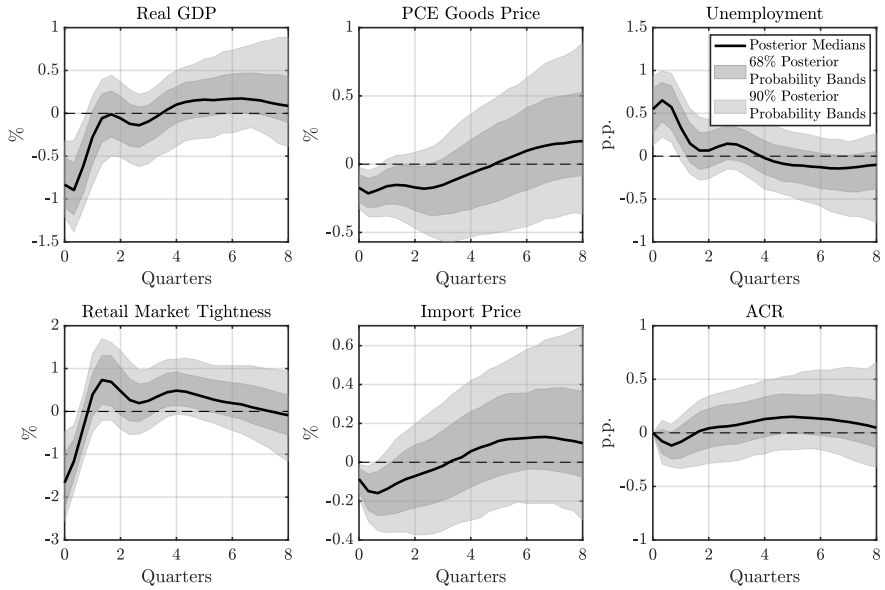


Figure 9: IRFs to an Adverse Shock to Aggregate Demand

Notes. The IRFs to a one standard deviation adverse shock to aggregate demand are identified using the ACR index and Restrictions 1, 2, and 3. The solid line shows the point-wise posterior medians, and the shaded bands represent the 68% and 90% equal-tailed point-wise posterior probability bands. The figure is based on 100,000 independent draws.

Figures 9, 10, and 11 show our baseline results for the responses of the endogenous variables to an adverse shock to aggregate demand, productive capacity, and the supply chain, respectively. The solid lines show the point-wise posterior median impulse response functions (IRFs) of the endogenous variables to each structural shock, and the gray-shaded areas represent the corresponding 68% and 90% posterior probability bands.[32] We begin by discussing the IRFs to an adverse shock to aggregate demand in Figure 9. On impact, real GDP declines significantly by approximately 0.8%, and unemployment rises sharply by more than 0.5%. Such responses persist with a high posterior probability for the first six months following the shock. Consistent with the movements of real GDP and unemployment, retail market tightness also decreases substantially by more than 1.5% on impact, then rebounds

[32]These results are based on 100,000 independent draws from the posterior distribution of the structural parameters, with the structural shocks normalized to one standard deviation.

to 0.5%, and gradually reverts to zero thereafter. In contrast, the response of the PCE goods price is muted, with an initial drop of about 0.2% before gradually reverting to zero after approximately five quarters. The import price exhibits a similar pattern, albeit returning to a statistically insignificant response quicker, at the three-quarter mark. Lastly, the ACR index's response is less precisely estimated, with a large posterior probability mass centered around zero.

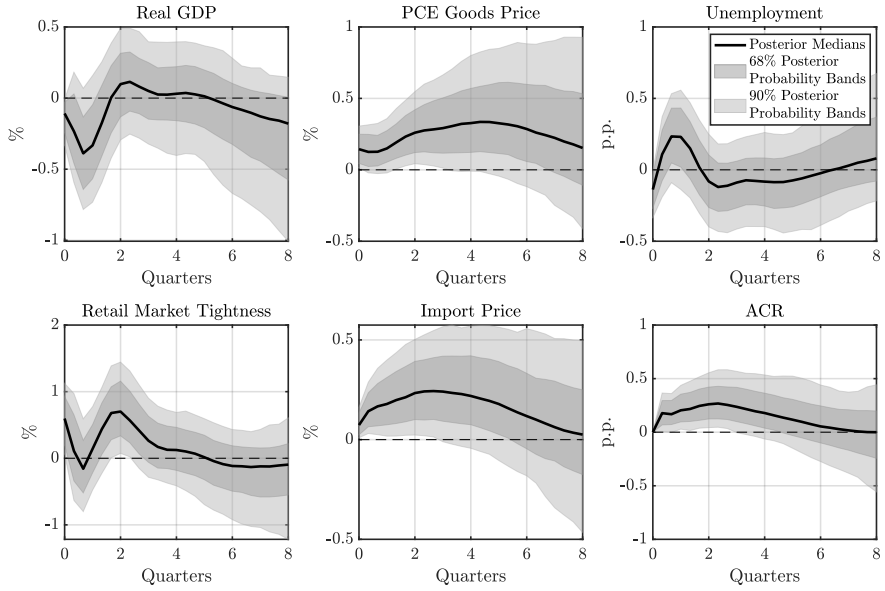


Figure 10: IRFs to an Adverse Shock to Productive Capacity

Notes. The IRFs to a one standard deviation adverse shock to productive capacity are identified using the ACR index and Restrictions 1, 2, and 3. The solid line shows the point-wise posterior medians, and the shaded bands represent the 68% and 90% equal-tailed point-wise posterior probability bands. The figure is based on 100,000 independent draws.

Figure 10 shows the IRFs to an adverse shock to productive capacity. On impact, the responses of real GDP and unemployment are negative, whereas the response of retail market tightness is positive, in accordance with Restriction 2. Subsequently, real GDP continues to decline, approaching a zero response close to the boundary of the 90% confidence interval near the trough, which occurs approximately one quarter after the shock. Largely due to the fall in real GDP, the initial decrease in unemployment quickly reverses, turning significantly positive within one quarter of the shock, peaking at around 0.25% before returning to zero. The post-impact response of retail market tightness reverts back to zero before increasing again. The PCE goods price rises and remains high for about two years, reflecting the lagged

effects of supply-side disruptions. The import price exhibits a similar pattern, although it reaches its peak at an earlier point. Lastly, the median response of the ACR index is zero on impact but remains consistently above zero for over a year thereafter.

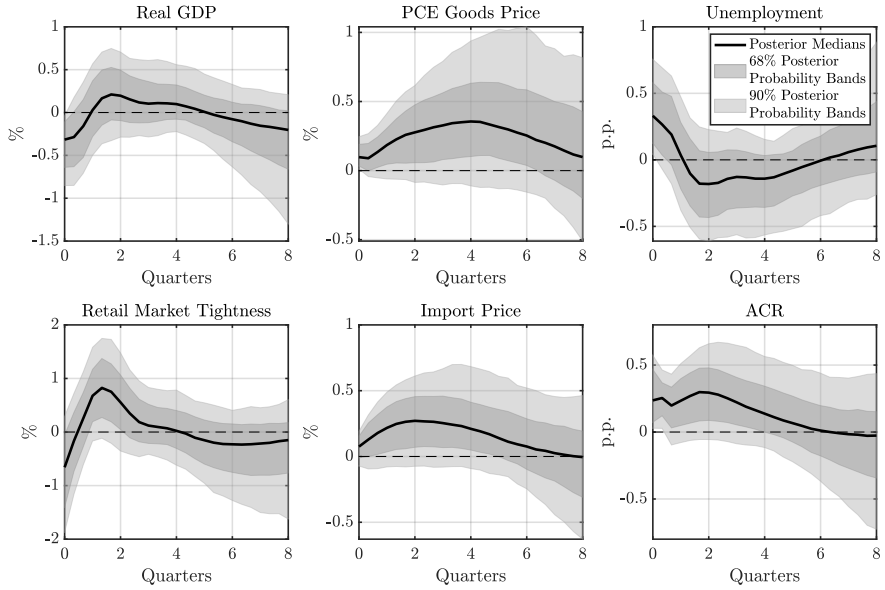


Figure 11: IRFs to an Adverse Shock to Supply Chain

Notes. The IRFs to a one standard deviation adverse shock to the supply chain are identified using the ACR index and Restrictions 1, 2, and 3. The solid line shows the point-wise posterior medians, and the shaded bands represent the 68% and 90% equal-tailed point-wise posterior probability bands. The figure is based on 100,000 independent draws.

Figure 11 shows the IRFs following a negative shock to the supply chain. The median response of real GDP is negative on impact and stays below zero for over a quarter after the shock. While real GDP decreases, unemployment increases by roughly the same magnitude and remains elevated for one quarter. In terms of the response of retail market tightness, which is unrestricted, it initially decreases before sharply increasing to peak at 0.5% after one quarter.[33] The surges in both the PCE goods price and the import price are consistent with the magnitudes observed following the negative capacity shock, highlighting the substantial impact of supply chain disruptions on price inflation. Despite the uncertainty around our estimates, as indicated by the wide posterior probability bands, the positive responses of

[33] In line with our theoretical prediction in Section 3.4, the initial decrease in tightness can be largely attributed to the rise in spare capacity following the supply chain disruption when prices have not adjusted. Subsequently, as prices continue to rise, more retailers are drawn into the product market, resulting in the elevated tightness.

both the PCE goods price and import price are still statistically significant at the 68% level of confidence. Lastly, the ACR index remains elevated for six quarters after the shock.

Figure 12 shows the proportions of forecast error variance explained by each of the three structural shocks. The aggregate demand shock accounts for the largest share of unexpected fluctuations in real GDP, unemployment, and retail market tightness across all horizons. Conversely, although the demand shock explains the majority of variations in PCE goods and import prices at shorter horizons, supply chain disturbances become the dominant factor accounting for the largest portion of unexpected fluctuations in both price indicators over longer horizons, suggesting that disruptions to the supply chain have enduring effects on price increases. Capacity shocks also contribute significantly to the price movements but are less influential than supply chain shocks. Moreover, supply chain shocks are more potent in explaining the unexpected variations in unemployment and retail market tightness than capacity shocks.

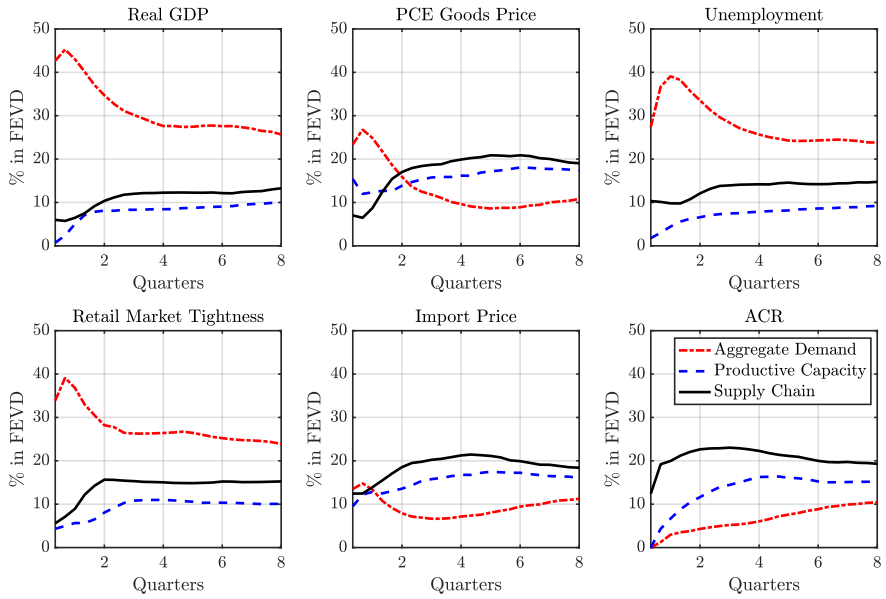


Figure 12: Forecast Error Variance Decomposition (FEVD) from the SVAR

Notes. Each line presents the median fraction of the forecast error variance for each endogenous variable, explained by each of the three identified structural shocks at various time horizons. The FEVD is estimated using the ACR index and Restrictions 1, 2, and 3, and based on 100,000 independent draws.

Finally, Figure 13 shows the cumulative historical contribution of each of the three struc-

tural shocks to U.S. goods inflation for the sample period from January 2017 to July 2022.[34] Our ACR index attributes the initial drop in inflation at the onset of the Covid-19 pandemic in early 2020 to a substantial decrease in aggregate demand, with the subsequent rise in inflation from April 2020 onwards due to adverse shocks to productive capacity and the supply chain, which remain influential throughout the sample period. Interestingly, our estimation indicates that supply chain disturbances consistently exerted a negative contribution to inflation prior to the start of the Covid-19 pandemic.[35,36]

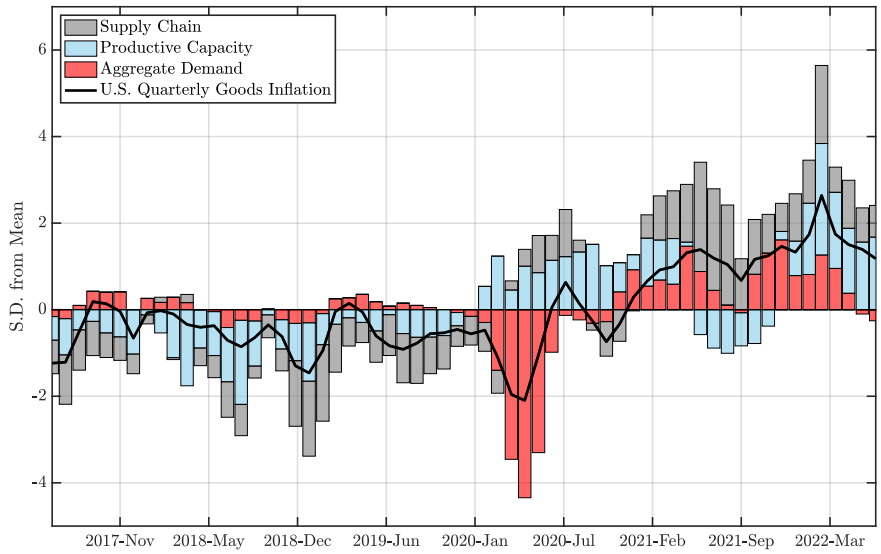


Figure 13: Historical Decomposition (HD) of U.S. Goods Inflation

Notes. The solid line represents the standardized quarterly goods inflation rate in the U.S., i.e., quarter-on-quarter growth of the PCE goods price index. The shaded bar represents the standardized cumulative historical contribution of each of the three structural shocks identified using the ACR index and Restrictions 1, 2, and 3 to U.S. goods inflation. The estimation results are based on all endogenous variables being measured as a percent change from the previous period, with the exceptions of unemployment and the ACR index, which are measured as a change from the previous period. The figure is derived from 100,000 independent draws.

[34] To facilitate the comparison of series across different scales, we have applied Z-score standardization, which rescales data to have a mean of zero and a standard deviation of one.

[35] The persistent negative contribution of supply chain shocks to U.S. inflation prior to the pandemic supports the notion of strategic enhancements to supply chain operations to alleviate inflationary pressures. For instance, several U.S. ports underwent considerable infrastructure upgrades between 2017 and 2019, aiming to increase their capacity, efficiency, and resilience against potential systemic disruptions.

[36] In Appendix F, we present the estimation results using alternative indices of supply chain disruptions found in the literature, including the HARPEX, the New York Fed's GSCPI, and the SDI by Smirnyagin & Tsyvinski (2022), among others. These results show significant variations among the indices in terms of the estimated impacts of aggregate demand, productive capacity, and supply chain shocks on U.S. goods inflation.

5. The Effectiveness of Monetary Policy

In this section, we study the interplay between supply chain disruptions and the effectiveness of monetary policy in simultaneously controlling inflation and output. We show through our theoretical model that a disruption to the supply chain increases the sensitivity of inflation and reduces the sensitivity of output to a contractionary monetary policy shock, generating state-dependence in the tradeoff for monetary policy. Subsequently, we test and empirically corroborate our theoretical predictions using a Threshold Vector Autoregression (TVAR) model.

5.1. Theoretical Prediction

We derive the theoretical prediction for the state-dependence of monetary policy using our theoretical model described in Section 3. The money supply parameter μ encapsulates the action of monetary policy, and the transportation cost parameter γ captures the disruption to the supply chain. We study the comparative statics of the impact of a tightening in monetary policy, focusing on whether the effects of the policy intervention on inflation and output are different amid the supply chain disruption.[37] Proposition 6 summarizes the results.

Proposition 6. *For any given threshold of reservation transportation cost $\tau > 0$ and parameter values relevant for monetary policy $\mu \in \mathbb{R}^+$ and transportation costs $\gamma \in \mathbb{R}$, when the product market tightness is sufficiently elevated to allow producers to recoup the increase in transportation costs due to the supply chain disruption, as represented by the following constraint:*

$$\frac{\partial\theta(\mu,\gamma)}{\partial\gamma} > \frac{\theta(1+\theta^{\xi})}{\big(1-G(\tau)\big)G(\tau)}\frac{1}{\sigma\sqrt{2\pi}}\exp\Big[-\frac{(\log\tau-\gamma)^2}{2\sigma^2}\Big], \tag{25}$$

where $G(\tau) \equiv \Phi[(\log\tau-\gamma)/\sigma]$, $\Phi(.)$ is the standard normal cumulative density function, the responses of the endogenous variables to a change in monetary policy are described by the

[37] In Appendix D.7, we derive the theoretical prediction for the effectiveness of monetary policy, depending on whether the productive capacity of the economy is constrained or not. Similar to the scenario in which the supply chain is disrupted, contractionary monetary policy is more effective at taming inflation and reducing the sensitivity of output when the productive capacity is constrained. The only difference is that the state-dependent effects of monetary policy are unconditional.

partial derivatives:

$$\frac{\partial c(\mu,\gamma)}{\partial \mu} > 0,\ \frac{\partial p(\mu,\gamma)}{\partial \mu} > 0,\ \frac{\partial \theta(\mu,\gamma)}{\partial \mu} > 0,\ \frac{\partial r(\mu,\gamma)}{\partial \mu} > 0,$$
$$\frac{\partial}{\partial \mu}\big[G(\tau)l - c(\mu,\gamma)\big] < 0,\ \frac{\partial}{\partial \mu}\big[l - c(\mu,\gamma)\big] < 0.$$

The cross derivatives of the endogenous variables that describe the optimal interplay between a change in monetary policy and the supply chain disruption are given by:

$$\frac{\partial^2 c(\mu,\gamma)}{\partial \mu \partial \gamma} < 0,\ \frac{\partial^2 p(\mu,\gamma)}{\partial \mu \partial \gamma} > 0,\ \frac{\partial^2 \theta(\mu,\gamma)}{\partial \mu \partial \gamma} > 0,\ \frac{\partial^2 r(\mu,\gamma)}{\partial \mu \partial \gamma} > 0,$$
$$\frac{\partial^2}{\partial \mu \partial \gamma}\big[G(\tau)l - c(\mu,\gamma)\big] > 0,\ \frac{\partial^2}{\partial \mu \partial \gamma}\big[l - c(\mu,\gamma)\big] > 0,$$

where $c, p, \theta, r, G(\tau)l - c$, and $l - c$ represent consumption (or equivalently, output), price, product market tightness, wholesale price, matching cost, and spare capacity (or equivalently, unemployment), respectively.

Proof. See Appendix D.6. ■

In words, the partial and cross derivatives in Proposition 6 imply that at an equilibrium where the increase in product market tightness is sufficiently large during the supply chain disruption and therefore producers have greater incentives to trade with the retailers (Equation (25)), a contractionary monetary policy shock increases the rise in inflation and dampens the fall in consumption (or equivalently, output), as evinced by the signs of the second derivatives.[38]

Figure 14 gives the graphical representation of our theoretical prediction. In response to a contractionary monetary policy shock, households reduce consumption due to decreased money holdings. This reduction causes the aggregate demand curve to shift inward, leading to lower prices and reduced consumption of goods. As a result, product market tightness decreases since retailers visit fewer producers to purchase goods. This reduction in demand and product market tightness leads to a lower wholesale price. Producers, facing diminished demand, sell a smaller fraction of their productive capacity to retailers, which leads to

[38] Proposition 6 also shows that the responses of product market tightness and wholesale price are greater while the responses of matching cost and spare capacity (or equivalently, unemployment) are weaker during the supply chain disruption.

a decrease in output. Consequently, matching costs and spare capacity (or equivalently, unemployment) increase.

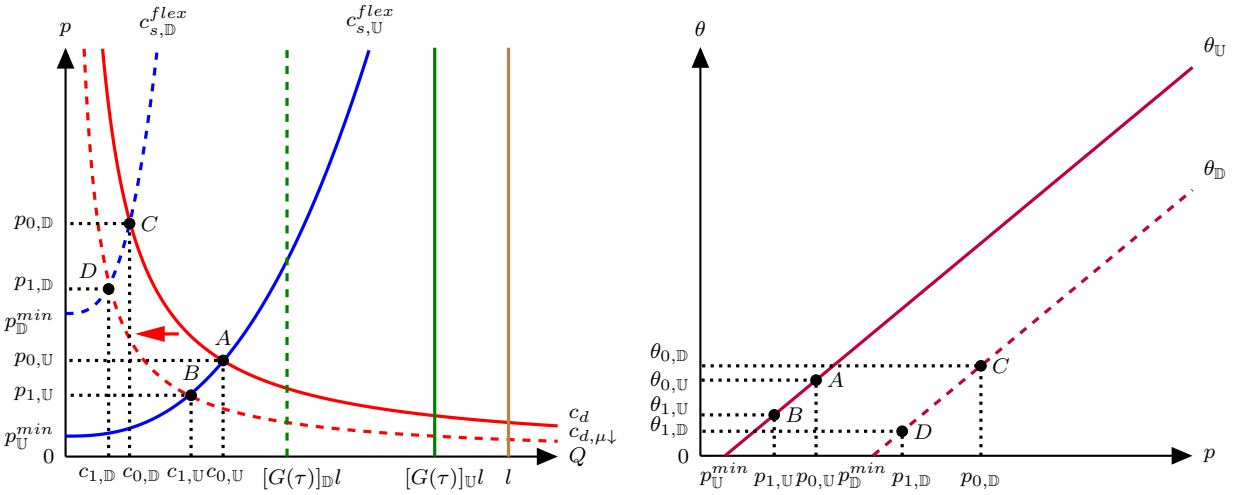


Figure 14: State-Dependent Effects of a Contractionary Monetary Policy Shock: Theoretical Prediction

Notes. The panels illustrate the adjustment of the economy to a contractionary monetary policy shock and to what extent the adjustment depends on disruptions to the supply chain. The two respective states – i.e., supply chain disrupted ($\mathbb{D}$) versus undisrupted ($\mathbb{U}$) – are plotted against each other. $c^{flex}s, \mathbb{D}$ and $c^{flex}s, \mathbb{U}$ represent the aggregate supply curves in the two states, while $\theta_{\mathbb{D}}$ and $\theta_{\mathbb{U}}$ represent the schedules of product market tightness in the two states. c_d and $c_{d,\mu\downarrow}$ denote the aggregate demand curves before and after the contractionary monetary policy shock, respectively. The labels on the axes corresponding to each state are differentiated by their subscripts, and the capital letters ($A \to B, C \to D$) indicate the movements of the equilibrium in the two states.

Recall from our discussion in Section 3.4 that the aggregate supply curve becomes steeper when the increase in product market tightness during the supply chain disruption is sufficiently large (Equation (25)). This steepening occurs because the probability of producers engaging in trade becomes less sensitive to price changes when the market is already tight, since the number of matches is constrained by the shorter side, i.e., the number of unmatched producers. As a result, the supply of goods becomes less responsive to price changes during the supply chain disruption. Consequently, a contractionary monetary policy shock significantly reduces inflation with only a relatively modest decrease in output.

5.2. Empirical Validation

We test our theoretical prediction for the state-dependence of monetary policy by developing a structural TVAR model – building on Chen & Lee (1995) – that allows for endogenous variations in the estimated parameters based on the estimated threshold of our ACR index. The reduced-form model is the following:

$$\boldsymbol{y}_t = I_t\Big[\sum_{l=1}^{L}\boldsymbol{B}'_{\mathbb{D},l}\boldsymbol{y}_{t-l} + \boldsymbol{C}'_{\mathbb{D}}\boldsymbol{\omega}_t + \boldsymbol{\Sigma}_{\mathbb{D}}^{1/2}\boldsymbol{\epsilon}_t\Big] + (1-I_t)\Big[\sum_{l=1}^{L}\boldsymbol{B}'_{\mathbb{U},l}\boldsymbol{y}_{t-l} + \boldsymbol{C}'_{\mathbb{U}}\boldsymbol{\omega}_t + \boldsymbol{\Sigma}_{\mathbb{U}}^{1/2}\boldsymbol{\epsilon}_t\Big], \quad (26)$$

where $1 \leq t \leq T$, $\boldsymbol{y}_t$ is an $n \times 1$ vector of endogenous variables, $\boldsymbol{\omega}_t = [1, t]'$ is a 2×1 vector of a constant and a linear trend, $\boldsymbol{\epsilon}_t$ is an $n \times 1$ vector of structural shocks, $\boldsymbol{B}_{\mathbb{D},l}$ and $\boldsymbol{B}_{\mathbb{U},l}$ are two $n \times n$ matrices of coefficients for the lagged endogenous variables $\boldsymbol{y}_{t-l}$, $\boldsymbol{C}_{\mathbb{D}}$ and $\boldsymbol{C}_{\mathbb{U}}$ are two $2 \times n$ matrices of coefficients for the constant and linear trend, $\boldsymbol{\Sigma}_{\mathbb{D}}$ and $\boldsymbol{\Sigma}_{\mathbb{U}}$ are the covariance matrices, L is the lag length, and T is the sample size.[39] The vector $\boldsymbol{\epsilon}_t$, conditional on past information and the initial conditions $\boldsymbol{y}_0, \ldots, \boldsymbol{y}_{1-L}$, is Gaussian with mean zero and covariance matrix $\mathbf{1}_{n\times n}$, i.e., an $n \times n$ identity matrix. Switches between the two regimes – i.e., supply chain disrupted ($\mathbb{D}$) vs. undisrupted ($\mathbb{U}$) – are governed by the indicator variable $I_t \in \{0, 1\}$, which is equal to one if the ACR in period $t-1$, ACR_{t-1}, is above the threshold $\overline{ACR}$, and equal to zero otherwise:

$$I_t = \begin{cases} 1, & \text{if } ACR_{t-1} > \overline{ACR}; \\ 0, & \text{if } ACR_{t-1} \leq \overline{ACR}. \end{cases} \quad (27)$$

Under the Normal-Inverse-Wishart conjugate prior for the TVAR parameters and conditional on the value of the threshold $\overline{ACR}$, the posterior distribution of the TVAR parameter vector is a conditional Normal-Inverse-Wishart distribution, and we use the Gibbs sampler to draw from the distribution. Since the posterior distribution of the threshold $\overline{ACR}$ conditional on the TVAR parameters is unknown, we use a Metropolis-Hastings algorithm to obtain its posterior distribution, similar to Chen & Lee (1995), Lopes & Salazar (2006), Pizzinelli et al. (2020). Appendix I.1 provides the details on the Normal-Inverse-Wishart prior.

[39] Note that we allow the covariance matrix to be regime-specific.

To retain comparability with our previous empirical results, we include the same variables used in our SVAR model in Section 4, with the addition of the Federal Funds Rate to reflect changes in the stance of U.S. monetary policy. For consistency, we also retain the same sample period from January 2017 to July 2022.[40]

To identify the contractionary monetary policy shock, we impose the following standard restriction on IRFs:

Restriction 4. ***A contractionary monetary policy shock*** *leads to a negative response of real GDP, PCE goods price, retail market tightness, and import price, as well as to a positive response of unemployment and the Federal Funds Rate at* $k = 1$*. ACR does not respond at* $k = 1$*.*[41]

We compute the identified set of IRFs using the Bayesian approach similar to Pizzinelli et al. (2020), Bratsiotis & Theodoridis (2022).[42] We use one lag in the baseline estimation, and select the one-month lag of the ACR index as the variable determining the state I_t.[43]

Figure 15 plots the IRFs to a contractionary monetary policy shock for both the supply chain disrupted (black) and undisrupted (red) regimes, reporting both the point-wise posterior medians (solid lines) and the 68% equal-tailed point-wise posterior probability bands (shaded area and dotted lines) from horizon $k = 0$ up to horizon $k = 12$ (i.e., four quarters). The figure shows significant differences in the responses of the endogenous variables to the contractionary monetary policy shock between the two regimes. In accordance with our theoretical results, the PCE goods price and import price are more responsive while real GDP and unemployment are less responsive in the regime where the supply chain is disrupted, and the differences in the responses are statistically significant. The responses of the retail

[40] All the series are seasonally adjusted, except the Federal Funds Rate. Real GDP, PCE goods price, retail market tightness, and import price enter the TVAR in log percent, whereas the Federal Funds Rate, unemployment, and the ACR index enter the TVAR in percent.

[41] Restriction 4 enriches Restriction 1, which is intended for the identification of an adverse shock to aggregate demand, by including the positive response of the Federal Funds Rate on impact, which is the main instrument to control monetary policy.

[42] To implement the sign and zero restrictions on IRFs, we use the penalty function approach (PFA) developed in Uhlig (2005), Mountford & Uhlig (2009). The PFA consists of using a loss function to find an orthogonal matrix that satisfies the zero restrictions and that satisfies or comes close to satisfying the sign restrictions. Appendix I.2 provides the details on the PFA.

[43] Appendix I.3 plots the posterior distribution of the threshold $\overline{ACR}$, together with the time series of the identified regimes using the median of the posterior $\overline{ACR}$.

market tightness between the two regimes, however, cannot be disentangled from each other.

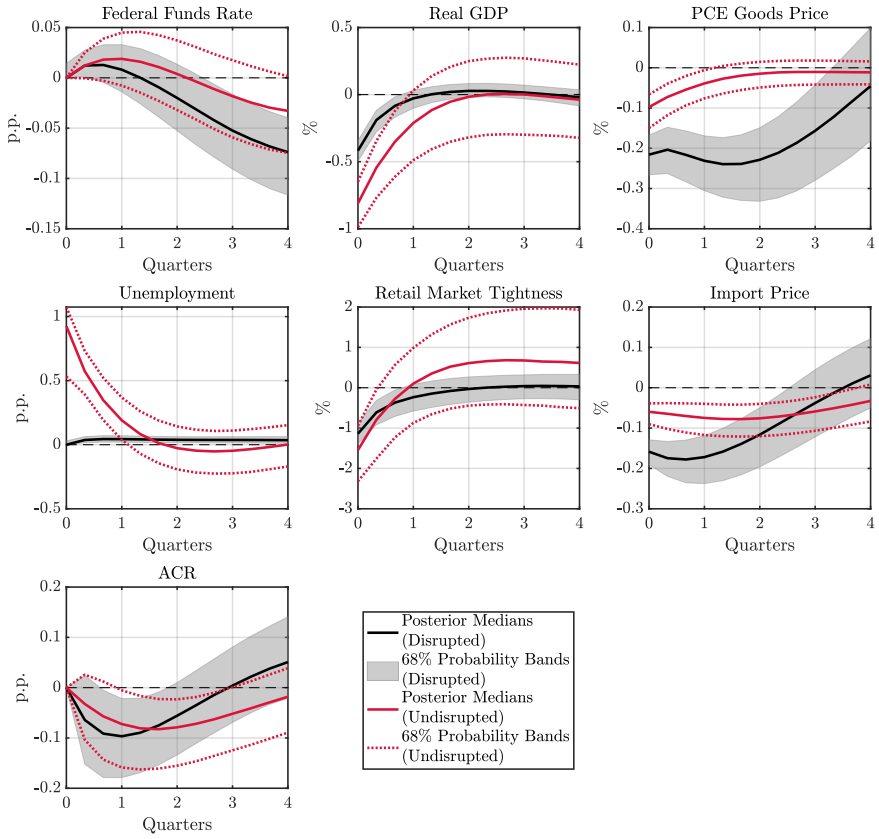


Figure 15: State-Dependent Effects of a Contractionary Monetary Policy Shock: Empirical Validation

Notes. The figure shows the IRFs to a one standard deviation contractionary monetary policy shock identified using Restriction 4 for both the supply chain disrupted and undisrupted regimes. The black solid (red solid) line shows the point-wise posterior medians, and the black shaded area (red dotted lines) depicts the 68% equal-tailed point-wise posterior probability bands for the supply chain disrupted (undisrupted) regime. The figure is based on 10,000 independent draws from the posterior.

Appendix J shows that our results hold across several variations to the benchmark model: (i) using the Wu-Xia Shadow Federal Funds Rate (Wu & Xia 2016) to reflect the stance of U.S. monetary policy; (ii) dropping the zero restriction imposed on the on-impact response of the ACR index; (iii) employing different lag structures; and (iv) adopting a looser prior (i.e., $\lambda = 0.5$ instead of 0.25; see Appendix I.1 for details on the tightness of the prior). Appendix K also shows that our results continue to hold when we use local projections with interaction terms, as in Ramey & Zubairy (2018), Ghassibe & Zanetti (2022), Arias et al. (2023), to estimate the state-dependent effects of a contractionary monetary policy shock.

6. Conclusion

Our study constructs the first index of global supply chain disruptions using data from the Automatic Identification System – the long-range identification and tracking system on containerships mandated by the International Maritime Organization (IMO) – whose records have been publicly available since 2017. We quantify supply chain disruptions from the estimation of the congestion in fifty major ports around the world by developing a novel spatial clustering algorithm. This algorithm identifies port zones and distinguishes between berth and anchorage areas within ports of different morphologies using the precise location, speed and heading of containerships. By aggregating the congestion rates across ports, we develop the first high-frequency index of Average Congestion Rate (ACR) worldwide.

We develop a new theoretical framework with separated production and retailing processes, search frictions in the exchange between producers and retailers, and transportation costs. The model simultaneously generates spare capacity for producers and a scarcity of supply for retailers, leading to sharp price increases and heightened search frictions that curtail output. Our framework demonstrates that disturbances to the supply chain reduce output and increase prices, as in standard models, *and importantly*, they increase the spare productive capacity. The co-movements of spare productive capacity, prices, and output allow us to uniquely identify the supply chain shocks and study their causal effects on macroeconomic outcomes through an SVAR model with sign and zero restrictions derived from our theory. The empirical model establishes that supply chain shocks exert an immediate, large increase in prices and a simultaneous detrimental effect on real GDP and unemployment.

We show, both theoretically and empirically, that monetary policy exerts a stronger influence on inflation, albeit with a diminished effect on output, amid supply chain disruptions. Therefore, disruptions to the supply chain enhance the effectiveness of contractionary monetary policy in taming inflation while reducing the sensitivity of output to the policy.

Our study opens several important avenues for future research. First, our new index reveals significant heterogeneity in the congestion of ports around the world. It would be interesting to study whether the spillovers between ports are primarily driven by geographical proximity or production synergies that Fernández-Villaverde et al. (2021, 2022, 2023)

find critical for the matching between producers and retailers. The presence of heterogeneity raises the possibility of reducing congestion from supply chain disturbances by strategically re-organizing the location of producers and retailers across ports in accordance with their production synergies. Second, our results show that spare capacity is central to the effect and ramifications of supply chain disturbances in the economy. Enriching the analysis by endogenizing the adjustment of spare capacity and studying its persistence is important to accelerate the speed of recovery in the aftermath of supply chain disruptions. Third, while our theoretical framework is based on single producer-retailer relationships to study the role of spare capacity and the resulting changes in prices and output, it would be worthwhile to extend the analysis to input-output networks and explore the role of spare capacity in the transmission of supply chain disruptions across firms in the network. The structure of the production network could potentially magnify or dampen the disturbances to the supply chain, which may trigger endogenous changes in the structure of the network, as documented in Ghassibe (2023). Fourth, the incorporation of predictive analytics into our spatial clustering algorithm will enable the algorithm to anticipate supply chain disruptions by identifying subtle changes and systematic patterns in the shipments using real-time position, speed, and weight of containerships. The enriched algorithm could prove a valuable tool to design preemptive policy actions to offset or minimize the disruptions to the supply chain. We plan to pursue some of these extensions in our future work.

References

Acharya, V. V., Crosignani, M., Eisert, T. & Eufinger, C. (2023), 'How Do Supply Shocks to Inflation Generalize? Evidence from the Pandemic Era in Europe', *NBER Working Paper 31790* .

Adland, R. & Jia, H. (2016), 'Dynamic speed choice in bulk shipping', *Maritime Economics & Logistics* **20**(3), 253–266.

Alessandria, G., Khan, S. Y., Khederlarian, A., Mix, C. & Ruhl, K. J. (2023), 'The aggregate effects of global and local supply chain disruptions: 2020–2022', *Journal of International Economics* p. 103788.

Allen, T. (2014), 'Information Frictions in Trade', *Econometrica* **82**, 2041–2083.

Allen, T. & Arkolakis, C. (2014), 'Trade and the Topography of the Spatial Economy', *The Quarterly Journal of Economics* **129**(3), 1085–1140.

Arias, J. E., Caldara, D. & Rubio-Ramírez, J. F. (2019), 'The systematic component of monetary policy in SVARs: An agnostic identification procedure', *Journal of Monetary Economics* **101**, 1–13.

Arias, J. E., Fernández-Villaverde, J., Rubio-Ramírez, J. F. & Shin, M. (2023), 'The Causal Effects of Lockdown Policies on Health and Macroeconomic Outcomes', *American Economic Journal: Macroeconomics* **15**(3), 287–319.

Arias, J. E., Rubio-Ramirez, J. F. & Waggoner, D. F. (2018), 'Inference Based on Structural Vector Autoregressions Identified With Sign and Zero Restrictions: Theory and Applications', *Econometrica* **86**, 685–720.

Attinasi, M. G., Balatti, M., Mancini, M. & Metelli, L. (2021), 'Supply chain disruptions and the effects on the global economy', *ECB Economic Bulletin Issue 8* .

Bai, X. & Li, Y. (2022), 'The Congestion Effect of Oil Transportation and Its Trade Implications', *Working Paper* .

Bai, X., Ma, Z., Hou, Y., Li, Y. & Yang, D. (2023), 'A Data-Driven Iterative Multi-Attribute Clustering Algorithm and Its Application in Port Congestion Estimation', *IEEE Transactions on Intelligent Transportation Systems* **24**, 12026–12037.

Baker, S. R., Bloom, N. & Davis, S. J. (2016), 'Measuring Economic Policy Uncertainty', *The Quarterly Journal of Economics* **131**, 1593–1636.

Barro, R. J. & Grossman, H. I. (1971), 'A General Disequilibrium Model of Income and Employment', *The American Economic Review* **61**(1), 82–93.

Bańbura, M., Giannone, D. & Reichlin, L. (2010), 'Large Bayesian vector auto regressions', *Journal of Applied Econometrics* **25**, 71–92.

Bekaert, G., Engstrom, E. & Ermolov, A. (2020), 'Aggregate Demand and Aggregate Supply Effects of COVID-19: A Real-time Analysis', *Finance and Economic Discussion Series 2020-049* .

Benguria, F. (2021), 'The matching and sorting of exporting and importing firms: Theory and evidence', *Journal of International Economics* **131**, 103430.

Benigno, G., di Giovanni, J., Groen, J. J. & Noble, A. I. (2022), 'The GSCPI: A New Barometer of Global Supply Chain Pressures', *Federal Reserve Bank of New York Staff Reports 1017* .

Benigno, P. & Eggertsson, G. B. (2023), 'It's Baaack: The Surge in Inflation in the 2020s and the Return of the Non-Linear Phillips Curve', *NBER Working Paper 31197* .

Benigno, P. & Ricci, L. A. (2011), 'The Inflation-Output Trade-Off with Downward Wage Rigidities', *American Economic Review* **101**(4), 1436–66.

Bernanke, B. S. & Mihov, I. (1998), 'Measuring Monetary Policy', *The Quarterly Journal of Economics* **113**, 869–902.

Bils, M., Chang, Y. & Kim, S.-B. (2011), 'Worker Heterogeneity and Endogenous Separations in a Matching Model of Unemployment Fluctuations', *American Economic Journal: Macroeconomics* **3**, 128–154.

Birant, D. & Kut, A. (2007), 'ST-DBSCAN: An algorithm for clustering spatial–temporal data', *Data & Knowledge Engineering* **60**, 208–221.

Blanchard, O. J. & Bernanke, B. S. (2023), 'What Caused the US Pandemic-Era Inflation?', *NBER Working Paper 31417* .

Brancaccio, G., Kalouptsidi, M. & Papageorgiou, T. (2020), 'Geography, transportation, and endogenous trade costs', *Econometrica* **88**(2), 657–691.

Brancaccio, G., Kalouptsidi, M., Papageorgiou, T. & Rosaia, N. (2023), 'Search Frictions and Efficiency in Decentralized Transport Markets', *The Quarterly Journal of Economics* p. qjad023.

Bratsiotis, G. J. & Theodoridis, K. (2022), 'Precautionary liquidity shocks, excess reserves and business cycles', *Journal of International Financial Markets, Institutions and Money* **77**, 101518.

Brinca, P., Duarte, J. B. & e Castro, M. F. (2021), 'Measuring labor supply and demand shocks during COVID-19', *European Economic Review* **139**, 103901.

Brown, J., Englert, D. & Hoffmann, J. (2021), 'International transport costs: Why and how to measure them?', World Bank Blogs - Transport. Available at: https://blogs.worldbank.org/transport/international-transport-costs-why-and-how-measure-them (Accessed: March 6, 2022).

Burriel, P., Kataryniuk, I., Pérez, C. M. & Viani, F. (2023), 'A New Supply Bottlenecks Index Based on Newspaper Data', *Banco de España Working Paper 2304* .

Chaney, T. (2014), 'The Network Structure of International Trade', *American Economic Review* **104**(11), 3600–3634.

Chen, C. W. & Lee, J. C. (1995), 'Bayesian Inference of Threshold Autoregressive Models', *Journal of Time Series Analysis* **16**, 483–492.

Chow, G. C. & Lin, A.-l. (1971), 'Best Linear Unbiased Interpolation, Distribution, and Extrapolation of Time Series by Related Series', *The Review of Economics and Statistics* **53**, 372–375.

Comin, D. A., Johnson, R. C. & Jones, C. J. (2023), 'Supply Chain Constraints and Inflation', *NBER Working Paper 31179* .

Costinot, A., Vogel, J. & Wang, S. (2013), 'An Elementary Theory of Global Supply Chains', *The Review of Economic Studies* **80**, 109–144.

Coşar, A. K. & Demir, B. (2018), 'Shipping inside the box: Containerization and trade', *Journal of International Economics* **114**, 331–345.

Dempsey, H. (2022), 'Is there an end in sight to supply chain disruption?', Financial Times. Available at: https://www.ft.com/content/21242e3b-298b-4a6f-a35f-32fdde905952 (Accessed: January 9, 2022).

den Haan, W. J., Ramey, G. & Haefke, C. (2005), 'Turbulence and Unemployment in a Job Matching Model', *Journal of the European Economic Association* **3**, 1360–1385.

di Giovanni, J., Şebnem Kalemli-Özcan, Silva, A. & Yildirim, M. A. (2022), 'Global Supply Chain Pressures, International Trade, and Inflation', *NBER Working Paper 30240* .

Du, Y., Chen, Q., Lam, J. S. L., Xu, Y. & Cao, J. X. (2015), 'Modeling the Impacts of Tides and the Virtual Arrival Policy in Berth Allocation', *Transportation Science* **49**(4), 939–956.

Dunn, J. & Leibovici, F. (2023), 'Navigating the Waves of Global Shipping: Drivers and Aggregate Implications', *Federal Reserve Bank of St. Louis Working Paper 2023-002* .

Eaton, J. & Kortum, S. (2002), 'Technology, Geography, and Trade', *Econometrica* **70**, 1741–1779.

Eichenbaum, M., Rebelo, S. & Wong, A. (2022), 'State-Dependent Effects of Monetary Policy: The Refinancing Channel', *American Economic Review* **112**(3), 721–61.

Ester, M., Kriegel, H.-P., Sander, J. & Xu, X. (1996), 'A Density-Based Algorithm for Discovering Clusters in Large Spatial Databases with Noise', *KDD-96 Proceedings* .

Fernández-Villaverde, J., Mandelman, F., Yu, Y. & Zanetti, F. (2021), 'The "Matthew effect" and market concentration: Search complementarities and monopsony power', *Journal of Monetary Economics* **121**, 62–90.

Fernández-Villaverde, J., Mandelman, F., Yu, Y. & Zanetti, F. (2022), 'Search Complementarities, Aggregate Fluctuations, and Fiscal Policy', *NBER Working Paper 26210* .

Fernández-Villaverde, J., Yu, Y. & Zanetti, F. (2023), 'Technological Synergies, Heterogenous Firms, and Idiosyncratic Volatility', *Working Paper* .

Finck, D. & Tillmann, P. (2022), 'The macroeconomic effects of global supply chain disruptions', *BOFIT Discussion Paper 14/2022* .

Forster van Aerssen, K., Gomez-Salvador, R., Soudan, M. & Spital, T. (2021), 'The US and UK labour markets in the post-pandemic recovery', *ECB Economic Bulletin Issue 8* .

Fuchs, S. & Wong, W. F. (2022), 'Multimodal Transport Networks', *Federal Reserve Bank of Atlanta Working Paper 2022-13* .

Fujita, S. (2018), 'Declining labor turnover and turbulence', *Journal of Monetary Economics* **99**, 1–19.

Fujita, S. & Ramey, G. (2012), 'Exogenous versus Endogenous Separation', *American Economic Journal: Macroeconomics* **4**, 68–93.

Ghassibe, M. (2023), 'Endogenous Production Networks and Non-Linear Monetary Transmission', *CREi Working Paper Series* .

Ghassibe, M. & Zanetti, F. (2022), 'State dependence of fiscal multipliers: the source of fluctuations matters', *Journal of Monetary Economics* **132**, 1–23.

Giacomini, R. & Kitagawa, T. (2021), 'Robust Bayesian Inference for Set-Identified Models', *Econometrica* **89**, 1519–1556.

Gordon, M. V. & Clark, T. E. (2023), 'The Impacts of Supply Chain Disruptions on Inflation', *Federal Reserve Bank of Cleveland Economic Commentary 2023-08* .

Grimes, C. & Edgecliffe-Johnson, A. (2021), 'The supply chain crisis and US ports: 'Disruption on top of disruption'', Financial Times. Available at: https://www.ft.com/content/aa24d82e-16c7-4e3e-868e-42bd32f593be (Accessed: October 14, 2021).

Hall, R. E. (2005), 'Employment Fluctuations with Equilibrium Wage Stickiness', *American Economic Review* **95**(1), 50–65.

Harding, M., Lindé, J. & Trabandt, M. (2023), 'Understanding Post-COVID Inflation Dynamics', *Journal of Monetary Economics* .

Heiland, I., Moxnes, A., Ulltveit-Moe, K. H. & Zi, Y. (2022), 'Trade From Space: Shipping Networks and The Global Implications of Local Shocks', *CEPR Discussion Paper 14193* .

Howitt, P. & McAfee, R. P. (1987), 'Costly Search and Recruiting', *International Economic Review* **28**(1), 89–107.

Ikeda, D., Li, S., Mavroeidis, S. & Zanetti, F. (2023), 'Testing the Effectiveness of Unconventional Monetary Policy in Japan and the United States', *American Economic Journal: Macroeconomics* p. forthcoming.

Kamali, P. & Wang, A. (2021), 'Longer Delivery Times Reflect Supply Chain Disruptions', IMF Blog. Available at: https://www.imf.org/en/Blogs/Articles/2021/10/25/longer-delivery-times-reflect-supply-chain-disruptions (Accessed: October 25, 2021).

Karimi-Mamaghan, M., Mohammadi, M., Pirayesh, A., Karimi-Mamaghan, A. M. & Irani, H. (2020), 'Hub-and-spoke network design under congestion: A learning based metaheuristic', *Transportation Research Part E: Logistics and Transportation Review* **142**, 102069.

Kasahara, H. & Lapham, B. (2013), 'Productivity and the decision to import and export: Theory and evidence', *Journal of International Economics* **89**, 297–316.

Kilian, L. & Murphy, D. P. (2012), 'Why Agnostic Sign Restrictions Are Not Enough: Understanding the Dynamics of Oil Market VAR Models', *Journal of the European Economic Association* **10**, 1166–1188.

Klachkin, O. (2021), 'Supply-chain headwinds pummel the economy', Oxford Economics. Available at: https://resources.oxfordeconomics.com/hubfs/press-release/Supply-chain-headwinds-pummel-the-economy.pdf (Accessed: September 22, 2021).

Krolikowski, P. M. & McCallum, A. H. (2021), 'Goods-market frictions and international trade', *Journal of International Economics* **129**, 103411.

Lane, P. R. (2022), 'Bottlenecks and monetary policy', ECB Blog. Available at: https://www.ecb.europa.eu/press/blog/date/2022/html/ecb.blog220210~1590dd90d6.en.html (Accessed: February 10, 2022).

Lenoir, C., Martin, J. & Mejean, I. (2022), 'Search Frictions in International Goods Markets', *Journal of the European Economic Association* **21**(1), 326–366.

Li, C., Qi, X. & Song, D. (2016), 'Real-time schedule recovery in liner shipping service with regular uncertainties and disruption events', *Transportation Research Part B: Methodological* **93**, 762–788.

Li, Y., Bai, X., Wang, Q. & Ma, Z. (2022), 'A big data approach to cargo type prediction and its implications for oil trade estimation', *Transportation Research Part E: Logistics and Transportation Review* **165**, 102831.

Litterman, R. B. (1986), 'Forecasting with Bayesian Vector Autoregressions: Five Years of Experience', *Journal of Business & Economic Statistics* **4**, 25–38.

Liu, P., Theodoridis, K., Mumtaz, H. & Zanetti, F. (2019), 'Changing Macroeconomic Dynamics at the Zero Lower Bound', *Journal of Business & Economic Statistics* **37**(3), 391–404.

Lopes, H. F. & Salazar, E. (2006), 'Bayesian Model Uncertainty In Smooth Transition Autoregressions', *Journal of Time Series Analysis* **27**, 99–117.

Mathieu, E., Ritchie, H., Rodés-Guirao, L., Appel, C., Giattino, C., Hasell, J., Macdonald, B., Dattani, S., Beltekian, D., Ortiz-Ospina, E. & Roser, M. (2020), 'Coronavirus pandemic (covid-19)', Our World in Data. Available at: https://ourworldindata.org/coronavirus (Accessed: August 17, 2022).

Melitz, J. & Toubal, F. (2014), 'Native language, spoken language, translation and trade', *Journal of International Economics* **93**, 351–363.

Melitz, M. J. (2003), 'The Impact of Trade on Intra-Industry Reallocations and Aggregate Industry Productivity', *Econometrica* **71**, 1695–1725.

Menzio, G. & Shi, S. (2011), 'Efficient Search on the Job and the Business Cycle', *Journal of Political Economy* **119**, 468–510.

Michaillat, P. & Saez, E. (2015), 'Aggregate Demand, Idle Time, and Unemployment', *The Quarterly Journal of Economics* **130**, 507–569.

Michaillat, P. & Saez, E. (2022), 'An economical business-cycle model', *Oxford Economic Papers* **74**, 382–411.

Mountford, A. & Uhlig, H. (2009), 'What are the effects of fiscal policy shocks?', *Journal of Applied Econometrics* **24**, 960–992.

Mumtaz, H. & Zanetti, F. (2012), 'Neutral Technology Shocks and the Dynamics Of Labor Input: Results from an Agnostic Identification', *International Economic Review* **53**, 235–254.

Mumtaz, H. & Zanetti, F. (2015), 'Labor Market Dynamics: A Time-Varying Analysis', *Oxford Bulletin of Economics and Statistics* **77**, 319–338.

Naudé, W. & Matthee, M. (2011), 'The impact of transport costs on new venture internationalisation', *Journal of International Entrepreneurship* **9**, 62–89.

Notteboom, T. E. (2006), 'The Time Factor in Liner Shipping Services', *Maritime Economics & Logistics* **8**, 19–39.

Notteboom, T., Pallis, A. & Rodrigue, J.-P. (2022), *Port Economics, Management and Policy*, 1 edn, Routledge.

Notteboom, T., Pallis, T. & Rodrigue, J. (2021), 'Disruptions and resilience in global container shipping and ports: the COVID-19 pandemic versus the 2008–2009 financial crisis', *Maritime Economics & Logistics* **23**, 179–210.

OECD & EUIPO (2021), *Misuse of Containerized Maritime Shipping in the Global Trade of Counterfeits*, OECD.

Pizzinelli, C., Theodoridis, K. & Zanetti, F. (2020), 'State Dependence in Labor Market Fluctuations', *International Economic Review* **61**, 1027–1072.

Plagborg-Møller, M. & Wolf, C. K. (2021), 'Local Projections and VARs Estimate the Same Impulse Responses', *Econometrica* **89**, 955–980.

Ramey, V. A. & Zubairy, S. (2018), 'Government spending multipliers in good times and in bad: Evidence from US historical data', *Journal of Political Economy* **126**, 850–901.

Ramondo, N. & Rodríguez-Clare, A. (2013), 'Trade, Multinational Production, and the Gains from Openness', *Journal of Political Economy* **121**, 273–322.

Rodrigue, J.-P. (2020), *The Geography of Transport Systems*, 5 edn, Routledge.

Rubio-Ramirez, J. F., Waggoner, D. F. & Zha, T. (2010), 'Structural Vector Autoregressions: Theory of Identification and Algorithms for Inference', *The Review of Economic Studies* **77**, 665–696.

Samuelson, P. A. (1954), 'The Transfer Problem and Transport Costs, II: Analysis of Effects of Trade Impediments', *The Economic Journal* **64**(254), 264–289.

Sea-Intelligence (2021), '20%–25% Weekly Capacity Blanked on Asia-NAWC', Sea-Intelligence. Available at: https://sea-intelligence.com/press-room/111-20-25-weekly-capacity-blanked-on-asia-nawc (Accessed: December 15, 2021).

Smirnyagin, V. & Tsyvinski, A. (2022), 'Macroeconomic and Asset Pricing Effects of Supply Chain Disasters', *NBER Working Paper 30503* .

Song, D.-P. & Dong, J.-X. (2012), 'Cargo routing and empty container repositioning in multiple shipping service routes', *Transportation Research Part B: Methodological* **46**(10), 1556–1575.

Stamer, V. (2021), 'Thinking Outside the Container: A Sparse Partial Least Squares Approach to Forecasting Trade Flows', *Kiel Working Papers 2179* .

Stopford, M. (2008), *Maritime Economics*, 3 edn, Routledge, London.

Talley, W. K. & Ng, M. W. (2016), 'Port multi-service congestion', *Transportation Research Part E: Logistics and Transportation Review* **94**, 66–70.

The White House (2021), 'Fact Sheet: Biden Administration Efforts to Address Bottlenecks at Ports of Los Angeles and Long Beach: Moving Goods from Ship to Shelf', The White House. Available at: https://www.whitehouse.gov/briefing-room/statements-releases/2021/10/13/fact-sheet-biden-administration-efforts-to-address-bottlenecks-at-ports-of-los-angeles-and-long-beach-moving-goods-from-ship-to-shelf/ (Accessed: October 13, 2021).

Uhlig, H. (2005), 'What are the effects of monetary policy on output? Results from an agnostic identification procedure', *Journal of Monetary Economics* **52**, 381–419.

UNCTAD (2019), 'Review of Maritime Transport 2019', UNCTAD. Available at: https://unctad.org/webflyer/review-maritime-transport-2019 (Accessed: November 1, 2021).

UNCTAD (2021), 'Global Transport Costs Dataset for International Trade', UNCTADstat. Available at: https://unctadstat.unctad.org/wds/TableViewer/tableView.aspx?ReportId=207046 (Accessed: January 20, 2022).

Wang, Y., Meng, Q. & Jia, P. (2019), 'Optimal port call adjustment for liner container shipping routes', *Transportation Research Part B: Methodological* **128**, 107–128.

Williamson, C. (2021), 'Understanding…PMI suppliers' delivery times: A widely used indicator of supply delays, capacity constraints and price pressures', S&P Global Market Intelligence Economics Commentary. Available at: https://ihsmarkit.com/research-analysis/understanding--pmi-suppliers-delivery-times-a-widely-used-indicator-of-supply-delays-capacity-constraints-and-price-pressures-Jul21.html (Accessed: May 2, 2022).

Wong, W. F. (2022), 'The Round Trip Effect: Endogenous Transport Costs and International Trade', *American Economic Journal: Applied Economics* **14**, 127–166.

World Bank (2022), *Global Economic Prospects, June 2022*, Washington, DC: World Bank.

Wu, J. C. & Xia, F. D. (2016), 'Measuring the Macroeconomic Impact of Monetary Policy at the Zero Lower Bound', *Journal of Money, Credit and Banking* **48**(2-3), 253–291.

Online Appendices

A. A Primer on Containerized Shipping Industry

Liner shipping service regularity. Numerous textbooks and research papers on maritime economics discuss the long-term contractual agreements prevalent in the containerized shipping industry (Stopford 2008, Song & Dong 2012, Wang et al. 2019, Brancaccio et al. 2020, 2023). For instance, Stopford (2008) states in his textbook (p.512): "A liner service is a fleet of ships … which provide a fixed service, at regular intervals, between named ports, …. A fixed itinerary, inclusion in a regular service, and the obligation to accept cargo from all comers and to sail … on the date fixed by a published schedule are what distinguish the liner from the tramp". Likewise, Brancaccio et al. (2020) state in their paper (p.2): "The transportation sector … can be split into two categories: those that operate on fixed itineraries, much like buses, and those that operate on flexible routes, much like taxis. Containerships … belong to the first group".

Congestion and speed adjustment. The current shipping industry generally adopts a "hurry up and wait" practice regarding the port call process (Du et al. 2015). For instance, a vessel departs the loading port at full speed, aiming to meet the original Requested Time of Arrival at Pilot Boarding Place (RTA PBP) scheduled for day 14. However, if three days into the voyage, the port encounters delays altering the RTA PBP to day 17, the ship may not receive this updated information in time to adjust its speed. Consequently, even if a port is experiencing congestion, vessels will still "hurry" to arrive and then "wait" at anchorage due to the lack of timely communication.

Oil price, speed adjustment, and congestion. Fuel costs account for approximately 50% to 60% of a vessel's operating costs for a liner shipping company (Notteboom 2006). Moreover, the fuel consumption of a vessel is widely acknowledged to be roughly a cubic function of the sailing speed (Li et al. 2016). Therefore, vessel sailing speed significantly impacts operating costs. In principle, shipping companies would dynamically adjust sailing speeds based on current bunker prices, which are primarily influenced by fluctuations in oil prices.

For example, when bunker prices are high, reducing speed could lead to substantial fuel cost savings. However, based on AIS data, researchers have found that this relationship between speed and oil prices is not readily apparent in practice (Adland & Jia 2016). This has been attributed to the rigidity of contractual structures and the lack of coordination between ports and vessels. Consequently, the observed impact of oil prices on vessel speed, and thus on congestion, is limited.

B. A Density-Based Spatial Clustering Algorithm

In this appendix, we provide the technical details of our density-based spatial clustering algorithm, namely the iterative, multi-attribute, density-based spatial clustering of applications with noise (IMA-DBSCAN).[1] This algorithm is used to estimate port congestion for major container ports worldwide.[2] In subsequent sections, we first delve into the methodology underpinning our algorithm. We then present an illustrative case where we apply the algorithm to the Port of Ningbo-Zhoushan in China, demonstrating its capability to identify anchorage and berth areas of a port where other methods fall short.

B.1. Methodology

As depicted in Figure B.1, the proposed IMA-DBSCAN algorithm has several distinct features. Foremost among these is its two-tiered, iterative structure. At the first level, we extract the trajectory of each containership at every port in question from the AIS data. For each ship, a traditional DBSCAN (Ester et al. 1996) is employed to filter out noise and cluster all its mooring points. While this level can pinpoint mooring areas, it does not adequately differentiate between anchorage and berth areas of a port. The second level addresses this limitation. Here, a spatial-temporal-DBSCAN (ST-DBSCAN; see Birant & Kut (2007)) is applied to the clustering. During this phase, we employ an iterative method to determine a generalized and optimal parameter setting for the clustering algorithm. Another hallmark

[1] Most of the details provided in this appendix can also be found in the companion paper (Bai et al. 2023).

[2] See https://www.worldshipping.org/top-50-ports (Accessed June 15, 2022) for the full list of ports. The Port of Tokyo Ko, Japan, is not included as its observations are merged with those of the Port of Keihin, Japan.

of IMA-DBSCAN is its integration of multiple attributes at the second level. Beyond spatial data (like coordinates), we also weave in non-spatial information (such as headings and timestamps) to enhance clustering accuracy. In the sections that follow, we elaborate on the specifics of each level of IMA-DBSCAN.

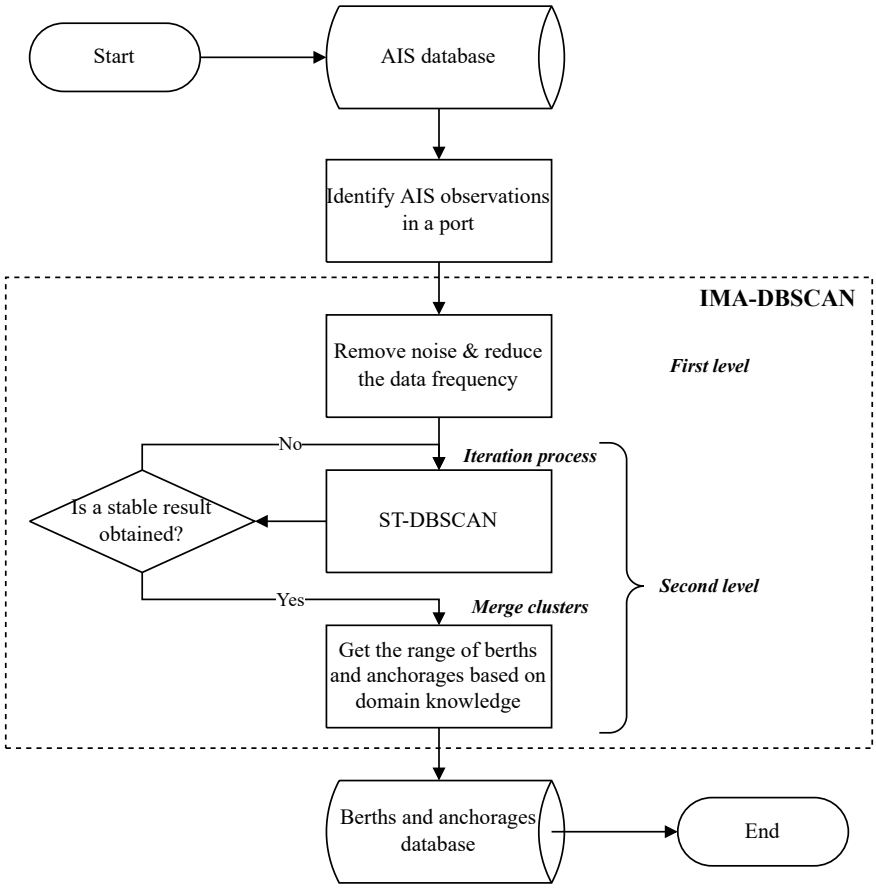


Figure B.1: Methodology Framework of IMA-DBSCAN

B.1.1. The First Level – Data Pre-Processing

While AIS data provides detailed information on the positions of each ship, direct clustering of these positions to determine the anchorage and berth areas of a port presents several challenges. Firstly, even if we restrict the data to a specific port area within a certain timeframe, the sheer volume of records means that inputting them directly into DBSCAN would lead to extended processing times. Secondly, a high incidence of incorrect AIS signal assignments could result in inaccurate clustering outcomes, such as identifying a cluster that

is not an actual berth or one that covers an unusually large geographical area. Thirdly, if a ship stays in a port area for an extended period (e.g., for maintenance), the dense AIS data could lead DBSCAN to mistakenly identify it as a cluster. Given these challenges, it is essential to preprocess the AIS data before using it to pinpoint the anchorage and berth areas of a port.

In the first level of IMA-DBSCAN, we begin by filtering the AIS data for each ship in the port area, focusing on records indicating speeds of less than one knot. Such positions suggest that a ship is either berthed, anchored, or in an unusual situation (e.g., under maintenance). We then tally these positions; if their number falls outside an acceptable range (e.g., less than 100 or more than 100,000), we deem the ship's data abnormal and exclude it from further analysis. Since a ship might dock at a port multiple times, we establish a period, Δt (e.g., 12 hours), as the cut-off between two consecutive arrivals. If the gap between two arrivals exceeds Δt, we treat them as separate port calls. To streamline the data while maintaining consistency, we retain only the first data point for each hour. For every port call of a ship, its positions are clustered using the traditional DBSCAN with parameters Eps and $MinPts$. We choose an Eps value small enough to identify the ship's mooring areas and an appropriate $MinPts$ value to ensure transient stops are classified as noise. At this stage, the AIS data preprocessing is complete. The refined samples are then used to identify the anchorage and berth areas of a port in the second level of IMA-DBSCAN. For reference, the pseudo-code for the first level of IMA-DBSCAN is detailed in Algorithm 1.

B.1.2. The Second Level – Multiple Attributes and Iteration

Information on Headings. As highlighted in the main text, AIS data integrates both spatial (i.e., geographical coordinates) and non-spatial (i.e., headings) information. In Figure 1 from the main text, we illustrate the positions of a ship in a port alongside their headings. We observe that the headings of a ship at a berth are either aligned in the same direction or are exact opposites. In contrast, headings in an anchorage area appear random, with no discernible pattern. This observation aligns with real-world scenarios, where ships in anchorage areas often struggle to maintain consistent headings over time due to significant wind and wave variations.

Consequently, in the second level of IMA-DBSCAN, we leverage this heading information to enhance estimation accuracy.[3] Specifically, IMA-DBSCAN incorporates three parameters, as opposed to the traditional two in DBSCAN. These are $Eps1$, $Eps2$, and $MinPts$. Here, $Eps1$ denotes the maximum geographical coordinate (spatial) distance, $Eps2$ represents the maximum non-spatial distance between two headings, and $MinPts$ is the minimum number of points within the distances defined by $Eps1$ and $Eps2$. The geographical coordinate (spatial) distance D is calculated using the Haversine formula:

$$D\Big[(x_1, x_2), (y_1, y_2)\Big] = 2 \cdot R \cdot \arcsin\left[\sqrt{\sin^2\left(\frac{x_1 - y_1}{2}\right) + \cos x_1 \cos y_1 \sin^2\left(\frac{x_2 - y_2}{2}\right)}\right], \quad \text{(B.1)}$$

where the coordinates are measured in radians, and $R = 6,371$ is the mean radius of Earth in kilometers. On the other hand, the non-spatial distance Δh is calculated as:

$$\Delta h(h_1, h_2) = \begin{cases} |h_1 - h_2|\,, & \text{if } |h_1 - h_2| \leq 180°; \\ 360° - |h_1 - h_2|\,, & \text{otherwise.} \end{cases} \quad \text{(B.2)}$$

With the two measures of distance defined above, the neighbors of a point are those with geographical coordinate (spatial) distance less than $Eps1$ and non-spatial distance less than $Eps2$, and a core is defined as a point with more than or equivalent to $MinPts$ neighbors. The clusters in IMA-DBSCAN contain only these cores.

Iteration Process. As previously discussed, there are three parameters to set in IMA-DBSCAN. Given that the geographical shapes of anchorage and berth areas vary significantly across ports, the values of these three parameters should ideally differ to achieve optimal estimation results. Therefore, we propose an iterative method to determine these parameter values. Specifically, while we fix $Eps2$ at 1°, our method allows the values of $Eps1$ and $MinPts$ to vary between different ports. During the iteration process, we define four intermediate variables: $Dist$, m, m', and $NumC$. Here, $Dist$ represents the average distance between a point in a cluster and the center of its respective cluster. m denotes the number of points, while m' represents the number of noisy points (initialized to zero). Lastly, $NumC$

[3] Such non-spatial information is also useful when we distinguish between different berths (see Algorithm 2). In our initial experiment, the coordinates could only help us identify the approximate locations of anchorage and berth areas of a port, not to mention the exact number of berths.

indicates the number of clusters.[4] Using these intermediate variables, $MinPts$ and $Eps1$ are calculated as:

$$Eps1 = \alpha \cdot Dist,\ MinPts = \beta \cdot \frac{m - m'}{NumC}.$$

Regarding α and β, even though there is no explicit constraint on their values, they should fall within a reasonable range to ensure both the algorithm's convergence and the validity of the identification results. After evaluating the performance of IMA-DBSCAN under various parameter settings, we find that an admissible range of ($0.4 \leq \alpha \leq 0.6$, $0.06 \leq \beta \leq 0.1$) is appropriate. We also introduce an intermediate variable, $Dist_0$, which records the value of $Dist$ from the previous iteration and is initialized to zero.

Following this, we iteratively execute ST-DBSCAN. In each iteration, ST-DBSCAN operates with $Eps1$ and $MinPts$ set to their current values, and $Eps2$ set to 1°. The outputs classify each point either into a cluster or as noise. Based on these outputs, the values of the intermediate variables, as well as those for $Eps1$ and $MinPts$, are updated. These updated values are then re-applied in ST-DBSCAN for the subsequent iteration. The entire process concludes when the difference $Dist - Dist_0$ is less than or equal to $\Delta Dist$ (e.g., 100 m). Consequently, each point is either assigned to a cluster or labeled as noise. We then interpret the cluster areas as berths and the areas of noisy points as anchorages.

Information on Timestamp. After running ST-DBSCAN, we find that there exists a large proportion of clusters that should be merged together as they essentially represent the same berth in reality. To achieve a more accurate identification of berth areas, we merge certain clusters by taking advantage of the time information (i.e., timestamps) in the AIS data (see Figure B.2 for an illustration). More precisely, we first calculate the start and end times of each port call in each cluster. Subsequently, since only one ship can dock at a berth for a given moment, for each cluster under consideration, we find the cluster that is the closest to it, and then check whether there is any overlap in the docking times. If there exists (at least) one overlap, the two clusters are considered to represent two different berths. If there is no overlap, the two clusters are merged together to represent one berth.

[4] Since there are no clusters at initialization, we treat all points as if they were part of the same cluster. Additionally, if all points are classified as noise, we set $NumC = 1$.

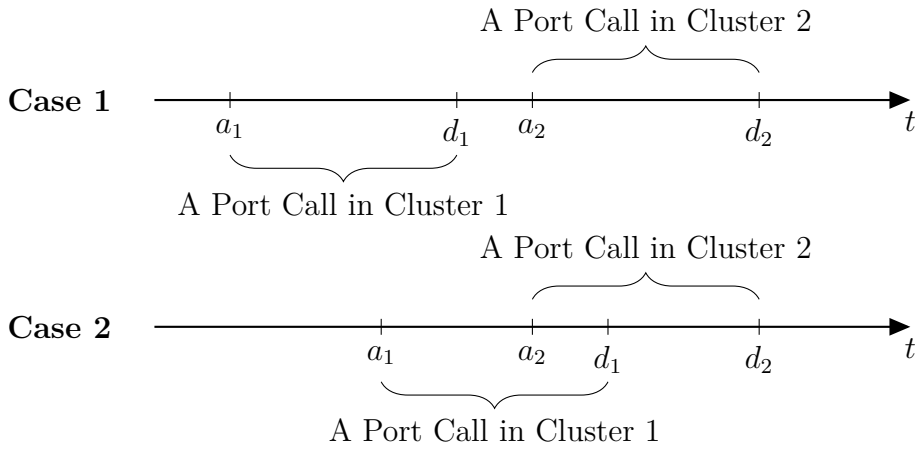


Figure B.2: Merging Clusters

Notes. The figure illustrates two scenarios and discusses the criteria for merging clusters after executing ST-DBSCAN on the second level. Here, a_1 and d_1 represent the arrival and departure times of a ship during a port call assigned to cluster 1. Similarly, a_2 and d_2 correspond to the times for a port call assigned to cluster 2, which is geographically the closest to cluster 1. In the first scenario, there is no overlap in the docking times, so clusters 1 and 2 are merged. In contrast, the second scenario shows an overlap in the docking times. As a result, clusters 1 and 2 are kept distinct since two ships cannot occupy a single berth simultaneously.

Furthermore, in order to differentiate between different anchorage areas, we perform another DBSCAN on those points that are classified as noise. In the process, the two parameters associated with the DBSCAN, i.e, Eps' and $MinPts'$, are set according to our domain knowledge. Finally, we remove clusters with less than N port calls, with N set according to our domain knowledge. For reference, the pseudo-codes for the second level of IMA-DBSCAN can be found in Algorithms 2, 3, and 4.

Lastly, in the estimation of port congestion for the major container ports worldwide, the parameter values set for IMA-DBSCAN are provided in Table B.1.

Table B.1: Parameter Values for IMA-DBSCAN

	Parameter					
First Level	Δt	Eps	$MinPts$			
Value	12 hours	50 m	10			
Second Level	α	β	$\Delta Dist$	Eps'	$MinPts'$	N
Value	0.5	0.08	100 m	1,000 m	50	5

Algorithm 1 Level 1 IMA-DBSCAN

Inputs:

$A_l = \{a_{1,l}, \ldots, a_{n,l}\}$: the set of coordinates recorded in the AIS data for a ship l
$S_l = \{s_{1,l}, \ldots, s_{n,l}\}$: the set of speeds recorded in the AIS data for a ship l
$T_l = \{t_{1,l}, \ldots, t_{n,l}\}$: the set of timestamps recorded in the AIS data for a ship l

Outputs:

$D_l = \{d_{1,l}, \ldots, d_{m,l}\}$: the coordinates of the first observation for each hour in B_l
$H_l = \{h_{1,l}, \ldots, h_{m,l}\}$: the headings of the first observation for each hour in B_l

/ Data Pre-Processing */*
$B_l = \{b_{1,l} \ldots b_{k,l}\} \leftarrow$ the set of coordinates in A_l that indicate a speed less than 1 knot
/ Exception Identification */*
if $|B_l| < 100$ **or** $|B_l| > 100,000$ **then**
    Remove the data and stop ▷ *The ship has an abnormal port call*
else
    Continue
end if
/ DBSCAN Clustering */*
$X \leftarrow b_{1,l}$
for $i \leftarrow 2 : k$ **do**
    if $t_i - t_{i-1} \leq \Delta t$ **then**
        Append $b_{i,l}$ to X
    else
        $DBSCAN(X, Eps, MinPts)$
        $X \leftarrow \emptyset$
        Append $b_{i,l}$ to X
    end if
end for
Remove the observations labeled as noise from B_l
Keep only the first observation for each hour in B_l ▷ *Note that only m observations remain in B_l at this stage*
$D_l = \{d_{1,l}, \ldots, d_{m,l}\} \leftarrow$ the coordinates of the first observation for each hour in B_l
$H_l = \{h_{1,l}, \ldots, h_{m,l}\} \leftarrow$ the headings of the first observation for each hour in B_l

Algorithm 2 Level 2 IMA-DBSCAN

Inputs:

$\boldsymbol{D} = \{D_1, \ldots, D_L\}$: the set of coordinates for all ships after Level 1 IMA-DBSCAN
$\boldsymbol{H} = \{H_1, \ldots, H_L\}$: the set of headings for all ships after Level 1 IMA-DBSCAN
$\boldsymbol{O} = \{\boldsymbol{D}, \boldsymbol{H}\} = \{o_1, \ldots, o_M\}$: the combined set of coordinates and headings

Outputs:

C_{berth}: the set of clusters marked as berths
$C_{anchorage}$: the set of clusters marked as anchorages

/ Parameter Initialization */*
$Dist \leftarrow$ the average distance between a point in $\boldsymbol{D}$ and the center of the mass of $\boldsymbol{D}$
$m \leftarrow |\boldsymbol{D}|$
$Eps1 \leftarrow \alpha \cdot Dist$
$MinPts \leftarrow \beta \cdot m$
/ Iteration Process */*
$Dist_0 \leftarrow 0$
while $Dist - Dist_0 > \Delta Dist$ km **do**
    $ST - DBSCAN(\boldsymbol{O}, Eps1, Eps2 = 1°, MinPts)$ ▷ *See function ST-DBSCAN*
    $Dist_0 \leftarrow Dist$
    $Dist \leftarrow$ the average distance between a non-noisy point in $\boldsymbol{D}$ and the center of the mass of its assigned cluster
    $m' \leftarrow |$noisy points in $\boldsymbol{O}|$
    $NumC \leftarrow |$clusters in $\boldsymbol{O}|$
    $Eps1 \leftarrow \alpha \cdot Dist$
    $MinPts \leftarrow \beta \cdot (m - m') / NumC$
end while
/ Merging Clusters */*
Use the center of the mass of each cluster to calculate the distance in between
for all clusters c in $\boldsymbol{O}$ **do**
    $c' \leftarrow$ the nearest cluster less than 500 m away from c
    if the docking times of c' and c do not overlap **then**
        Replace the cluster label of c' with that of c
    end if
end for
/ Berth and Anchorage Detection */*
$C_{berth} \leftarrow$ clusters in $\boldsymbol{O}$
$C_{anchorage} \leftarrow DBSCAN($Noisy points in $\boldsymbol{O}, Eps', MinPts')$
/ Exception Removal */*
for all clusters c **in** C_{berth} **and** $C_{anchorage}$ **do**
    $NumP \leftarrow$ the number of port calls in cluster c
    if $NumP < N$ **then**
        Remove c
    end if
end for

Algorithm 3 ST-DBSCAN

Inputs:

$\boldsymbol{O} = \{o_1, \ldots, o_M\}$: the combined set of coordinates and headings
$Eps1$: maximum geographical coordinate (spatial) distance
$Eps2$: maximum non-spatial distance
$MinPts$: minimum number of points within the distance of $Eps1$ and $Eps2$

Outputs:

$C = \{c_1, \ldots, c_M\}$: the set of clusters in $\boldsymbol{O}$

```
/* The codes are adapted from those in Birant & Kut (2007).                    */
function ST − DBSCAN(D, Eps1, Eps2, MinPts)
    ClusterLabel = 0
    for i ← 1 : m do
        if o_i is not in a cluster then
            Y ← RetrieveNeighbors(o_i, Eps1, Eps2)    ▷ See function RetrieveNeighbors
            if |Y| < MinPts then
                Mark o_i as noise
            else                                                ▷ Construct a new cluster
                ClusterLabel ← ClusterLabel + 1
                for j ← 1 : |Y| do
                    Mark all objects in Y with current ClusterLabel
                end for
                Push(all objects in Y)
                while not IsEmpty() do
                    CurrentObj = Pop()
                    Z ← RetrieveNeighbors(CurrentObj, Eps1, Eps2)
                    if |Z| ≥ MinPts then
                        for all objects o in Z do
                            if o is not marked as noise or it is not in a cluster then
                                Mark o with current ClusterLabel
                                Push(o)
                            end if
                        end for
                    end if
                end while
            end if
        end if
    end for
    C = {c_1, ..., c_M} ← the set of clusters in O
end function
```

Algorithm 4 RetrieveNeighbors

Inputs:

o: an observation in $\boldsymbol{O}$
$Eps1$: maximum geographical coordinate (spatial) distance
$Eps2$: maximum non-spatial distance

Outputs:

$Neighbors$: the set of neighbors for o

function $RetrieveNeighbors(o, Eps1, Eps2)$
  $Neighbors \leftarrow \emptyset$
  for all observations o' **in** O **do**
    $Dist1 \leftarrow D(o, o')$ ▷ *See Equation* (B.1)
    $Dist2 \leftarrow \Delta h(o, o')$ ▷ *See Equation* (B.2)
    if $Dist1 \leq Eps1$ **and** $Dist2 \leq Eps2$ **then**
      Append o' to $Neighbors$
    end if
  end for
  return $Neighbors$
end function

B.2. Illustrative Case: Port of Ningbo-Zhoushan, China

To demonstrate the capability of IMA-DBSCAN in accurately identifying anchorage and berth areas of a port, which other methods might fail to achieve, we apply the algorithm to the Port of Ningbo-Zhoushan in China. We choose this specific example primarily due to its intricate port layout. Figure B.3a showcases the first 50,000 AIS observations from January 2020 within the Port of Ningbo-Zhoushan.[5] The observations are represented by blue dots on the map, with each dot indicating the position of a low-speed containership. Before applying IMA-DBSCAN to the AIS data, we mark the approximate locations of anchorages and berths using both satellite images and nautical charts as benchmarks. The red boxes indicate the anchorage areas, while the yellow rectangles denote the berth locations.

Figure B.3b presents the clustering results of IMA-DBSCAN for the Port of Ningbo-Zhoushan, mirroring the map in Figure B.3a for a direct comparison between our algorithm's

[5]This example focuses on a one-month snapshot. It is reasonable to assume that the identification results would be indicative of anchorage and berth areas in subsequent months, given that we do not expect significant short-term changes in the port areas. In real-world applications of IMA-DBSCAN, periodic identification can be conducted to monitor potential changes in port anchorages and berths.

outcomes and the actual observations. The clusters in Figure B.3b (colored in red, yellow, blue, purple, cyan, and orange) correspond closely with the anchorage areas in Figure B.3a (represented by red polygons).[6] Additionally, in Figure B.3e, we spotlight the locations of four terminals within Ningbo-Zhoushan: Beilun, Daxie, Pukou, and Yuandong. Using satellite maps as a reference, we confirm the accuracy of these identifications; each berth in the terminals is pinpointed precisely, and the delineated areas align closely with reality.[7]

To assess the performance of IMA-DBSCAN, we contrast it with the outcomes from ST-DBSCAN.[8] Given that ST-DBSCAN is capable of processing spatial-temporal databases and is recognized as one of the most prominent spatial clustering algorithms in the literature, this comparison is relevant. Figure B.3c illustrates the results derived from ST-DBSCAN, underscoring its lesser precision in comparison to IMA-DBSCAN. Notably, while ST-DBSCAN can generally detect points within the anchorages (highlighted in blue in B.3c), it mistakenly identifies several high-density regions as berths, even though they are not genuine berths. For example, within the blue rectangle in Figure B.3f, points that ought to be categorized as noise are marked as berths, given that ships stayed in these locations for extended periods (potentially for maintenance tasks). Additionally, in the black rectangle, ST-DBSCAN mislabels several points as berths when they should be designated as mooring areas. Consequently, while employing ST-DBSCAN on the sample data offers insights into the arrangement of anchorages, it does not succeed in precisely pinpointing berth locations.

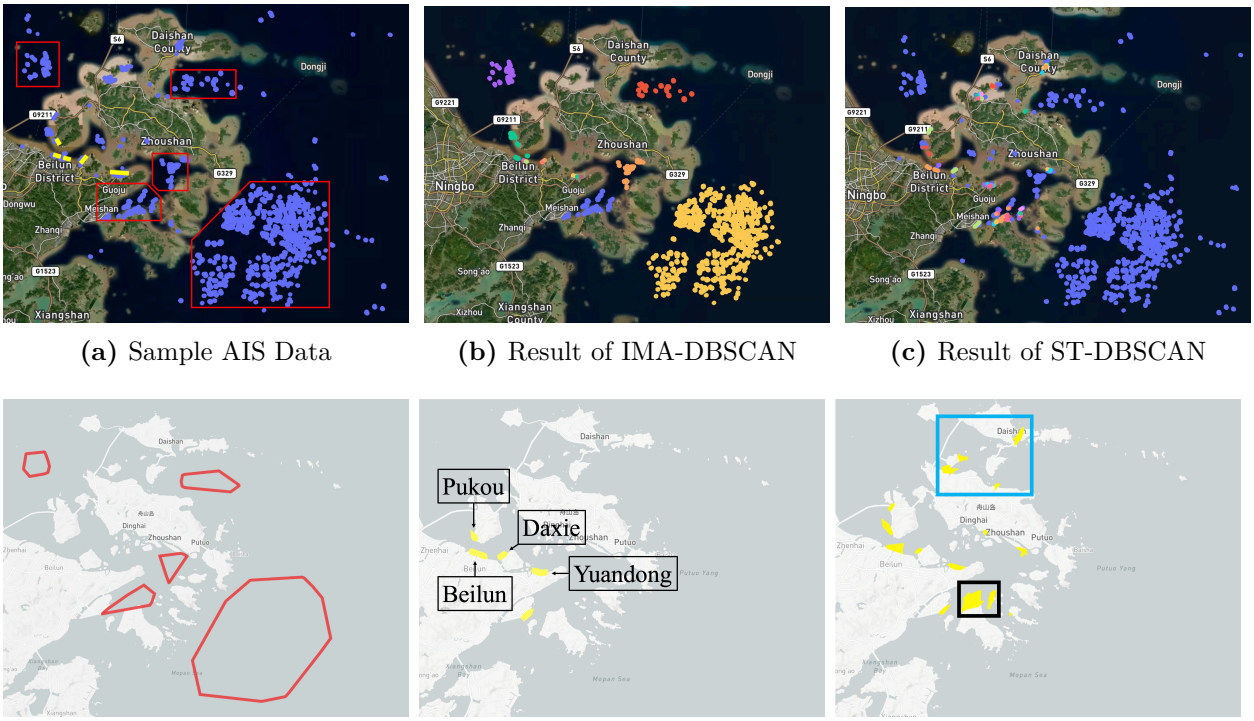
Furthermore, in Figure B.4, we present the detailed results of berth identification for each of the four terminals, i.e., Beilun, Daxie, Pukou, and Yuandong, within the Port of Ningbo-Zhoushan. The outcomes from ST-DBSCAN are ambiguous and feature overlapping sections (proximate in position but with significant differences in heading). Although the general range of these terminals can be discerned, individual berths are scarcely distinguishable. In contrast, our IMA-DBSCAN method can produce clusters that align precisely with each berth within a terminal. Admittedly, increasing the $MinPts$ or reducing the $Eps1$ value could enhance the ST-DBSCAN results. However, this would require constant parameter

[6] For clarity, we also display the convex hulls formed by these clusters in Figure B.3d.

[7] Moreover, some of the blue dots in Figure B.3a do not correspond to any anchorage or berth in Figure B.3b, indicating that ships anchored in these areas for only a short duration.

[8] For this comparison, the input parameters of ST-DBSCAN are set to $Eps1 = 2500$m, $Eps2 = 1°$, and $MinPts = 100$, as recommended by Ester et al. (1996).

adjustments, which is challenging to execute consistently for each port. Our IMA-DBSCAN algorithm, conversely, operates iteratively to automatically determine a set of parameters that can accurately identify both berths and anchorages.



(a) Sample AIS Data **(b)** Result of IMA-DBSCAN **(c)** Result of ST-DBSCAN

(d) Anchorages (IMA-DBSCAN) **(e)** Berths (IMA-DBSCAN) **(f)** Berths (ST-DBSCAN)

Figure B.3: Identification of Anchorage and Berth Areas in the Port of Ningbo-Zhoushan

Notes. In Figure (a), the sample data comprises the first 50,000 AIS observations taken in January 2020 within the Port of Ningbo-Zhoushan. These observations are represented by blue dots on the map, corresponding to coordinates ranging from 121.60°E to 123.00°E and from 29.50°N to 30.35°N. As a benchmark, using satellite maps and nautical charts, we identify the approximate areas of the anchorages with red polygons and the approximate locations of the berths with yellow rectangles. We apply two clustering algorithms, IMA-DBSCAN and ST-DBSCAN, to the sample data. The resulting clusters are depicted in Figures (b) and (c) respectively. Notably, blue dots in Figure (b) represent the identified anchorage areas, while those in Figure (c) represent noise, which outlines the general layout of anchorage areas but does not distinctly identify each one. In Figure (d), the anchorages from Figure (b) are shown separately in red. In Figure (e), the berths from Figure (b) are displayed separately in yellow. The four terminals are identified as Pukou, Daxie, Beilun, and Yuandong. Lastly, in Figure (f), the yellow areas depict the approximate positions of the berths as identified by ST-DBSCAN. The blue and black rectangles indicate misidentifications of noise as berths and confusion between anchorages and berths, respectively.



(a) Terminal Beilun **(b)** Terminal Daxie **(c)** Terminal Pukou **(d)** Terminal Yuandong

Figure B.4: Detailed Results of Berth Identification: IMA-DBSCAN (Top Row) vs. ST-DBSCAN (Bottom Row)

Notes. The figure displays the detailed results of berth identification for each of the four terminals: Beilun, Daxie, Pukou, and Yuandong, within the Port of Ningbo-Zhoushan. The berths identified by IMA-DBSCAN are presented in yellow on the top row, while those pinpointed by ST-DBSCAN are depicted in brown on the bottom row.

C. Discussion on the Assumptions in the Model

In this appendix, we discuss two critical assumptions in the model: matching frictions in the product market and endogenous separation of producer-retailer matches on transportation cost. First, to represent the matching frictions in a tractable manner, we assume that the number of trades between producers and retailers are governed by a matching function. Second, to succinctly capture the decision-making process between a producer and a retailer when their trade is subject to a transportation cost, we assume that upon meeting, both parties choose to endogenously separate from each other once the idiosyncratic transportation cost to pay lies above a reservation threshold. We discuss each of these two assumptions in turn.

The matching function. There is ample literature that studies the origins of matching frictions in the product market, including but not limited to locating and building connections with buyers in different locations (Benguria 2021, Krolikowski & McCallum 2021, Lenoir et al. 2022), costly information acquisition about market conditions elsewhere (Allen 2014, Chaney 2014), and informal trade barriers such as common language (Melitz & Toubal 2014) and geography (Eaton & Kortum 2002). Common across all these theories is the existence of prevalent trade barriers between producers and retailers, implying that not all the unmatched producers engage in trade, while not all the sourcing visits by retailers are successful. Consistent with these theories, we assume a constant-returns-to-scale matching function that summarizes how unmatched producers and visits of retailers are transformed into trades through the matching process. Thus, we abstract away from modeling the complex matching process while still preserving its main implication: the unmatched producers only engage in trade with probability $f(\theta)G(\tau) < 1$ and the visits of retailers to producers are only successful with probability $q(\theta)G(\tau) < 1$.

Endogenous separation on transportation cost. Much in the same way the separation margin on the labor market could be modeled endogenously when workers face productivity shocks to their employment matches and bad draws possibly lead to separations (Bils et al. 2011, Menzio & Shi 2011, Fujita & Ramey 2012), the separation margin in the product market

could be modeled endogenously when producers face idiosyncratic transportation costs to their trading relationships with retailers and bad draws possibly lead to terminations of such relationships. Such a modeling assumption is reasonable only if we find convincing evidence that (1) transportation cost is taken into account when trading partners decide on a potential trade, and (2) there exists a threshold of transportation cost above which trading partners choose to sever their relationship.

The prediction that transportation cost affects the possibility of a trade has been examined empirically in the trade literature. To name a few, evidence in Rodrigue (2020) underlines that across all modes, raising transportation costs by 10% reduces trade volumes by more than 20%. In the context of maritime transportation, Brancaccio et al. (2020) exploit changes in tariffs across the trade network to estimate the elasticity of world trade value with respect to shipping costs. They estimate that a 1% change in shipping costs leads to approximately a 1% change in world trade value. Similarly, Wong (2022) estimates the containerized trade elasticity with respect to freight rates using the round-trip effect as an instrument (in particular, for route i, j, the author uses a Bartik-style instrument to proxy for the predicted trade value on route j, i). The author reports that a 1% increase in per unit container freight rates decreases containerized trade value by 2.8% when dyad-by-product controls are included in the regression. Together, these elasticities emphasize that transportation costs are indeed taken into account when trading partners choose to form a relationship, and that a rise in transportation cost deters trade substantially.

Both theory and casual observation also suggest the presence of a reservation transportation cost, which trading partners often consider when assessing the profitability of a potential trade in the product market. Notably, to reconcile the empirical evidence that export and import intensities vary across plants, Kasahara & Lapham (2013) extend the model in Melitz (2003) by allowing for heterogeneity in transportation costs. Incorporating heterogeneous transportation costs provides a plausible self-selection mechanism regarding trade decisions, as plants with low transportation costs self-select into exporting and importing. As such, there must exist a threshold value of transportation cost below which plants choose to engage in trade.[9] Casual observations are also consistent with this theoretical prediction. For in-

[9] A similar argument can be found in the discussion of transport infrastructure and its effects on firm's

stance, according to the Global Transport Costs Dataset for International Trade (UNCTAD 2021), the cost of transporting medical care commodities by sea from China to the U.S. normally accounts for 5% of their Free On Board values. When the transportation cost rises above 5%, producers in China will reconsider whether it is still profitable to export medical care commodities to the U.S. Hence, following the Covid-19 pandemic, as the transportation cost skyrocketed while the initial increase in the final price of medical care commodities was not on par, trades collapsed as producers in China exited the market, leading to a great shortage of medical supplies in the U.S. Furthermore, it is noted that the reservation transportation cost is largely fixed in the short run, given that transportation technology and price outlook for shipping fuel are unlikely to vary in few years' time. As such, our modeling assumption regarding the flexible-price aggregate supply is consistent with the reality.

Lastly, the modeling assumption that transportation cost follows a log-normal distribution is borrowed from Kasahara & Lapham (2013). We make this crude but convenient assumption for two reasons. First, since transportation cost varies across countries, routes, directions, and commodities in reality (Brown et al. 2021), an assumption that it is randomly distributed according to a distribution is more plausible than a fixed value (for instance, the "iceberg" formulation of trade costs as in Samuelson (1954)). Second, using a log-normally distributed transportation cost provides us with a purely exogenous measure of transportation cost. With the scale parameter of the log-normal distribution of transportation costs acting as the model counterpart to the ACR index, our model mimics the positive relationship between the ACR index and shipping costs, as shown in Figure F.1.[10]

exporting decision. For instance, Naudé & Matthee (2011) argue that the availability of transport infrastructure will have a threshold effect – a certain minimum of transport infrastructure is required for a firm to start exporting, but once the threshold is reached, improved infrastructure will not necessarily have a large impact on the extent of an individual firm's exports. Since the availability of transport infrastructure (at least partially) determines the transportation cost, this argument is consistent with the presence of a reservation transportation cost that firms take into account when making an exporting decision.

[10] Alternatively, we could augment the current model with a full-fledged transportation sector in which the interactions between producers and shipowners determine the transportation cost. Such an endogenous setting can be found in Brancaccio et al. (2020), Bai & Li (2022). Nonetheless, we maintain the current setting for its tractability.

D. Long Proofs

D.1. Proof of Proposition 1

We first derive Equation (14). Rewriting Equations (12) and (13) and applying the property $\theta = f(\theta)/q(\theta)$, we obtain that:

$$\theta(p, \bar{z}) = \frac{1-\eta}{\eta\rho}\big(p - \bar{z} + \beta \mathbb{E}_{z'} S(z')\big). \tag{D.1}$$

Then we rewrite $\mathbb{E}_{z'} S(z')$. Using the definition of $S(z)$, we have:

$$S(z) = p - z + \big(1 - \eta f(\theta)\big)\beta \mathbb{E}_{z'} S(z').$$

Subtracting Equation (12) from the above equation yields $S(z) = \bar{z} - z$. Replacing $S(z')$ in $\mathbb{E}_{z'} S(z')$ with $\bar{z} - z'$, we derive that:

$$\begin{aligned}
\mathbb{E}_{z'} S(z') &= \int_0^{\bar{z}} (\bar{z} - z') dG(z') \\
&= (\bar{z} - z') G(z') \Big|_0^{\bar{z}} + \int_0^{\bar{z}} G(z') dz' \\
&= \int_0^{\bar{z}} G(z') dz'.
\end{aligned}$$

Subsequently, replacing $\mathbb{E}_{z'} S(z')$ in Equation (D.1) with $\int_0^{\bar{z}} G(z') dz'$ gives Equation (14).

The first property is obvious. Since θ cannot be negative, for a given $\bar{z}$, p is bounded on $[p^{min}, +\infty)$, where p^{min} is such that it solves $p^{min} - \bar{z} + \beta \int_0^{\bar{z}} G(z') dz' = 0$ for any $\bar{z} > 0$. As for the second and third properties, we derive that:

$$\frac{\partial \theta(p, \bar{z})}{\partial p} = \frac{1-\eta}{\eta\rho} > 0.$$

Hence, the product market tightness $\theta(p, \bar{z})$ is strictly increasing and linear on $[p^{min}, +\infty)$.

The fourth property is also obvious from the definition of $\bar{z}^{max}$, as θ cannot be negative. In terms of the fifth and last properties, we derive that:

$$\frac{\partial \theta(p, \bar{z})}{\partial \bar{z}} = \frac{1-\eta}{\eta\rho}\big(-1 + \beta G(\bar{z})\big) < 0,$$

$$\frac{\partial^2\theta(p,\bar{z})}{\partial\bar{z}^2} = \frac{(1-\eta)\beta}{\eta\rho}\frac{1}{\bar{z}\sigma}\phi(\frac{\log\bar{z}-\gamma}{\sigma}) > 0,$$

where $\phi(.)$ is the standard normal probability density function. Hence, the product market tightness $\theta(p,\bar{z})$ is strictly decreasing and convex on $(0,\bar{z}^{max}]$.

D.2. Proof of Proposition 2

The first property is obvious. When $p = p^{min}$, $\theta(p^{min}) = 0$, $f\big(\theta(p^{min})\big) = 0$, and $c_s^{flex}(p^{min}) = 0$. When $p \to +\infty$, $\lim_{p\to+\infty}\theta(p) = +\infty$, $\lim_{p\to+\infty} f\big(\theta(p)\big) = 1$, and hence $\lim_{p\to+\infty} c_s^{flex}(p) = G(\tau)l$. In terms of the second and third properties, we derive that:

$$\frac{dc_s^{flex}(p)}{dp} = \frac{1-\eta}{\eta\rho}\frac{\big(1-G(\tau)\big)q(\theta)^{1+\xi}G(\tau)l}{\big(1-G(\tau)+f(\theta)G(\tau)\big)^2} > 0,$$

$$\begin{aligned}\frac{d^2c_s^{flex}(p)}{dp^2} =& -\Big(\frac{1-\eta}{\eta\rho}\Big)^2\big(1-G(\tau)\big)G(\tau)l \\ &\cdot\frac{\big(1-G(\tau)+f(\theta)G(\tau)\big)\theta^{\xi-1}(1+\xi)(1+\theta^{\xi})^{-\frac{1+\xi}{\xi}-1} + 2G(\tau)q(\theta)^{2(1+\xi)}}{\big(1-G(\tau)+f(\theta)G(\tau)\big)^3} < 0.\end{aligned}$$

Hence, the flexible-price aggregate supply c_s^{flex} is strictly increasing and concave on $[p^{min},+\infty)$.

D.3. Proof of Proposition 4

Since we look for a flexible-price equilibrium with positive consumption, we restrict our search of price p within the range $[p^{min},+\infty)$. The equilibrium condition (21) can be re-written as:

$$\frac{f\big(\theta(p)\big)p}{1-G(\tau)+f\big(\theta(p)\big)G(\tau)} = \frac{\chi^{\epsilon}}{1+\chi^{\epsilon}}\frac{\mu}{G(\tau)l}. \tag{D.2}$$

For any $\tau > 0$, the right hand side is a constant that is strictly positive. For the left hand side, when $p = p^{min}$, $\theta(p^{min}) = 0$, and $f\big(\theta(p^{min})\big) = 0$, it has a limit of zero; when $p \to +\infty$, $\lim_{p\to+\infty}\theta(p) = +\infty$, and $\lim_{p\to+\infty} f\big(\theta(p)\big) = 1$, it has a limit of positive infinity. For $p \in [p^{min},+\infty)$, the derivative of the left hand side with respect to p is given by:

$$\frac{d}{dp}\Big[\frac{f\big(\theta(p)\big)p}{1-G(\tau)+f\big(\theta(p)\big)G(\tau)}\Big] = \frac{\big(1-G(\tau)\big)\frac{1-\eta}{\eta\rho}q(\theta)^{1+\xi}p + f(\theta)\big(1-G(\tau)+f(\theta)G(\tau)\big)}{\big(1-G(\tau)+f(\theta)G(\tau)\big)^2} > 0.$$

Therefore, the left hand side is strictly increasing from zero to positive infinity on $[p^{min}, +\infty)$. As such, there is a unique $p \in [p^{min}, +\infty)$ that solves Equation (D.2).

D.4. Proof of Proposition 5

We first consider an adverse shock to aggregate demand. No matter whether the negative aggregate demand shock is represented by a decrease in money supply μ or in the taste for consumption of goods χ, the right hand side of Equation (D.2) will decrease. To balance both sides of Equation (D.2), price p will decrease, since the derivative of the left hand side with respect to p is positive (see the proof for Proposition 4). As p decreases, by the second property in Proposition 1 and the second property in Proposition 2, product market tightness θ and consumption (or equivalently, output) c will decrease. Since both p and θ decrease, according to Equation (10), wholesale price r will decline as well. For the matching cost, $G(\tau)l - c$, and spare capacity (or equivalently, unemployment), $l - c$, since they both are strictly decreasing in c, they will increase following an adverse shock to aggregate demand.

Next, we consider an adverse shock to productive capacity, which is parameterized by a decrease in l. On impact, the right hand side of Equation (D.2) increases. Similar to the above reasoning, price p will increase. As p increases, by the second property in Proposition 1 and Proposition 3, product market tightness θ will increase while consumption (or equivalently, output) c will fall. Again, since both p and θ increase, according to Equation (10), wholesale price r will rise. In terms of the matching cost and spare capacity (or equivalently, unemployment), they can be alternatively expressed as:

$$matching\ cost = \frac{\big(1 - G(\tau)\big)\big(1 - f(\theta)\big)}{1 - \big(1 - f(\theta)\big)G(\tau)} G(\tau)l,$$

$$spare\ capacity = \frac{1 - G(\tau)}{1 - G(\tau) + f(\theta)G(\tau)} l,$$

respectively. With θ increasing and l decreasing following the capacity shock, it is easy to verify that both the matching cost and spare capacity will decrease.

Lastly, we consider an adverse shock to the supply chain, which is represented by an increase in γ, i.e., the scale parameter of the log-normal distribution of transportation costs $G(.)$. We first look at the effect on price. Using the re-arranged equilibrium condition (D.2),

we define a function $\mathbb{T} : [p^{min}, +\infty) \times \mathbb{R} \to \mathbb{R}$:

$$\mathbb{T}(p,\gamma) = \frac{\chi^{\epsilon}}{1+\chi^{\epsilon}}\frac{\mu}{G(\tau)l} - \frac{f(\theta)p}{1-G(\tau)+f(\theta)G(\tau)}$$
$$= \frac{\chi^{\epsilon}}{1+\chi^{\epsilon}}\frac{\mu}{\Phi(\frac{\log\tau-\gamma}{\sigma})l} - \frac{\big\{1+\big[\frac{1-\eta}{\eta\rho}\big(p-\tau+\beta\int_0^{\tau}\Phi(\frac{\log z'-\gamma}{\sigma})dz'\big)\big]^{-\xi}\big\}^{-\frac{1}{\xi}}p}{1-\Phi(\frac{\log\tau-\gamma}{\sigma})+\big\{1+\big[\frac{1-\eta}{\eta\rho}\big(p-\tau+\beta\int_0^{\tau}\Phi(\frac{\log z'-\gamma}{\sigma})dz'\big)\big]^{-\xi}\big\}^{-\frac{1}{\xi}}\Phi(\frac{\log\tau-\gamma}{\sigma})},$$

where $\Phi(.)$ is the standard normal cumulative density function. Assuming the existence of a tuple $(p_0,\gamma_0) \in [p^{min}, +\infty) \times \mathbb{R}$ such that $\mathbb{T}(p_0,\gamma_0) = 0$ and $\partial\mathbb{T}(p,\gamma)/\partial p|_{p=p_0,\gamma=\gamma_0} \neq 0$, by the Implicit Function Theorem, there is a neighborhood of (p_0,γ_0) such that whenever γ is sufficiently close to γ_0, there is a unique p so that $\mathbb{T}(p,\gamma) = 0$. This assignment makes p a continuous function of γ. Applying implicit differentiation to $\mathbb{T}(p,\gamma)$ around (p_0,γ_0) yields:

$$\frac{dp(\gamma)}{d\gamma} = -\frac{\partial\mathbb{T}(p,\gamma)/\partial\gamma}{\partial\mathbb{T}(p,\gamma)/\partial p}.$$

In terms of $\partial\mathbb{T}(p,\gamma)/\partial\gamma$, we derive that:

$$\frac{\partial\mathbb{T}(p,\gamma)}{\partial\gamma} = \frac{\chi^{\epsilon}}{1+\chi^{\epsilon}}\frac{\mu}{l}\frac{\frac{1}{\sigma}g(\tau)}{G(\tau)^2} + \frac{\big(1-G(\tau)\big)\frac{(1-\eta)\beta}{\eta\rho}\big[\int_0^{\tau}\frac{1}{\sigma}g(z')dz'\big]q(\theta)^{1+\xi}p}{\big(1-G(\tau)+f(\theta)G(\tau)\big)^2}$$
$$+ \frac{\big(1-f(\theta)\big)f(\theta)p\frac{1}{\sigma}g(\tau)}{\big(1-G(\tau)+f(\theta)G(\tau)\big)^2} > 0,$$

where $g(\tau) \equiv \phi[(\log\tau-\gamma)/\sigma]$, $g(z') \equiv \phi[(\log z'-\gamma)/\sigma]$, while $\phi(.)$ is the standard normal probability density function. In terms of $\partial\mathbb{T}(p,\gamma)/\partial p$, it can be written as:

$$\frac{\partial\mathbb{T}(p,\gamma)}{\partial p} = -\frac{\big(1-G(\tau)\big)\frac{1-\eta}{\eta\rho}q(\theta)^{1+\xi}p + f(\theta)\big(1-G(\tau)+f(\theta)G(\tau)\big)}{\big(1-G(\tau)+f(\theta)G(\tau)\big)^2} < 0.$$

By combining $\partial\mathbb{T}(p,\gamma)/\partial\gamma$ with $\partial\mathbb{T}(p,\gamma)/\partial p$ and collecting terms, we have:

$$\begin{aligned}\frac{dp(\gamma)}{d\gamma} =& \big[\big(1-G(\tau)\big)\frac{1-\eta}{\eta\rho}q(\theta)^{1+\xi}p + f(\theta)\big(1-G(\tau)+f(\theta)G(\tau)\big)\big]^{-1}\\ &\cdot\Big\{\big(1-G(\tau)+f(\theta)G(\tau)\big)f(\theta)\frac{1}{\sigma}g(\tau)\frac{p}{G(\tau)}\\ &+\big(1-G(\tau)\big)\frac{(1-\eta)\beta}{\eta\rho}\big[\int_0^{\tau}\frac{1}{\sigma}g(z')dz'\big]q(\theta)^{1+\xi}p\\ &+\big(1-f(\theta)\big)f(\theta)p\frac{1}{\sigma}g(\tau)\Big\} > 0.\end{aligned} \tag{D.3}$$

Hence, price p will increase on impact of an adverse shock to the supply chain. In terms of

consumption (or equivalently, output), it is written as:

$$c(\gamma) = \frac{\chi^{\epsilon}}{1+\chi^{\epsilon}} \frac{\mu}{p(\gamma)},$$

where p is an implicit function of γ. Therefore, the derivative of c with respect to γ is:

$$\begin{aligned}
\frac{dc(\gamma)}{d\gamma} = &- \frac{\chi^{\epsilon}}{1+\chi^{\epsilon}} \frac{\mu}{p} \big[\big(1-G(\tau)\big) \frac{1-\eta}{\eta\rho} q(\theta)^{1+\xi} p + f(\theta)\big(1-G(\tau)+f(\theta)G(\tau)\big) \big]^{-1} \\
&\cdot \Big\{ \big(1-G(\tau)+f(\theta)G(\tau)\big) f(\theta) \frac{1}{\sigma} g(\tau) \frac{1}{G(\tau)} \\
&+ \big(1-G(\tau)\big) \frac{(1-\eta)\beta}{\eta\rho} \big[\int_0^{\tau} \frac{1}{\sigma} g(z')dz' \big] q(\theta)^{1+\xi} \\
&+ \big(1-f(\theta)\big) f(\theta) \frac{1}{\sigma} g(\tau) \Big\} < 0.
\end{aligned}$$

Hence, consumption (or equivalently, output) c will fall. Next, in terms of product market tightness, it is given by:

$$\theta(\gamma) = \frac{1-\eta}{\eta\rho} \big(p(\gamma) - \tau + \beta \int_0^{\tau} \Phi(\frac{\log z' - \gamma}{\sigma}) dz' \big). \tag{D.4}$$

Accordingly, the derivative of θ with respect to γ is:

$$\begin{aligned}
\frac{d\theta(\gamma)}{d\gamma} = &\frac{1-\eta}{\eta\rho} \big[\big(1-G(\tau)\big) \frac{1-\eta}{\eta\rho} q(\theta)^{1+\xi} p + f(\theta)\big(1-G(\tau)+f(\theta)G(\tau)\big) \big]^{-1} \\
&\cdot \Big\{ \big(1-G(\tau)+f(\theta)G(\tau)\big) f(\theta) \frac{1}{\sigma} g(\tau) \frac{p}{G(\tau)} + \big(1-f(\theta)\big) f(\theta) p \frac{1}{\sigma} g(\tau) \\
&- \big(1-G(\tau)+f(\theta)G(\tau)\big) f(\theta) \beta \big[\int_0^{\tau} \frac{1}{\sigma} g(z')dz' \big] \Big\},
\end{aligned} \tag{D.5}$$

whose value depends on the values of θ and p; as we will discuss later in Appendix D.6, this dependence is crucial for the state-dependence result of a contractionary monetary policy shock. Similarly, by substituting Equation (D.4) into Equation (10), the wholesale price can be expressed as:

$$r(\gamma) = p(\gamma) + (1-\eta)\beta \int_0^{\tau} \Phi(\frac{\log z' - \gamma}{\sigma}) dz' + (1-\eta)(z-\tau).$$

Differentiating $r(\gamma)$ with respect to γ yields:

$$\begin{aligned}\frac{dr(\gamma)}{d\gamma} =&\big[\big(1-G(\tau)\big)\frac{1-\eta}{\eta\rho}q(\theta)^{1+\xi}p + f(\theta)\big(1-G(\tau)+f(\theta)G(\tau)\big)\big]^{-1}\\ &\cdot\Big\{\big(1-G(\tau)+f(\theta)G(\tau)\big)f(\theta)\frac{1}{\sigma}g(\tau)\frac{p}{G(\tau)}\\ &+\big(1-G(\tau)\big)\frac{(1-\eta)\beta}{\rho}\big[\int_0^\tau \frac{1}{\sigma}g(z')dz'\big]q(\theta)^{1+\xi}p\\ &+\big(1-f(\theta)\big)f(\theta)p\frac{1}{\sigma}g(\tau)\\ &-\big(1-G(\tau)+f(\theta)G(\tau)\big)f(\theta)(1-\eta)\beta\big[\int_0^\tau \frac{1}{\sigma}g(z')dz'\big]\Big\},\end{aligned}$$

whose value is also dependent on the values of θ and p. As for the matching cost, given that it is measured by the difference between $G(\tau)l$ and c, its derivative with respect to γ can be written as:

$$\begin{aligned}\frac{d}{d\gamma}\big[\textit{matching cost}(\gamma)\big] =&\big[\big(1-G(\tau)\big)\frac{1-\eta}{\eta\rho}q(\theta)^{1+\xi}p + f(\theta)\big(1-G(\tau)+f(\theta)G(\tau)\big)\big]^{-1}\\ &\cdot\Big(\frac{\chi^\epsilon}{1+\chi^\epsilon}\frac{\mu}{p}\Big\{\big(1-G(\tau)+f(\theta)G(\tau)\big)f(\theta)\frac{1}{\sigma}g(\tau)\frac{1}{G(\tau)}\\ &+\big(1-G(\tau)\big)\frac{(1-\eta)\beta}{\eta\rho}\big[\int_0^\tau \frac{1}{\sigma}g(z')dz'\big]q(\theta)^{1+\xi}\\ &+\big(1-f(\theta)\big)f(\theta)\frac{1}{\sigma}g(\tau)\Big\}\\ &-\big(1-G(\tau)\big)\frac{1-\eta}{\eta\rho}q(\theta)^{1+\xi}p\frac{1}{\sigma}g(\tau)l\\ &-f(\theta)\big(1-G(\tau)+f(\theta)G(\tau)\big)\frac{1}{\sigma}g(\tau)l\Big),\end{aligned}$$

whose value is again dependent on the values of θ and p. On the contrary, since the spare capacity (or equivalently, unemployment) is measured by the difference between l and c, its derivative with respect to γ is positive, i.e.,

$$\begin{aligned}\frac{d}{d\gamma}\big[\textit{spare capacity}(\gamma)\big] =&\frac{\chi^\epsilon}{1+\chi^\epsilon}\frac{\mu}{p}\big[\big(1-G(\tau)\big)\frac{1-\eta}{\eta\rho}q(\theta)^{1+\xi}p + f(\theta)\big(1-G(\tau)+f(\theta)G(\tau)\big)\big]^{-1}\\ &\cdot\Big\{\big(1-G(\tau)+f(\theta)G(\tau)\big)f(\theta)\frac{1}{\sigma}g(\tau)\frac{1}{G(\tau)}\\ &+\big(1-G(\tau)\big)\frac{(1-\eta)\beta}{\eta\rho}\big[\int_0^\tau \frac{1}{\sigma}g(z')dz'\big]q(\theta)^{1+\xi}\\ &+\big(1-f(\theta)\big)f(\theta)\frac{1}{\sigma}g(\tau)\Big\} > 0.\end{aligned}$$

D.5. Slope of the Aggregate Supply Curve and Its Dependence on Product Market Tightness

Given Equation (18), the slope of the aggregate supply curve is given by:

$$\frac{dc_s^{flex}}{dp} = \frac{(1-\eta)l}{\eta\rho} \frac{\big(1-G(\tau)\big)G(\tau)\big(1+\theta^{\xi}\big)^{-\frac{1+\xi}{\xi}}}{\big[1-G(\tau)+\big(1+\theta^{-\xi}\big)^{-\frac{1}{\xi}}G(\tau)\big]^2}.$$

Differentiating it with respect to θ yields:

$$\begin{aligned}\frac{d^2c_s^{flex}}{dpd\theta} = &-\frac{(1-\eta)l}{\eta\rho}\frac{1}{\big[1-G(\tau)+\big(1+\theta^{-\xi}\big)^{-\frac{1}{\xi}}G(\tau)\big]^3} \\ &\cdot\Big\{\big[1-G(\tau)+\big(1+\theta^{-\xi}\big)^{-\frac{1}{\xi}}G(\tau)\big]\big(1-G(\tau)\big)G(\tau)\theta^{\xi-1}(1+\xi)\big(1+\theta^{\xi}\big)^{-\frac{1+\xi}{\xi}-1} \\ &+2\big(1-G(\tau)\big)G(\tau)^2\big(1+\theta^{\xi}\big)^{-\frac{2(1+\xi)}{\xi}}\Big\} < 0.\end{aligned}$$

Therefore, the aggregate supply curve becomes steeper in the (Q,p) plane as the product market tightness increases.

Furthermore, to complement our discussion in Section 3.4 about the response of the system to an adverse shock to the supply chain, the alternative scenario in which the price increase fails to elevate product market tightness at the new equilibrium is depicted in the following figure.

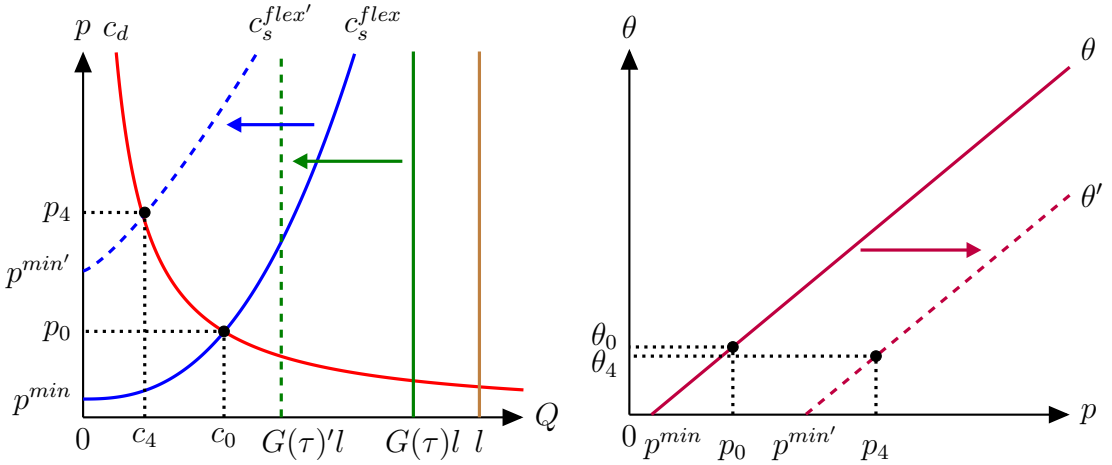


Figure D.1: Alternative Scenario When There Is an Adverse Shock to Supply Chain

D.6. Proof of Proposition 6

We start the proof by re-visiting the function $\mathbb{T} : [p^{min}, +\infty) \times \mathbb{R}^+ \times \mathbb{R} \to \mathbb{R}$:

$$\mathbb{T}(p,\mu,\gamma) = \frac{\chi^\epsilon}{1+\chi^\epsilon}\frac{\mu}{G(\tau)l} - \frac{f(\theta)p}{1-G(\tau)+f(\theta)G(\tau)}$$
$$= \frac{\chi^\epsilon}{1+\chi^\epsilon}\frac{\mu}{\Phi(\frac{\log\tau-\gamma}{\sigma})l} - \frac{\left\{1+\left[\frac{1-\eta}{\eta\rho}\left(p-\tau+\beta\int_0^\tau \Phi(\frac{\log z'-\gamma}{\sigma})dz'\right)\right]^{-\xi}\right\}^{-\frac{1}{\xi}}p}{1-\Phi(\frac{\log\tau-\gamma}{\sigma})+\left\{1+\left[\frac{1-\eta}{\eta\rho}\left(p-\tau+\beta\int_0^\tau \Phi(\frac{\log z'-\gamma}{\sigma})dz'\right)\right]^{-\xi}\right\}^{-\frac{1}{\xi}}\Phi(\frac{\log\tau-\gamma}{\sigma})},$$

where $\Phi(.)$ is the standard normal cumulative density function. Subsequently, assuming the existence of a tuple $(p_0,\mu_0,\gamma_0) \in [p^{min},+\infty)\times\mathbb{R}^+\times\mathbb{R}$ such that $\mathbb{T}(p_0,\mu_0,\gamma_0)=0$ and $\partial\mathbb{T}(p,\mu,\gamma)/\partial p|_{p=p_0,\mu=\mu_0,\gamma=\gamma_0} \neq 0$, by the Implicit Function Theorem, there is a neighborhood of (p_0,μ_0,γ_0) such that whenever (μ,γ) is sufficiently close to (μ_0,γ_0), there is a unique p so that $\mathbb{T}(p,\mu,\gamma)=0$. This assignment makes p a continuous function of μ and γ. Applying implicit differentiation to $\mathbb{T}(p,\mu,\gamma)$ around (p_0,μ_0,γ_0) yields:

$$\frac{\partial p(\mu,\gamma)}{\partial\mu} = -\frac{\partial\mathbb{T}(p,\mu,\gamma)/\partial\mu}{\partial\mathbb{T}(p,\mu,\gamma)/\partial p}.$$

The numerator can be written as:

$$\frac{\partial\mathbb{T}(p,\mu,\gamma)}{\partial\mu} = \frac{\chi^\epsilon}{1+\chi^\epsilon}\frac{1}{G(\tau)l} > 0,$$

whereas the denominator is given by:

$$\frac{\partial\mathbb{T}(p,\mu,\gamma)}{\partial p} = -\frac{\big(1-G(\tau)\big)\frac{1-\eta}{\eta\rho}q(\theta)^{1+\xi}p + f(\theta)\big(1-G(\tau)+f(\theta)G(\tau)\big)}{\big(1-G(\tau)+f(\theta)G(\tau)\big)^2} < 0.$$

By combining $\partial\mathbb{T}(p,\mu,\gamma)/\partial\mu$ with $\partial\mathbb{T}(p,\mu,\gamma)/\partial p$, we derive that:

$$\frac{\partial p(\mu,\gamma)}{\partial\mu} = \frac{\chi^\epsilon}{1+\chi^\epsilon}\frac{1}{G(\tau)l}\frac{\big(1-G(\tau)+f(\theta)G(\tau)\big)^2}{\big(1-G(\tau)\big)\frac{1-\eta}{\eta\rho}q(\theta)^{1+\xi}p + f(\theta)\big(1-G(\tau)+f(\theta)G(\tau)\big)}$$
$$= \frac{1}{\mu}\left[\frac{\big(1-G(\tau)\big)\frac{1-\eta}{\eta\rho}q(\theta)^{1+\xi}}{f(\theta)\big(1-G(\tau)+f(\theta)G(\tau)\big)} + \frac{1}{p}\right]^{-1} > 0,$$

where the last step is obtained because:

$$\mathbb{T}(p,\mu,\gamma)=0 \;\Rightarrow\; \frac{\chi^\epsilon}{1+\chi^\epsilon}\frac{1}{G(\tau)l} = \frac{f(\theta)p}{\mu\big(1-G(\tau)+f(\theta)G(\tau)\big)}.$$

In terms of the partial derivative of consumption (or equivalently, output) with respect to μ, using the expression of the aggregate demand in Equation (20), we can derive that:

$$\begin{aligned}\frac{\partial c(\mu,\gamma)}{\partial \mu} &= \frac{\chi^{\epsilon}}{1+\chi^{\epsilon}} \frac{\big(1-G(\tau)\big)^{\frac{1-\eta}{\eta\rho}} q(\theta)^{1+\xi}}{\big(1-G(\tau)\big)^{\frac{1-\eta}{\eta\rho}} q(\theta)^{1+\xi} p + f(\theta)\big(1-G(\tau)+f(\theta)G(\tau)\big)} \\ &= \frac{\chi^{\epsilon}}{1+\chi^{\epsilon}} \Big[p + \frac{f(\theta)\big(1-G(\tau)+f(\theta)G(\tau)\big)}{\big(1-G(\tau)\big)^{\frac{1-\eta}{\eta\rho}} q(\theta)^{1+\xi}}\Big]^{-1} > 0.\end{aligned}$$

Hence, both the partial derivatives $\partial p(\mu,\gamma)/\partial\mu$ and $\partial c(\mu,\gamma)/\partial\mu$ depend on the fraction:

$$\frac{\big(1-G(\tau)\big)^{\frac{1-\eta}{\eta\rho}} q(\theta)^{1+\xi}}{f(\theta)\big(1-G(\tau)+f(\theta)G(\tau)\big)}. \tag{D.6}$$

Next, we study the dependence of the fraction (D.6) on γ, as it directly determines the signs of the cross derivatives $\partial^2 p(\mu,\gamma)/\partial\mu\partial\gamma$ and $\partial^2 c(\mu,\gamma)/\partial\mu\partial\gamma$. It is given by:

$$\begin{aligned}\frac{\partial}{\partial\gamma}\Big[\frac{\big(1-G(\tau)\big)^{\frac{1-\eta}{\eta\rho}} q(\theta)^{1+\xi}}{f(\theta)\big(1-G(\tau)+f(\theta)G(\tau)\big)}\Big] &= \frac{f(\theta)\big(1-G(\tau)+f(\theta)G(\tau)\big)\big[\frac{1}{\sigma}g(\tau)\frac{1-\eta}{\eta\rho}q(\theta)^{1+\xi}\big]}{\big[f(\theta)\big(1-G(\tau)+f(\theta)G(\tau)\big)\big]^2} \\ &- \frac{f(\theta)\big(1-G(\tau)+f(\theta)G(\tau)\big)\big[\big(1-G(\tau)\big)^{\frac{1-\eta}{\eta\rho}}\frac{\partial\theta(\mu,\gamma)}{\partial\gamma}(1+\xi)\theta^{\xi-1}(1+\theta^{\xi})^{-\frac{1+\xi}{\xi}-1}\big]}{\big[f(\theta)\big(1-G(\tau)+f(\theta)G(\tau)\big)\big]^2} \\ &- \frac{\big(1-G(\tau)\big)^{\frac{1-\eta}{\eta\rho}} q(\theta)^{1+\xi}\big[\frac{\partial\theta(\mu,\gamma)}{\partial\gamma}q(\theta)^{1+\xi}\big(1-G(\tau)+f(\theta)G(\tau)\big)\big]}{\big[f(\theta)\big(1-G(\tau)+f(\theta)G(\tau)\big)\big]^2} \\ &- \frac{\big(1-G(\tau)\big)^{\frac{1-\eta}{\eta\rho}} q(\theta)^{1+\xi}\big[f(\theta)\big(\frac{1}{\sigma}g(\tau)+\frac{\partial\theta(\mu,\gamma)}{\partial\gamma}q(\theta)^{1+\xi}G(\tau)-f(\theta)\frac{1}{\sigma}g(\tau)\big)\big]}{\big[f(\theta)\big(1-G(\tau)+f(\theta)G(\tau)\big)\big]^2},\end{aligned}$$

and is proportional to:

$$\begin{aligned}\frac{\partial}{\partial\gamma}\Big[\frac{\big(1-G(\tau)\big)^{\frac{1-\eta}{\eta\rho}} q(\theta)^{1+\xi}}{f(\theta)\big(1-G(\tau)+f(\theta)G(\tau)\big)}\Big] &\propto f(\theta)^2\frac{1}{\sigma}g(\tau) \\ &- f(\theta)\big(1-G(\tau)+f(\theta)G(\tau)\big)\big(1-G(\tau)\big)\frac{\partial\theta(\mu,\gamma)}{\partial\gamma}(1+\xi)\frac{\theta^{\xi-1}}{1+\theta^{\xi}} \\ &- \big(1-G(\tau)\big)\frac{\partial\theta(\mu,\gamma)}{\partial\gamma}q(\theta)^{1+\xi}\big(1-G(\tau)+f(\theta)G(\tau)\big) \\ &- \big(1-G(\tau)\big)f(\theta)\frac{\partial\theta(\mu,\gamma)}{\partial\gamma}q(\theta)^{1+\xi}G(\tau),\end{aligned}$$

where $g(\tau)\equiv\phi[(\log\tau-\gamma)/\sigma]$ and $\phi(.)$ is the standard normal probability density function.

When the partial derivative of θ with respect to γ satisfies:

$$\frac{\partial\theta(\mu,\gamma)}{\partial\gamma} > \frac{f(\theta)^2\frac{1}{\sigma}g(\tau)}{\big(1-G(\tau)\big)f(\theta)q(\theta)^{1+\xi}G(\tau)} = \frac{\theta(1+\theta^{\xi})\frac{1}{\sigma}g(\tau)}{\big(1-G(\tau)\big)G(\tau)} > 0,$$

it is easy to verify that:

$$\frac{\partial}{\partial\gamma}\Big[\frac{\big(1-G(\tau)\big)\frac{1-\eta}{\eta\rho}q(\theta)^{1+\xi}}{f(\theta)\big(1-G(\tau)+f(\theta)G(\tau)\big)}\Big] < 0,$$

and the values of the cross derivatives can thus be determined:

$$\begin{aligned}\frac{\partial^2 p(\mu,\gamma)}{\partial\mu\partial\gamma} = &-\Big\{\frac{\partial}{\partial\gamma}\Big[\frac{\big(1-G(\tau)\big)\frac{1-\eta}{\eta\rho}q(\theta)^{1+\xi}}{f(\theta)\big(1-G(\tau)+f(\theta)G(\tau)\big)}\Big] - \frac{\partial p(\mu,\gamma)}{\partial\gamma}\frac{1}{p^2}\Big\}\\ &\cdot\Big[\frac{\big(1-G(\tau)\big)\frac{1-\eta}{\eta\rho}q(\theta)^{1+\xi}}{f(\theta)\big(1-G(\tau)+f(\theta)G(\tau)\big)}+\frac{1}{p}\Big]^{-2}\frac{1}{\mu} > 0,\end{aligned}$$

$$\begin{aligned}\frac{\partial^2 c(\mu,\gamma)}{\partial\mu\partial\gamma} = &-\Big\{\frac{\partial p(\mu,\gamma)}{\partial\gamma} - \frac{\partial}{\partial\gamma}\Big[\frac{\big(1-G(\tau)\big)\frac{1-\eta}{\eta\rho}q(\theta)^{1+\xi}}{f(\theta)\big(1-G(\tau)+f(\theta)G(\tau)\big)}\Big]\Big[\frac{\big(1-G(\tau)\big)\frac{1-\eta}{\eta\rho}q(\theta)^{1+\xi}}{f(\theta)\big(1-G(\tau)+f(\theta)G(\tau)\big)}\Big]^{-2}\Big\}\\ &\cdot\Big[p+\frac{f(\theta)\big(1-G(\tau)+f(\theta)G(\tau)\big)}{\big(1-G(\tau)\big)\frac{1-\eta}{\eta\rho}q(\theta)^{1+\xi}}\Big]^{-2}\frac{\chi^{\epsilon}}{1+\chi^{\epsilon}} < 0,\end{aligned}$$

where $\partial p(\mu,\gamma)/\partial\gamma > 0$ according to Equation (D.3). With them, it is straightforward to derive the rest of the cross derivatives. In terms of product market tightness, we have:

$$\frac{\partial\theta(\mu,\gamma)}{\partial\mu} = \frac{1-\eta}{\eta\rho}\frac{\partial p(\mu,\gamma)}{\partial\mu} > 0,\ \ \frac{\partial^2\theta(\mu,\gamma)}{\partial\mu\partial\gamma} = \frac{1-\eta}{\eta\rho}\frac{\partial^2 p(\mu,\gamma)}{\partial\mu\partial\gamma} > 0.$$

As for wholesale price, its cross derivative with respect to μ and γ is given by:

$$\frac{\partial r(\mu,\gamma)}{\partial\mu} = \frac{\partial p(\mu,\gamma)}{\partial\mu} > 0,\ \ \frac{\partial^2 r(\mu,\gamma)}{\partial\mu\partial\gamma} = \frac{\partial^2 p(\mu,\gamma)}{\partial\mu\partial\gamma} > 0.$$

Similarly, for matching cost, its cross derivative is written as:

$$\frac{\partial}{\partial\mu}\big[G(\tau)l - c(\mu,l)\big] = -\frac{\partial c(\mu,\gamma)}{\partial\mu} < 0,\ \ \frac{\partial^2}{\partial\mu\partial\gamma}\big[G(\tau)l - c(\mu,l)\big] = -\frac{\partial^2 c(\mu,\gamma)}{\partial\mu\partial\gamma} > 0.$$

Finally, in terms of spare capacity (or equivalently, unemployment), we derive that:

$$\frac{\partial}{\partial\mu}\big[l - c(\mu,l)\big] = -\frac{\partial c(\mu,\gamma)}{\partial\mu} < 0,\ \ \frac{\partial^2}{\partial\mu\partial\gamma}\big[l - c(\mu,l)\big] = -\frac{\partial^2 c(\mu,\gamma)}{\partial\mu\partial\gamma} > 0.$$

D.7. Theoretical Prediction on the Effectiveness of Monetary Policy When Productive Capacity Is Constrained

In this appendix, we derive our theoretical prediction for the effectiveness of monetary policy in controlling inflation and output, depending on whether the productive capacity of the economy is constrained or not. Similar to the scenario in which the supply chain is disrupted (as in Proposition 6), contractionary monetary policy is more effective at taming inflation and reducing the sensitivity of output when the productive capacity is constrained. The only difference, as we will elaborate below, is that the state-dependent effects of monetary policy are no longer conditional.

Referring to our theoretical model described in Section 3, we describe a change in the stance of monetary policy through a change in money supply μ. The productive capacity being constrained or not is represented by a change in labor supply l. The comparative statics are summarized in Proposition 6′.

Proposition 6′. *For any given threshold of reservation transportation cost $\tau > 0$ and parameter values relevant for monetary policy $\mu \in \mathbb{R}^+$ and productive capacity $l \in \mathbb{R}^+$, the responses of the endogenous variables to a change in monetary policy are described by the following partial derivatives:*

$$\frac{\partial c(\mu,l)}{\partial \mu} > 0,\ \frac{\partial p(\mu,l)}{\partial \mu} > 0,\ \frac{\partial \theta(\mu,l)}{\partial \mu} > 0,\ \frac{\partial r(\mu,l)}{\partial \mu} > 0,$$
$$\frac{\partial}{\partial \mu}\big[G(\tau)l - c(\mu,l)\big] < 0,\ \frac{\partial}{\partial \mu}\big[l - c(\mu,l)\big] < 0.$$

The cross derivatives that describe the variations in the responses of the endogenous variables ascribed to the constrained productive capacity satisfy:

$$\frac{\partial^2 c(\mu,l)}{\partial \mu \partial l} > 0,\ \frac{\partial^2 p(\mu,l)}{\partial \mu \partial l} < 0,\ \frac{\partial^2 \theta(\mu,l)}{\partial \mu \partial l} < 0,\ \frac{\partial^2 r(\mu,l)}{\partial \mu \partial l} < 0,$$
$$\frac{\partial^2}{\partial \mu \partial l}\big[G(\tau)l - c(\mu,l)\big] < 0,\ \frac{\partial^2}{\partial \mu \partial l}\big[l - c(\mu,l)\big] < 0,$$

where $c, p, \theta, r, G(\tau)l - c$, and $l - c$ represent consumption (or equivalently, output), price, product market tightness, wholesale price, matching cost, and spare capacity (or equivalently, unemployment), respectively.

Proof. Once again, we reply on the Implicit Function Theorem to derive the partial derivative $\partial p(\mu, l)/\partial \mu$. Consider the function $\mathbb{T} : [p^{min}, +\infty) \times \mathbb{R}^+ \times \mathbb{R}^+ \to \mathbb{R}$:

$$\begin{aligned}\mathbb{T}(p, \mu, l) &= \frac{\chi^\epsilon}{1+\chi^\epsilon}\frac{\mu}{G(\tau)l} - \frac{f(\theta)p}{1-G(\tau)+f(\theta)G(\tau)} \\ &= \frac{\chi^\epsilon}{1+\chi^\epsilon}\frac{\mu}{G(\tau)l} - \frac{\left\{1+\left[\frac{1-\eta}{\eta\rho}\left(p-\tau+\beta\int_0^\tau G(z')dz'\right)\right]^{-\xi}\right\}^{-\frac{1}{\xi}}p}{1-G(\tau)+\left\{1+\left[\frac{1-\eta}{\eta\rho}\left(p-\tau+\beta\int_0^\tau G(z')dz'\right)\right]^{-\xi}\right\}^{-\frac{1}{\xi}}G(\tau)}.\end{aligned}$$

Subsequently, assuming the existence of a tuple $(p_0, \mu_0, l_0) \in [p^{min}, +\infty) \times \mathbb{R}^+ \times \mathbb{R}^+$ such that $\mathbb{T}(p_0, \mu_0, l_0) = 0$ and $\partial \mathbb{T}(p, \mu, l)/\partial p|_{p=p_0, \mu=\mu_0, l=l_0} \neq 0$, by the Implicit Function Theorem, there is a neighborhood of (p_0, μ_0, l_0) such that whenever (μ, l) is sufficiently close to (μ_0, l_0), there is a unique p so that $\mathbb{T}(p, \mu, l) = 0$. This assignment makes p a continuous function of μ and l. Applying implicit differentiation to $\mathbb{T}(p, \mu, l)$ around (p_0, μ_0, l_0) yields:

$$\frac{\partial p(\mu, l)}{\partial \mu} = -\frac{\partial \mathbb{T}(p, \mu, l)/\partial \mu}{\partial \mathbb{T}(p, \mu, l)/\partial p}.$$

The numerator can be written as:

$$\frac{\partial \mathbb{T}(p, \mu, l)}{\partial \mu} = \frac{\chi^\epsilon}{1+\chi^\epsilon}\frac{1}{G(\tau)l} > 0,$$

whereas the denominator is given by:

$$\frac{\partial \mathbb{T}(p, \mu, l)}{\partial p} = -\frac{\left(1-G(\tau)\right)\frac{1-\eta}{\eta\rho}q(\theta)^{1+\xi}p + f(\theta)\left(1-G(\tau)+f(\theta)G(\tau)\right)}{\left(1-G(\tau)+f(\theta)G(\tau)\right)^2} < 0.$$

By combining $\partial \mathbb{T}(p, \mu, l)/\partial \mu$ with $\partial \mathbb{T}(p, \mu, l)/\partial p$, we derive that:

$$\frac{\partial p(\mu, l)}{\partial \mu} = \frac{1}{\mu}\left[\frac{\left(1-G(\tau)\right)\frac{1-\eta}{\eta\rho}q(\theta)^{1+\xi}}{f(\theta)\left(1-G(\tau)+f(\theta)G(\tau)\right)} + \frac{1}{p}\right]^{-1} > 0.$$

Using the expression of the aggregate demand in Equation (20), we can also derive the partial derivative of consumption (or equivalently, output):

$$\frac{\partial c(\mu, \gamma)}{\partial \mu} = \frac{\chi^\epsilon}{1+\chi^\epsilon}\left[p + \frac{f(\theta)\left(1-G(\tau)+f(\theta)G(\tau)\right)}{\left(1-G(\tau)\right)\frac{1-\eta}{\eta\rho}q(\theta)^{1+\xi}}\right]^{-1} > 0.$$

Next, we study the dependence of the partial derivatives on l by calculating the corre-

sponding cross derivatives. For price, it is written as:

$$\begin{aligned}\frac{\partial^2 p(\mu,l)}{\partial\mu\partial l} =&\Big[\frac{\big(1-G(\tau)\big)\frac{1-\eta}{\eta\rho}\theta^{\xi-1}(1+\xi)(1+\theta^{\xi})^{-\frac{1+\xi}{\xi}-1}}{f(\theta)\big(1-G(\tau)+f(\theta)G(\tau)\big)}\frac{\partial\theta(\mu,l)}{\partial l}\\&+\frac{\big(1-G(\tau)\big)\frac{1-\eta}{\eta\rho}q(\theta)^{2(1+\xi)}\big(1-G(\tau)+2f(\theta)G(\tau)\big)}{\big[f(\theta)\big(1-G(\tau)+f(\theta)G(\tau)\big)\big]^2}\frac{\partial\theta(\mu,l)}{\partial l}+\frac{1}{p^2}\frac{\partial p(\mu,l)}{\partial l}\Big]\\&\cdot\Big[\frac{\big(1-G(\tau)\big)\frac{1-\eta}{\eta\rho}q(\theta)^{1+\xi}}{f(\theta)\big(1-G(\tau)+f(\theta)G(\tau)\big)}+\frac{1}{p}\Big]^{-2}\frac{1}{\mu}<0,\end{aligned}$$

since the partial derivatives of product market tightness and price with respect to l are both negative, i.e., $\partial\theta(\mu,l)/\partial l<0$ and $\partial p(\mu,l)/\partial l<0$.[11] For consumption (or equivalently, output), it is given by:

$$\begin{aligned}\frac{\partial^2 c(\mu,l)}{\partial\mu\partial l} =&-\Big\{\frac{\partial p(\mu,l)}{\partial l}+\Big[\frac{\big(1-G(\tau)\big)\frac{1-\eta}{\eta\rho}\theta^{\xi-1}(1+\xi)(1+\theta^{\xi})^{-\frac{1+\xi}{\xi}-1}}{f(\theta)\big(1-G(\tau)+f(\theta)G(\tau)\big)}\frac{\partial\theta(\mu,l)}{\partial l}\\&+\frac{\big(1-G(\tau)\big)\frac{1-\eta}{\eta\rho}q(\theta)^{2(1+\xi)}\big(1-G(\tau)+2f(\theta)G(\tau)\big)}{\big[f(\theta)\big(1-G(\tau)+f(\theta)G(\tau)\big)\big]^2}\frac{\partial\theta(\mu,l)}{\partial l}\Big]\Big[\frac{\big(1-G(\tau)\big)\frac{1-\eta}{\eta\rho}q(\theta)^{1+\xi}}{f(\theta)\big(1-G(\tau)+f(\theta)G(\tau)\big)}\Big]^{-2}\Big\}\\&\cdot\Big[p+\frac{f(\theta)\big(1-G(\tau)+f(\theta)G(\tau)\big)}{\big(1-G(\tau)\big)\frac{1-\eta}{\eta\rho}q(\theta)^{1+\xi}}\Big]^{-2}\frac{\chi^{\epsilon}}{1+\chi^{\epsilon}}>0.\end{aligned}$$

With $\partial^2 p(\mu,l)/\partial\mu\partial l<0$ and $\partial^2 c(\mu,l)/\partial\mu\partial l>0$, it is straightforward to derive the rest of the cross derivatives in Proposition 6′. In terms of product market tightness, we derive that:

$$\frac{\partial\theta(\mu,l)}{\partial\mu}=\frac{1-\eta}{\eta\rho}\frac{\partial p(\mu,l)}{\partial\mu}>0,\ \ \frac{\partial^2\theta(\mu,l)}{\partial\mu\partial l}=\frac{1-\eta}{\eta\rho}\frac{\partial^2 p(\mu,l)}{\partial\mu\partial l}<0.$$

As for wholesale price, its cross derivative is written as:

$$\frac{\partial r(\mu,l)}{\partial\mu}=\frac{\partial p(\mu,l)}{\partial\mu}>0,\ \ \frac{\partial^2 r(\mu,l)}{\partial\mu\partial l}=\frac{\partial^2 p(\mu,l)}{\partial\mu\partial l}<0.$$

Lastly, for matching cost and spare capacity (or equivalently, unemployment), we have:

$$\begin{aligned}&\frac{\partial}{\partial\mu}\big[G(\tau)l-c(\mu,l)\big]=-\frac{\partial c(\mu,l)}{\partial\mu}<0,\ \ \frac{\partial^2}{\partial\mu\partial l}\big[G(\tau)l-c(\mu,l)\big]=-\frac{\partial^2 c(\mu,l)}{\partial\mu\partial l}<0,\\&\frac{\partial}{\partial\mu}\big[l-c(\mu,l)\big]=-\frac{\partial c(\mu,l)}{\partial\mu}<0,\ \ \frac{\partial^2}{\partial\mu\partial l}\big[l-c(\mu,l)\big]=-\frac{\partial^2 c(\mu,l)}{\partial\mu\partial l}<0.\end{aligned}$$

■

[11] Recall our discussion in Section 3.4 and Appendix D.4, both product market tightness and price will increase following an adverse shock to productive capacity.

D.8. Fixed-Price Aggregate Supply

In contrast to the flexible-price aggregate supply as discussed in the main text, we consider here the alternative pricing mechanism in which the price of goods is fixed while the reservation transportation cost can vary. A careful exposition of such a fixed-price mechanism is essential to understand how the matching frictions and endogenous separation mechanism could affect aggregate supply differently. The fixed-price aggregate supply is defined below, and its key analytical properties are summarized in Proposition 2′.

Definition 2″. *For an arbitrary price $\kappa \in (0, +\infty)$, the fixed-price aggregate supply c_s^{fix} is the function of reservation transportation cost $\bar{z}$ defined by:*

$$c_s^{fix}(\bar{z}) = \frac{\left\{1 + \left[\frac{1-\eta}{\eta\rho}\left(\kappa - \bar{z} + \beta \int_0^{\bar{z}} G(z')dz'\right)\right]^{-\xi}\right\}^{-\frac{1}{\xi}} G(\bar{z})l}{1 - G(\bar{z}) + \left\{1 + \left[\frac{1-\eta}{\eta\rho}\left(\kappa - \bar{z} + \beta \int_0^{\bar{z}} G(z')dz'\right)\right]^{-\xi}\right\}^{-\frac{1}{\xi}} G(\bar{z})}, \tag{D.7}$$

for all $\bar{z} \in (0, \bar{z}^{max}]$, where $\bar{z}^{max}$ satisfies:

$$\kappa - \bar{z}^{max} + \beta \int_0^{\bar{z}^{max}} G(z')dz' = 0. \tag{D.8}$$

Proposition 2′. *The fixed-price aggregate supply c_s^{fix} has the following properties:*

1. $\lim_{\bar{z}\to 0^+} c_s^{fix}(\bar{z}) = 0$;
2. $c_s^{fix}(\bar{z}^{max}) = 0$; *and*
3. *There exists at least one $\bar{z}^* \in (0, \bar{z}^{max}]$ such that $dc_s^{fix}(\bar{z})/d\bar{z}|_{\bar{z}=\bar{z}^*} = 0$.*

Proof. It is straightforward to prove the first property. When $\bar{z} \to 0^+$, $\lim_{\bar{z}\to 0^+} \theta(\bar{z}) = (1-\eta)\kappa/(\eta\rho)$, $\lim_{\bar{z}\to 0^+} f\big(\theta(\bar{z})\big) = \{1 + [(1-\eta)\kappa/(\eta\rho)]^{-\xi}\}^{-1/\xi} > 0$. At the same time, when $\bar{z} \to 0^+$, $\lim_{\bar{z}\to 0^+} G(\bar{z}) = 0$. Therefore, $\lim_{\bar{z}\to 0^+} c_s^{fix}(\bar{z}) = 0$. In terms of the second property, it is obvious from the definition of $\bar{z}^{max}$, together with that $f(0) = 0$. Regarding the last

property, the derivative of c_s^{fix} with respect to $\bar{z}$ can be written as:

$$\frac{dc_s^{fix}(\bar{z})}{d\bar{z}} = \big(1 - G(\bar{z}) + f(\theta)G(\bar{z})\big)^{-2} \cdot \Big[\underbrace{\big(1 - G(\bar{z})\big)\frac{1-\eta}{\eta\rho}\big(-1 + \beta G(\bar{z})\big)\theta^{-\xi-1}f(\theta)^{1+\xi}G(\bar{z})l}_{\substack{\text{Product Market Tightness} \\ \text{Channel} < 0}} + \underbrace{f(\theta)\frac{1}{\bar{z}\sigma}g(\bar{z})l}_{\substack{\text{Separation Margin} \\ \text{Channel} > 0}} \Big],$$

where $G(\bar{z}) \equiv \Phi[(\log \bar{z} - \gamma)/\sigma]$, $g(\bar{z}) \equiv \phi[(\log \bar{z} - \gamma)/\sigma]$, while $\Phi(.)$ and $\phi(.)$ are the standard normal cumulative density function and probability density function respectively. The product market tightness channel is negative, because a higher reservation transportation cost would reduce the total surplus to be shared between producers and retailers at the margin, hence dampening the incentives for retailers to visit producers, leading to a slack product market as well as a lower aggregate supply. The separation margin channel is positive, because a larger proportion of matches that would otherwise have been dismissed could now continue, hence contributing to a higher aggregate supply. These two channels jointly determine the fixed-price aggregate supply, and the extent to which one channel dominates the other depends on both the parameter values and reservation transportation cost itself.

When $\bar{z} \to 0^+$, it can be shown that:

$$\lim_{\bar{z}\to 0^+} \frac{dc_s^{fix}(\bar{z})}{d\bar{z}} = \Big\{1 + \Big[\frac{(1-\eta)\kappa}{\eta\rho}\Big]^{-\xi}\Big\}^{-\frac{1}{\xi}} \lim_{\bar{z}\to 0^+} \frac{1}{\bar{z}\sigma} g(\bar{z})l > 0,$$

since the probability density function of a log-normal distribution is always positive. When $\bar{z} \to \bar{z}^{max}$, it can be derived that:

$$\lim_{\bar{z}\to \bar{z}^{max}} \frac{dc_s^{fix}(\bar{z})}{d\bar{z}} = \frac{1}{1 - G(\bar{z}^{max})} \frac{1-\eta}{\eta\rho}\big(-1 + \beta G(\bar{z}^{max})\big)G(\bar{z}^{max})l < 0.$$

Consider an infinitesimal number $\epsilon > 0$ such that $dc_s^{fix}(\bar{z})/d\bar{z}|_{\bar{z}=\epsilon}$ and $\lim_{\bar{z}\to 0^+} dc_s^{fix}(\bar{z})/d\bar{z}$ have the same sign. By the Intermediate Value Theorem, since $dc_s^{fix}(\bar{z})/d\bar{z}$ is continuous on $[\epsilon, \bar{z}^{max}]$, there must exist at least one $\bar{z}^* \in [\epsilon, \bar{z}^{max}]$ such that $dc_s^{fix}(\bar{z})/d\bar{z}|_{\bar{z}=\bar{z}^*} = 0$. Since $[\epsilon, \bar{z}^{max}]$ is a sub-interval of $(0, \bar{z}^{max}]$, the last property thus holds. ■

To plot the fixed-price aggregate supply, we also need to pin down its curvature. Since the value of the second derivative of c_s^{fix} cannot be determined analytically, we resort to

numerical methods for an approximation.[12] Figure D.2 plots the fixed-price aggregate supply, its theoretical upper bound if the matching frictions were absent, and the productive capacity. As seen, the non-monotonic behavior of the fixed-price aggregate supply clearly illustrates the two aforementioned, counteracting channels at play; specifically, when the reservation transportation cost is relatively low, the separation margin channel dominates the product market tightness channel, and vice versa. Therefore, there exists a level of reservation transportation cost such that the aggregate supply is maximized. Such a behavior is similar to the one considered in Michaillat & Saez (2015), where both the matching frictions on the product market and matching cost per visit give rise to the non-standard behavior of the aggregate supply curve.[13]

In terms of the other variables of interest, as the reservation transportation cost increases, the matching cost $(G(\bar{z})l - c)$ rises, the transportation cost $((1 - G(\bar{z}))l)$ declines, and the spare capacity (or equivalently, unemployment) represented by $l - c$ first decreases and then increases.

[12] For reference, the second derivative of c_s^{fix} with respect to $\bar{z}$ is given by:

$$\frac{d^2 c_s^{fix}(\bar{z})}{d\bar{z}^2} = \big(1 - G(\bar{z}) + f(\theta)G(\bar{z})\big)^2 \cdot \Big(\frac{(1-\eta)l}{\eta\rho} \frac{1}{\bar{z}\sigma} g(\bar{z}) \big(-1 + 2\beta G(\bar{z}) + 2G(\bar{z}) - 3\beta G(\bar{z})^2 \big) q(\theta)^{1+\xi}$$
$$- \frac{(1-\eta)l}{\eta\rho} \big(1 - G(\bar{z})\big) G(\bar{z}) \big(-1 + \beta G(\bar{z})\big)^2 \frac{1-\eta}{\eta\rho} \theta^{\xi-1} (1+\xi) \big(1 + \theta^{\xi}\big)^{-\frac{1+\xi}{\xi}-1}$$
$$+ \frac{1-\eta}{\eta\rho} \big(-1 + \beta G(\bar{z})\big) \theta^{-\xi-1} \big(1 + \theta^{-\xi}\big)^{-\frac{1}{\xi}-1} \frac{1}{\bar{z}\sigma} g(\bar{z}) l - f(\theta) l \big\{ \frac{1}{\bar{z}^2\sigma} g(\bar{z}) + \frac{\log \bar{z} - \gamma}{\bar{z}^2 \sigma^3 \sqrt{2\pi}} \exp\big[- \frac{(\log \bar{z} - \gamma)^2}{2\sigma^2} \big] \big\} \Big)$$
$$- \big[\frac{(1-\eta)l}{\eta\rho} \big(1 - G(\bar{z})\big) G(\bar{z}) \big(-1 + \beta G(\bar{z})\big) q(\theta)^{1+\xi} + f(\theta) \frac{1}{\bar{z}\sigma} g(\bar{z}) l \big]$$
$$\cdot \big[\frac{1-\eta}{\eta\rho} \big(-1 + \beta G(\bar{z})\big) \theta^{-\xi-1} \big(1 + \theta^{-\xi}\big)^{-\frac{1}{\xi}-1} G(\bar{z}) - \big(1 - f(\theta)\big) \frac{1}{\bar{z}\sigma} g(\bar{z}) \big] 2 \big(1 - G(\bar{z}) + f(\theta) G(\bar{z})\big),$$

[13] In contrast to our fixed-price aggregate supply curve which is plotted in the $(c, \bar{z})$ plane, the aggregate supply curve in Michaillat & Saez (2015) is plotted in the (c, x) plane, where x refers to the product market tightness. See Figure I of their paper for details.

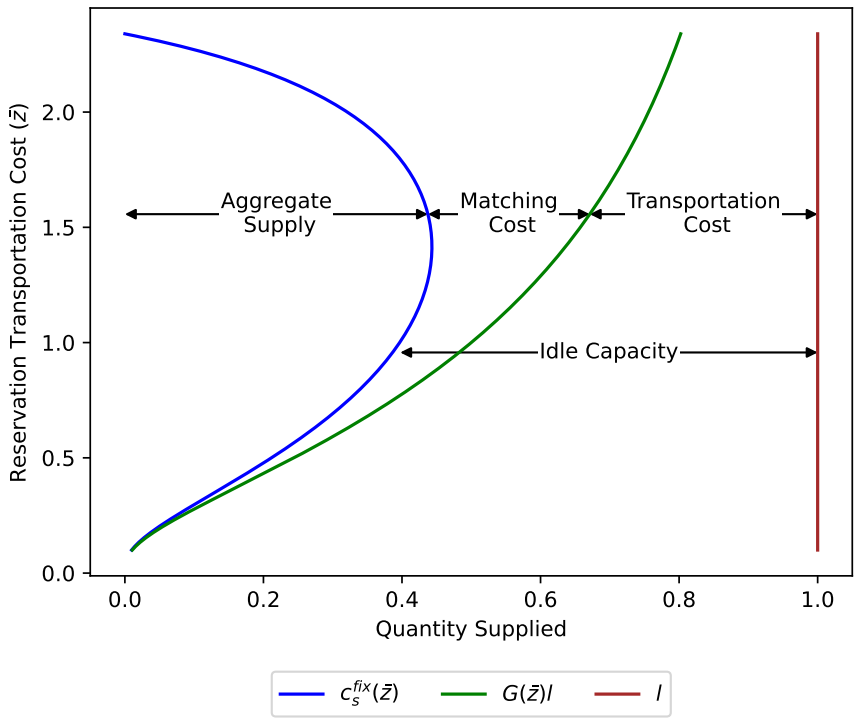


Figure D.2: Supply Side of the Economy When the Price of Goods Is Fixed

Notes. The figure depicts the fixed-price aggregate supply, $c_s^{fix}(\bar{z})$, its theoretical upper bound $G(\bar{z})l$ in the absence of matching frictions, and the productive capacity l for specific values of the reservation transportation cost $\bar{z}$. The difference between $c_s^{fix}(\bar{z})$ and $G(\bar{z})l$ signifies the matching cost, while the difference between $G(\bar{z})l$ and l denotes the transportation cost (measured in units of goods). The gap between $c_s^{fix}(\bar{z})$ and l represents the spare capacity of producers, or equivalently, unemployment. For the numerical approximation, the parameter values are set as follows: $\eta = 0.5, \rho = 0.5, \kappa = 1.2, \beta = 0.99, \xi = 2, l = 1, \gamma = 0$, and $\sigma = 1$. The value of $\bar{z}$ is derived from 1,000 evenly spaced numbers over the interval $[0.1, \bar{z}^{max}]$, where $\bar{z}^{max}$ is numerically determined based on its definition in Equation (D.8).

E. Robustness of SVAR Results

E.1. Dropping Zero Restrictions

In this appendix, we conduct a robustness check of our baseline results by relaxing the zero restrictions that are imposed on the on-impact responses of the ACR index to demand and capacity shocks in the SVAR estimation. While we impose such zero restrictions in the baseline estimation to sharpen our identification of supply chain disturbances, removing them facilitates the comparison of our ACR index with other indices of supply chain disruptions found in the existing literature. As we will elaborate later in Appendix F, these indices often face potential endogeneity issues – such as higher demand for tradable goods translating into higher shipping prices – and large, time-varying measurement errors. For example, an increase in "delivery times" – the average duration that suppliers take to provide inputs to their customers' factories – reported in the PMI could stem from either a supply chain disruption or a reduction in productive capacity.

Specifically, without the zero restrictions, the identifying restrictions are given by:

Restriction 1′. ***An adverse shock to aggregate demand*** *leads to a negative response of real GDP, PCE goods price, retail market tightness, and import price, as well as to a positive response of unemployment at* $k = 1$.

Restriction 2′. ***An adverse shock to productive capacity*** *leads to a negative response of real GDP and unemployment, as well as to a positive response of PCE goods price, retail market tightness, and import price at* $k = 1$.

Restriction 3′. ***An adverse shock to supply chain*** *leads to a negative response of real GDP, as well as to a positive response of PCE goods price, unemployment, and ACR at* $k = 1$.

The estimation is still performed using the Bayesian approach as in Arias et al. (2018, 2019, 2023). All the estimation specifications, except for the identifying restrictions, are kept the same as those applied in the baseline. As can be clearly seen in Figures E.1 through E.5, our main results still hold.

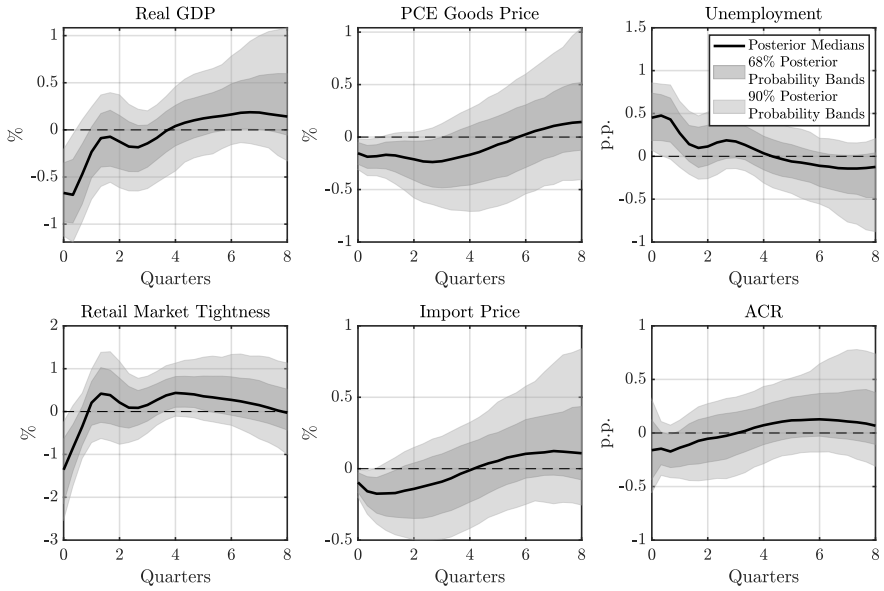


Figure E.1: IRFs to an Adverse Shock to Aggregate Demand: Dropping Zero Restrictions

Notes. The IRFs to a one standard deviation adverse shock to aggregate demand are identified using the ACR index and Restrictions 1′, 2′, and 3′. The solid line shows the point-wise posterior medians, and the shaded bands show the 68% and 90% equal-tailed point-wise posterior probability bands. The figure is based on 100,000 independent draws.

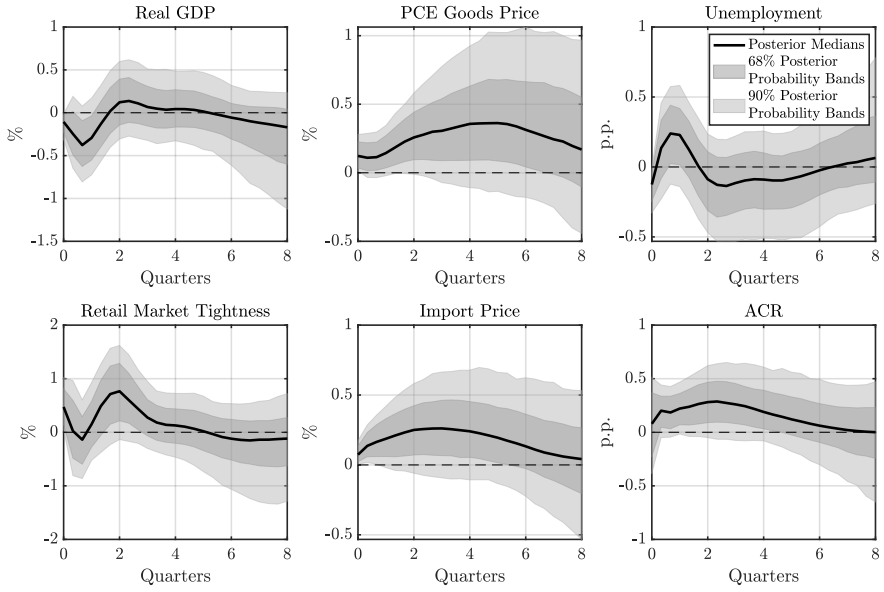


Figure E.2: IRFs to an Adverse Shock to Productive Capacity: Dropping Zero Restrictions

Notes. The IRFs to a one standard deviation adverse shock to productive capacity are identified using the ACR index and Restrictions 1′, 2′, and 3′. The solid line shows the point-wise posterior medians, and the shaded bands show the 68% and 90% equal-tailed point-wise posterior probability bands. The figure is based on 100,000 independent draws.

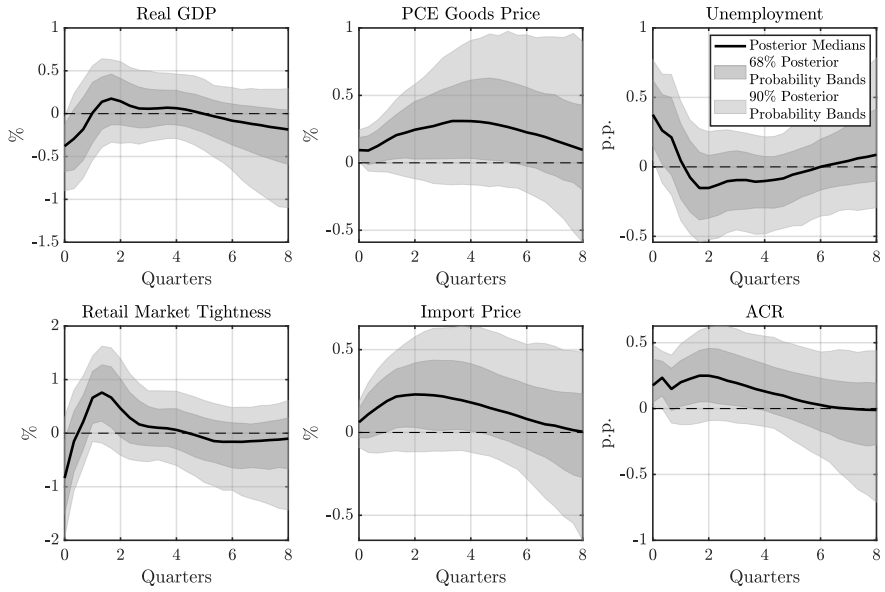


Figure E.3: IRFs to an Adverse Shock to Supply Chain: Dropping Zero Restrictions

Notes. The IRFs to a one standard deviation adverse shock to the supply chain are identified using the ACR index and Restrictions 1′, 2′, and 3′. The solid line shows the point-wise posterior medians, and the shaded bands show the 68% and 90% equal-tailed point-wise posterior probability bands. The figure is based on 100,000 independent draws.

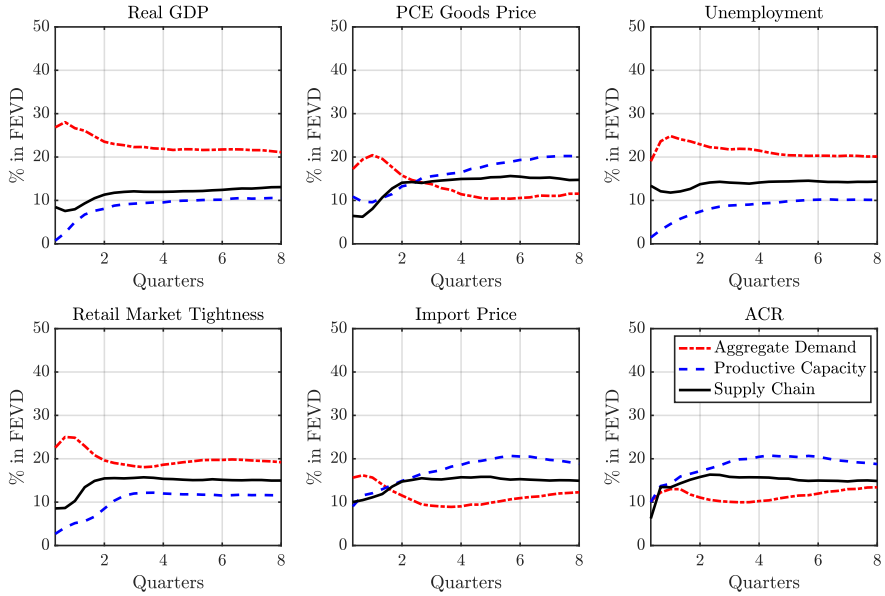


Figure E.4: FEVD from the SVAR: Dropping Zero Restrictions

Notes. Each line presents the median fraction of the forecast error variance for each endogenous variable, explained by each of the three identified structural shocks at various time horizons. The FEVD is estimated using the ACR index and Restrictions 1′, 2′, and 3′, and based on 100,000 independent draws.

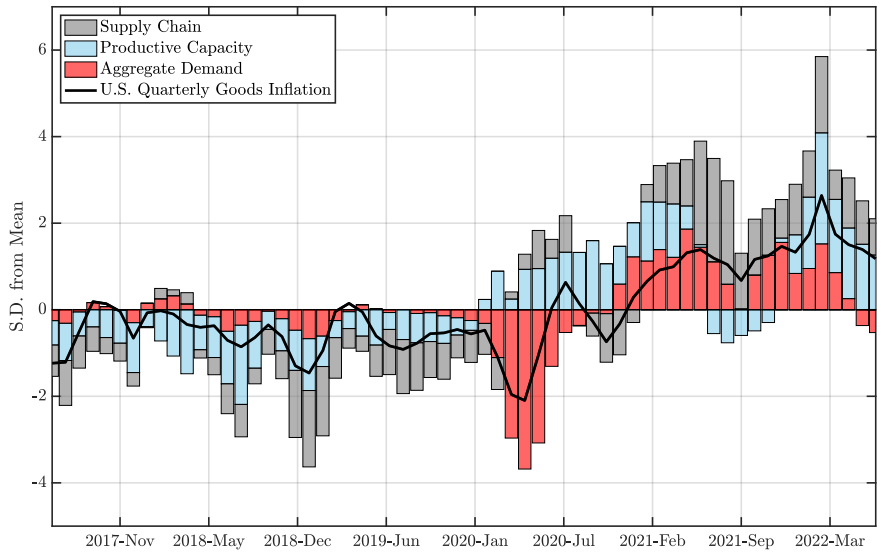


Figure E.5: HD of U.S. Goods Inflation: Dropping Zero Restrictions

Notes. The solid line represents the standardized quarterly goods inflation rate in the U.S., i.e., quarter-on-quarter growth of the PCE goods price index. The shaded bar represents the standardized cumulative historical contribution of each of the three structural shocks identified using the ACR index and Restrictions 1′, 2′, and 3′ to U.S. goods inflation. The estimation results are based on all endogenous variables being measured as a percent change from the previous period, with the exceptions of unemployment and the ACR index, which are measured as a change from the previous period. The figure is derived from 100,000 independent draws.

E.2. Different Lag Structures

In Figures E.6 through E.14, we show that the IRFs are robust to considering different lag structures, i.e., one, three, or four lags. We do not consider higher lags due to parameter uncertainty resulting from our limited sample length.

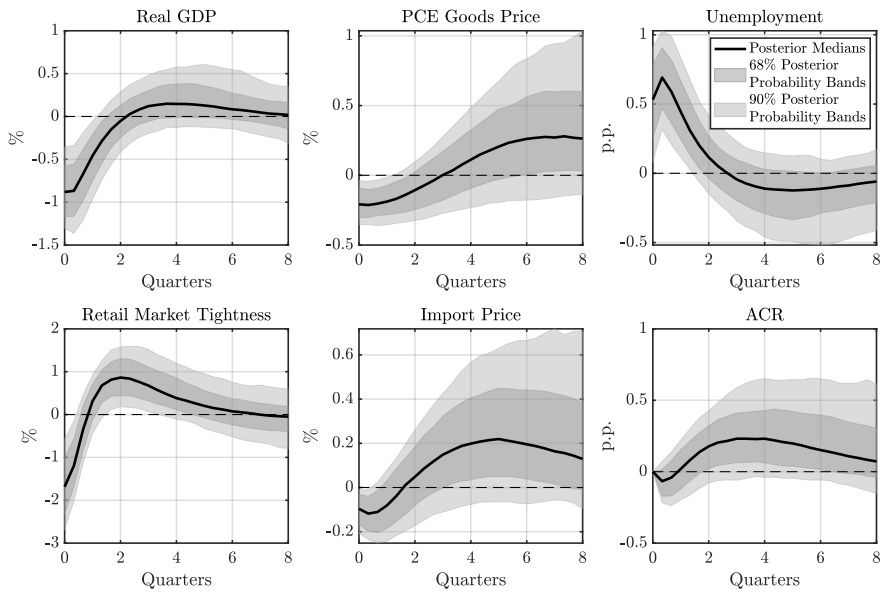


Figure E.6: IRFs to an Adverse Shock to Aggregate Demand: One Lag

Notes. The IRFs to a one standard deviation adverse shock to aggregate demand are identified using an SVAR specification as in Equation (24) with one lag, as well as Restrictions 1, 2, and 3. The solid line shows the point-wise posterior medians, and the shaded bands show the 68% and 90% equal-tailed point-wise posterior probability bands. The figure is based on 100,000 independent draws.

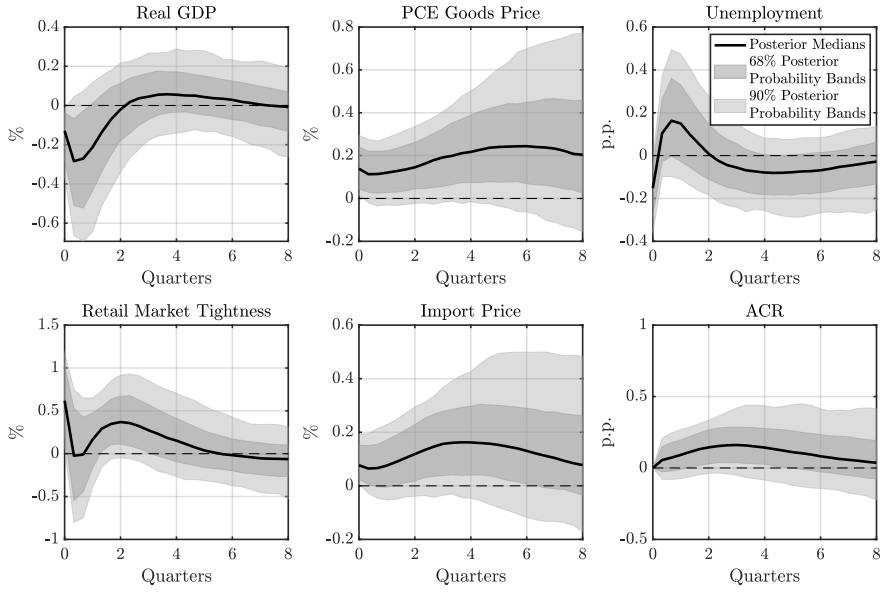


Figure E.7: IRFs to an Adverse Shock to Productive Capacity: One Lag

Notes. The IRFs to a one standard deviation adverse shock to productive capacity are identified using an SVAR specification as in Equation (24) with one lag, as well as Restrictions 1, 2, and 3. The solid line shows the point-wise posterior medians, and the shaded bands show the 68% and 90% equal-tailed point-wise posterior probability bands. The figure is based on 100,000 independent draws.

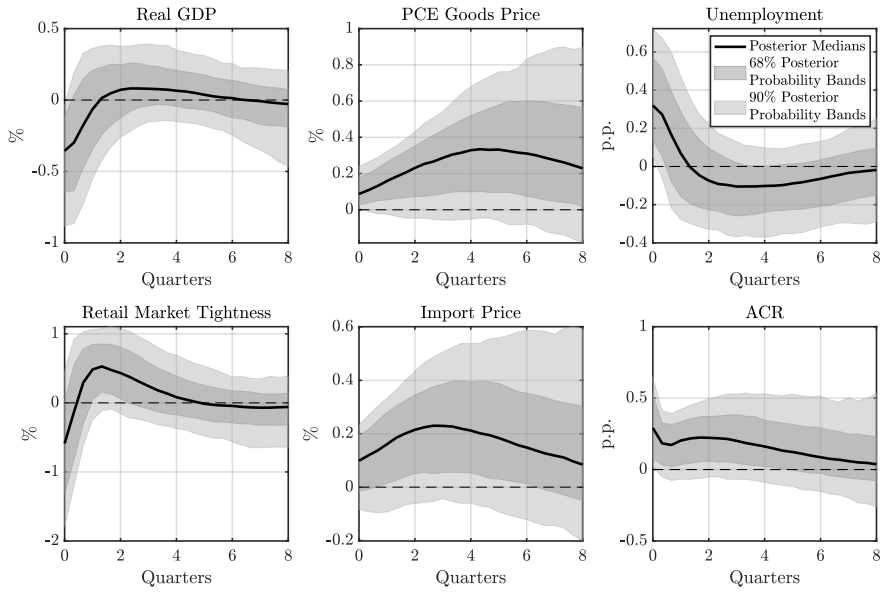


Figure E.8: IRFs to an Adverse Shock to Supply Chain: One Lag

Notes. The IRFs to a one standard deviation adverse shock to the supply chain are identified using an SVAR specification as in Equation (24) with one lag, as well as Restrictions 1, 2, and 3. The solid line shows the point-wise posterior medians, and the shaded bands show the 68% and 90% equal-tailed point-wise posterior probability bands. The figure is based on 100,000 independent draws.

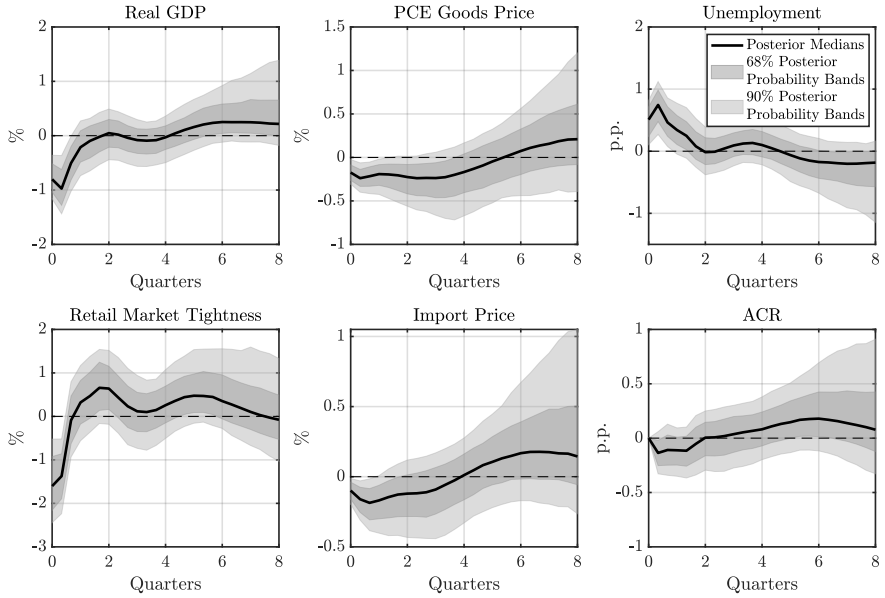


Figure E.9: IRFs to an Adverse Shock to Aggregate Demand: Three Lags

Notes. The IRFs to a one standard deviation adverse shock to aggregate demand are identified using an SVAR specification as in Equation (24) with three lags, as well as Restrictions 1, 2, and 3. The solid line shows the point-wise posterior medians, and the shaded bands show the 68% and 90% equal-tailed point-wise posterior probability bands. The figure is based on 100,000 independent draws.

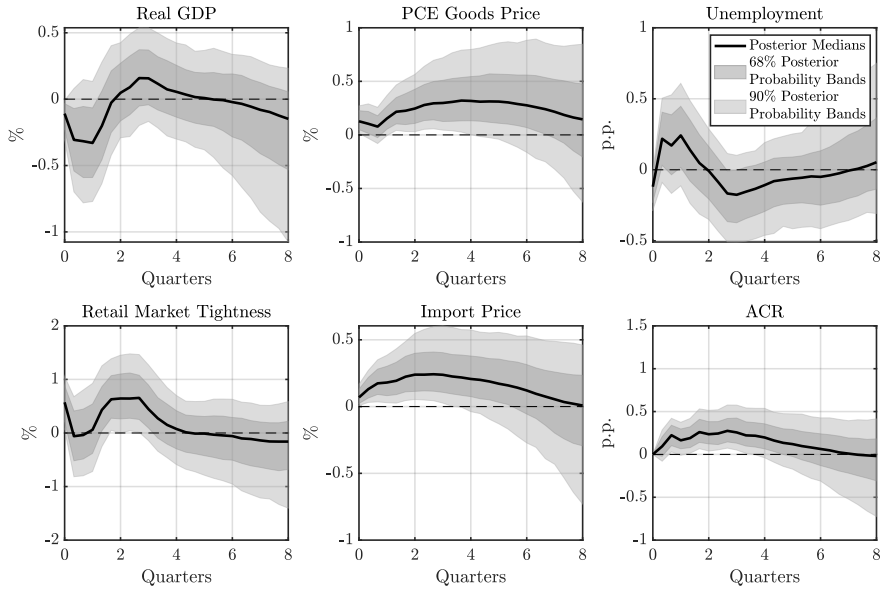


Figure E.10: IRFs to an Adverse Shock to Productive Capacity: Three Lags

Notes. The IRFs to a one standard deviation adverse shock to productive capacity are identified using an SVAR specification as in Equation (24) with three lags, as well as Restrictions 1, 2, and 3. The solid line shows the point-wise posterior medians, and the shaded bands show the 68% and 90% equal-tailed point-wise posterior probability bands. The figure is based on 100,000 independent draws.

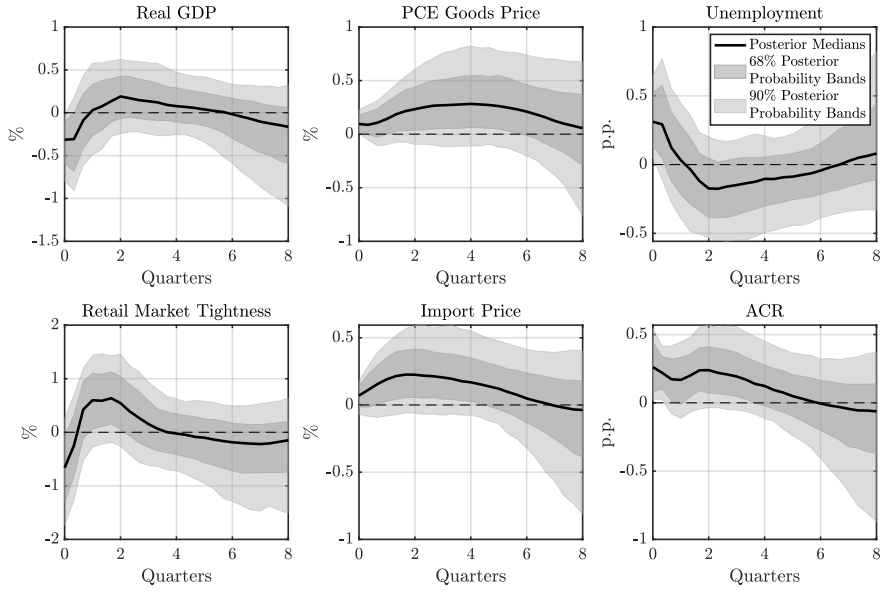


Figure E.11: IRFs to an Adverse Shock to Supply Chain: Three Lags

Notes. The IRFs to a one standard deviation adverse shock to the supply chain are identified using an SVAR specification as in Equation (24) with three lags, as well as Restrictions 1, 2, and 3. The solid line shows the point-wise posterior medians, and the shaded bands show the 68% and 90% equal-tailed point-wise posterior probability bands. The figure is based on 100,000 independent draws.

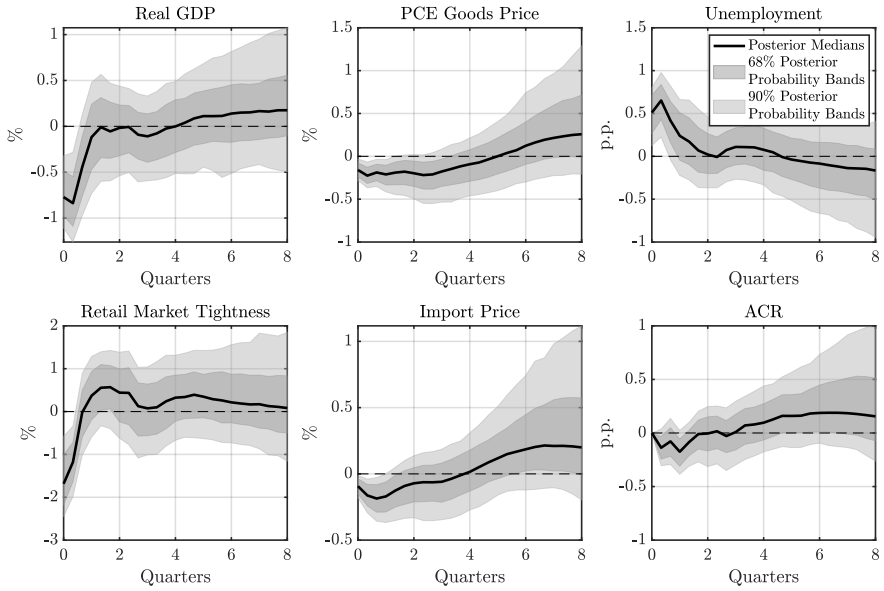


Figure E.12: IRFs to an Adverse Shock to Aggregate Demand: Four Lags

Notes. The IRFs to a one standard deviation adverse shock to aggregate demand are identified using an SVAR specification as in Equation (24) with four lags, as well as Restrictions 1, 2, and 3. The solid line shows the point-wise posterior medians, and the shaded bands show the 68% and 90% equal-tailed point-wise posterior probability bands. The figure is based on 100,000 independent draws.

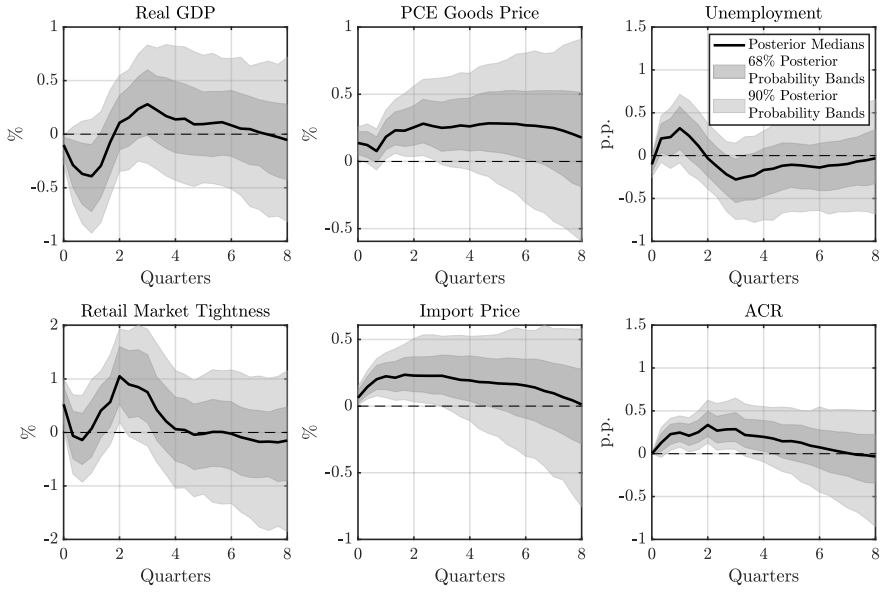


Figure E.13: IRFs to an Adverse Shock to Productive Capacity: Four Lags

Notes. The IRFs to a one standard deviation adverse shock to productive capacity are identified using an SVAR specification as in Equation (24) with four lags, as well as Restrictions 1, 2, and 3. The solid line shows the point-wise posterior medians, and the shaded bands show the 68% and 90% equal-tailed point-wise posterior probability bands. The figure is based on 100,000 independent draws.

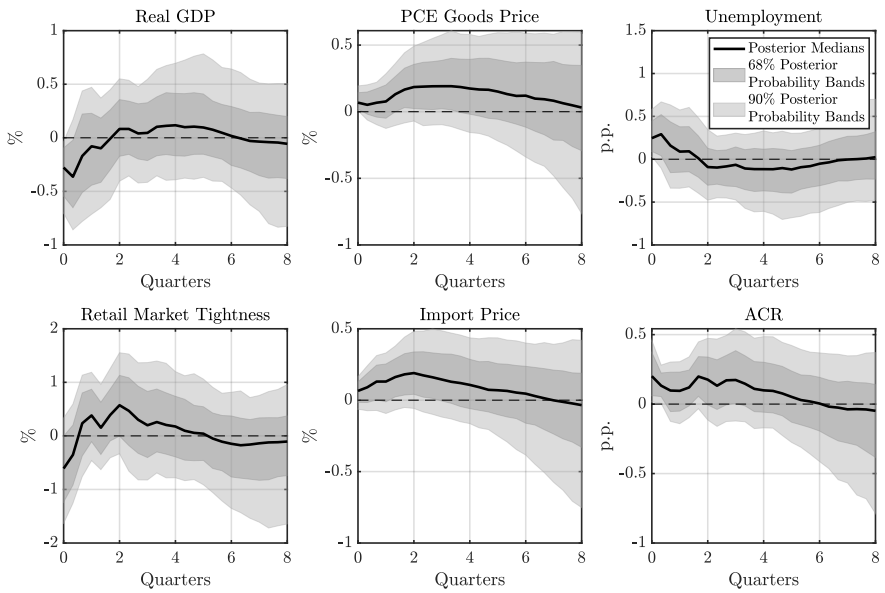


Figure E.14: IRFs to an Adverse Shock to Supply Chain: Four Lags

Notes. The IRFs to a one standard deviation adverse shock to the supply chain are identified using an SVAR specification as in Equation (24) with four lags, as well as Restrictions 1, 2, and 3. The solid line shows the point-wise posterior medians, and the shaded bands show the 68% and 90% equal-tailed point-wise posterior probability bands. The figure is based on 100,000 independent draws.

E.3. Alternative Proxies for Output, Spare Capacity, and Retail Market Tightness

In this appendix, we examine the robustness of our baseline results by replacing real GDP with real PCE of goods and unemployment with the U.S. spare capacity in the SVAR estimation. The monthly time series for real PCE of goods is retrieved directly from FRED using the mnemonic `DGDSRX1`. The series for U.S. spare capacity is constructed by subtracting the capacity utilization rate, denoted by `TCU`, from one hundred. As indicated in Figures E.15 through E.20, the IRFs are consistent with those in the baseline estimation.

For an additional robustness check, manufacturers' inventories are replaced with merchant wholesalers' inventories, referenced by the mnemonic `WHLSLRIMSA`, in constructing the retail market tightness measure. The behavior of the IRFs, as shown in Figures E.21 through E.23, is quantitatively similar to that observed in Figures 9, 10, and 11.

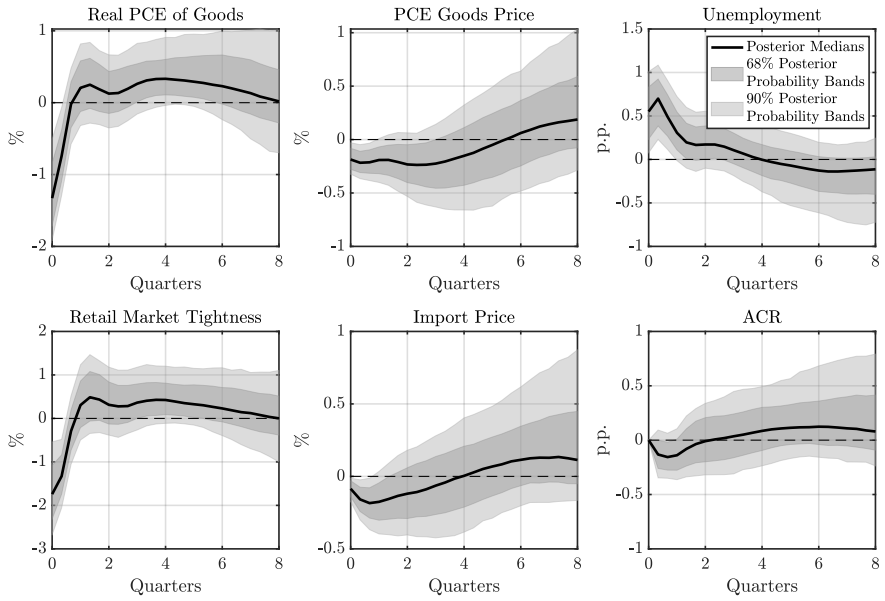


Figure E.15: IRFs to an Adverse Shock to Aggregate Demand: Real PCE of Goods

Notes. The IRFs to a one standard deviation adverse shock to aggregate demand are identified using the real PCE of goods as the proxy for output and Restrictions 1, 2, and 3. The solid line shows the point-wise posterior medians, and the shaded bands show the 68% and 90% equal-tailed point-wise posterior probability bands. The figure is based on 100,000 independent draws.

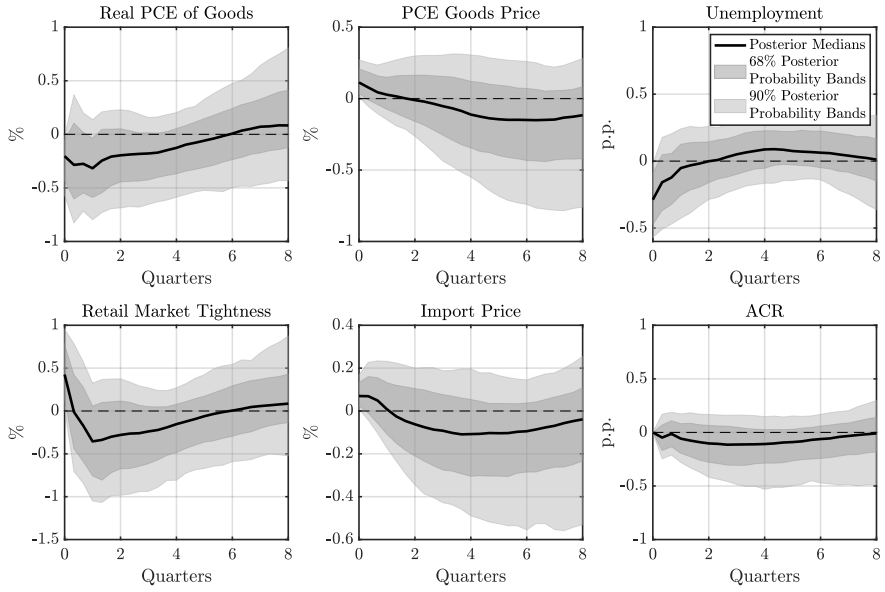


Figure E.16: IRFs to an Adverse Shock to Productive Capacity: Real PCE of Goods

Notes. The IRFs to a one standard deviation adverse shock to productive capacity are identified using the real PCE of goods as the proxy for output and Restrictions 1, 2, and 3. The solid line shows the point-wise posterior medians, and the shaded bands show the 68% and 90% equal-tailed point-wise posterior probability bands. The figure is based on 100,000 independent draws.

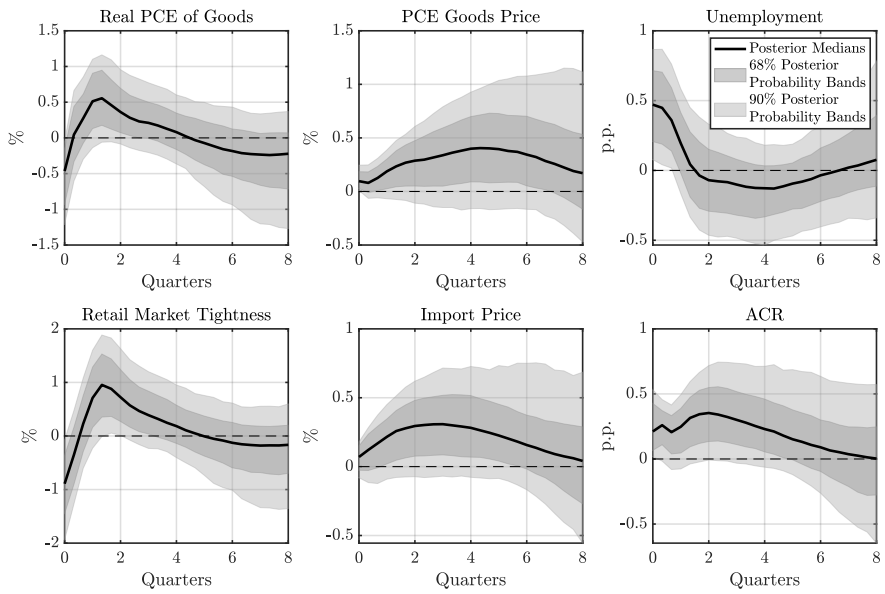


Figure E.17: IRFs to an Adverse Shock to Supply Chain: Real PCE of Goods

Notes. The IRFs to a one standard deviation adverse shock to the supply chain are identified using the real PCE of goods as the proxy for output and Restrictions 1, 2, and 3. The solid line shows the point-wise posterior medians, and the shaded bands show the 68% and 90% equal-tailed point-wise posterior probability bands. The figure is based on 100,000 independent draws.

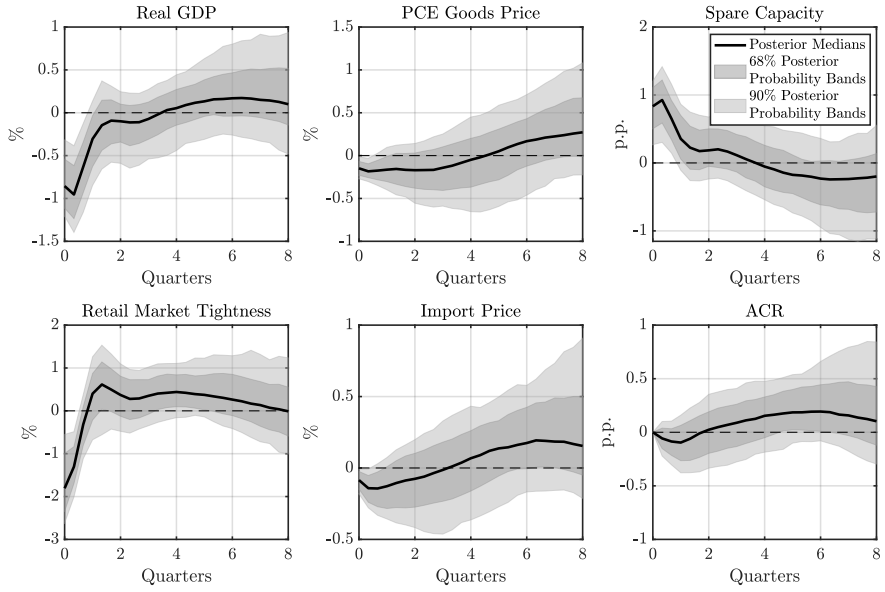


Figure E.18: IRFs to an Adverse Shock to Aggregate Demand: Spare Capacity

Notes. The IRFs to a one standard deviation adverse shock to aggregate demand are identified using the U.S. spare capacity (constructed by subtracting the capacity utilization rate from one hundred) and Restrictions 1, 2, and 3. The solid line shows the point-wise posterior medians, and the shaded bands show the 68% and 90% equal-tailed point-wise posterior probability bands. The figure is based on 100,000 independent draws.

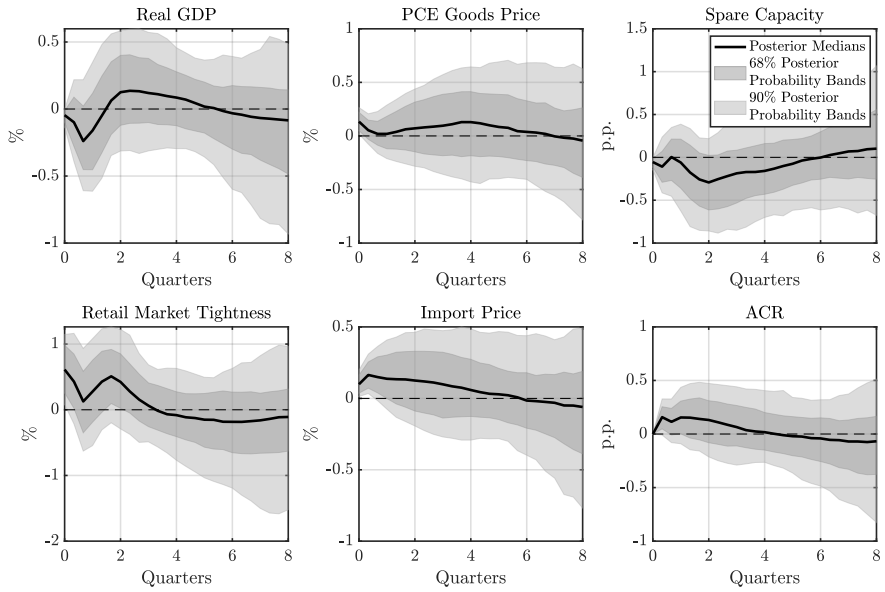


Figure E.19: IRFs to an Adverse Shock to Productive Capacity: Spare Capacity

Notes. The IRFs to a one standard deviation adverse shock to productive capacity are identified using the U.S. spare capacity (constructed by subtracting the capacity utilization rate from one hundred) and Restrictions 1, 2, and 3. The solid line shows the point-wise posterior medians, and the shaded bands show the 68% and 90% equal-tailed point-wise posterior probability bands. The figure is based on 100,000 independent draws.

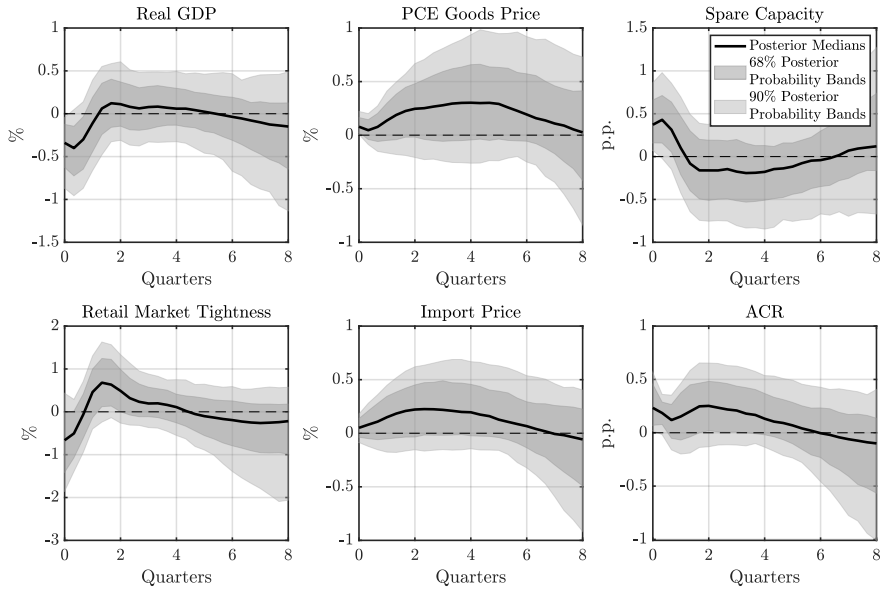


Figure E.20: IRFs to an Adverse Shock to Supply Chain: Spare Capacity

Notes. The IRFs to a one standard deviation adverse shock to the supply chain are identified using the U.S. spare capacity (constructed by subtracting the capacity utilization rate from one hundred) and Restrictions 1, 2, and 3. The solid line shows the point-wise posterior medians, and the shaded bands show the 68% and 90% equal-tailed point-wise posterior probability bands. The figure is based on 100,000 independent draws.

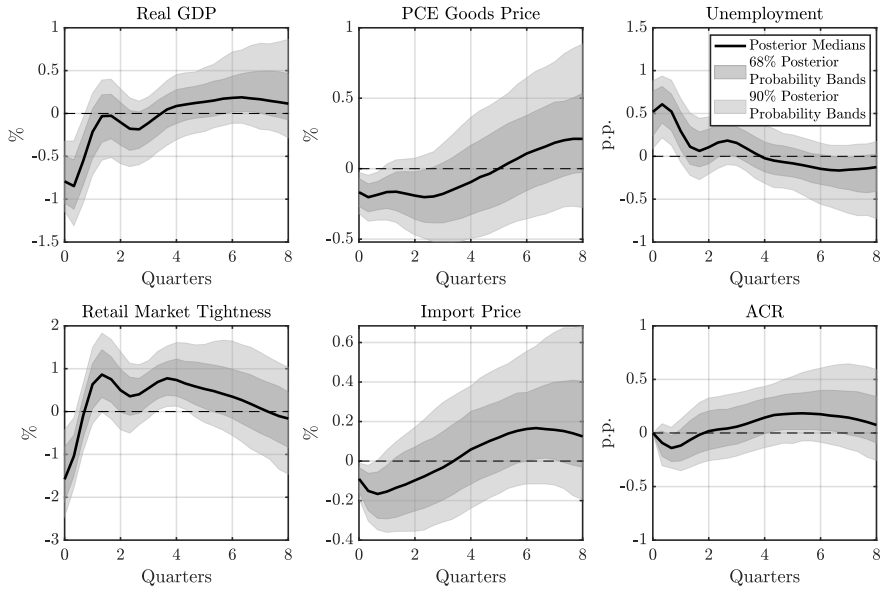


Figure E.21: IRFs to an Adverse Shock to Aggregate Demand: Wholesalers' Inventories

Notes. The IRFs to a one standard deviation adverse shock to aggregate demand are identified using the merchant wholesalers' inventories to construct the retail market tightness and Restrictions 1, 2, and 3. The solid line shows the point-wise posterior medians, and the shaded bands show the 68% and 90% equal-tailed point-wise posterior probability bands. The figure is based on 100,000 independent draws.

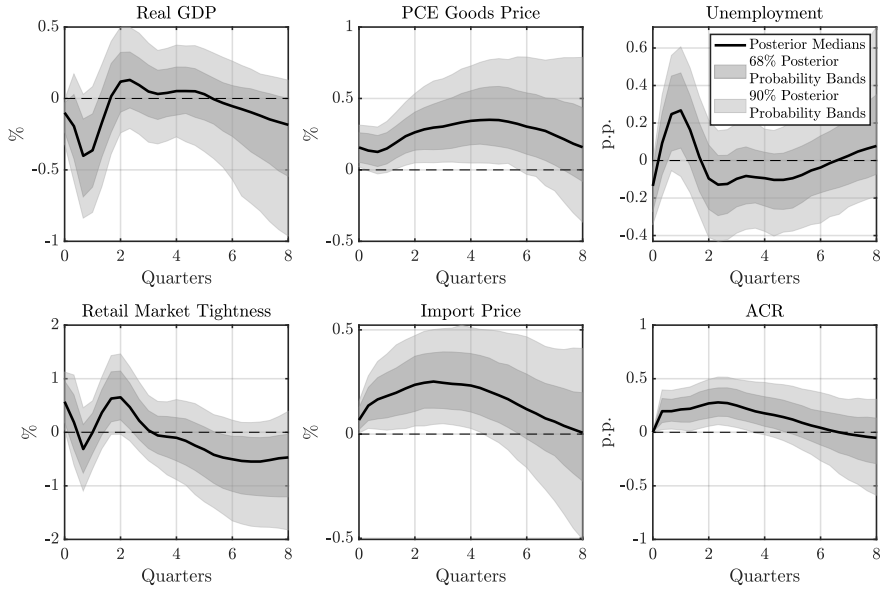


Figure E.22: IRFs to an Adverse Shock to Productive Capacity: Wholesalers' Inventories

Notes. The IRFs to a one standard deviation adverse shock to productive capacity are identified using the merchant wholesalers' inventories to construct the retail market tightness and Restrictions 1, 2, and 3. The solid line shows the point-wise posterior medians, and the shaded bands show the 68% and 90% equal-tailed point-wise posterior probability bands. The figure is based on 100,000 independent draws.

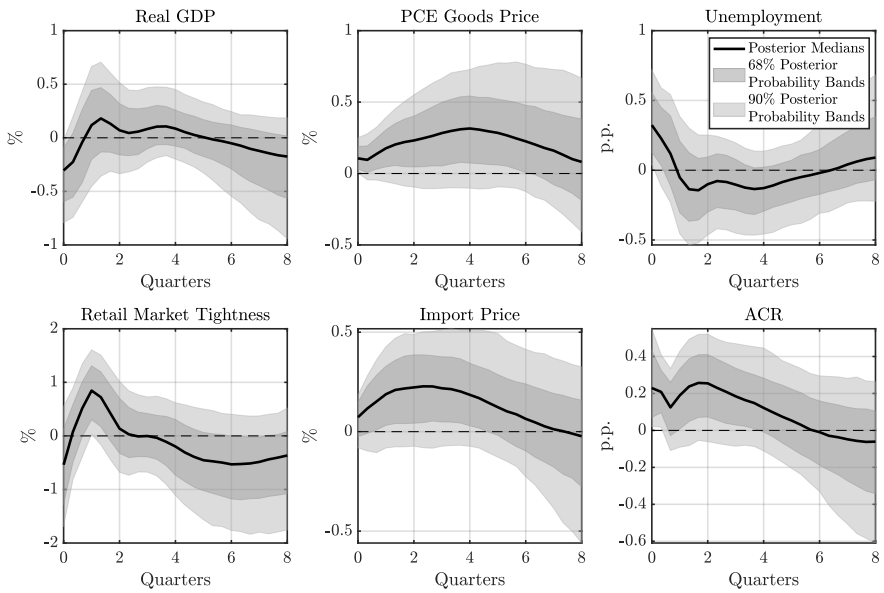


Figure E.23: IRFs to an Adverse Shock to Supply Chain: Wholesalers' Inventories

Notes. The IRFs to a one standard deviation adverse shock to the supply chain are identified using the merchant wholesalers' inventories to construct the retail market tightness and Restrictions 1, 2, and 3. The solid line shows the point-wise posterior medians, and the shaded bands show the 68% and 90% equal-tailed point-wise posterior probability bands. The figure is based on 100,000 independent draws.

E.4. Prior Robustness

Figures E.24, E.25, and E.26 show that the main conclusions from our baseline SVAR analysis are robust to using the prior robust approach for the SVARs proposed by Giacomini & Kitagawa (2021). Such an approach removes the need to specify the prior for the structural parameter given the reduced-form parameter, which is the component of the prior that is responsible for the asymptotic disagreement between Bayesian and frequentist inference. This is mainly achieved by constructing a class of priors that shares a single prior for the reduced-form parameter but allows for arbitrary conditional priors for the structural parameters given the reduced-form parameter.

In practice, we apply their Algorithm 1 to numerically approximate the set of posterior means and the associated robust credible regions for the IRFs of the selected endogenous variables to each structural shock. We make two modifications in the implementation of Algorithm 1. First, in Step 2 of Algorithm 1, to draw the orthonormal Q's subject to Restrictions 1, 2, and 3, we apply the QR decomposition method as in Arias et al. (2018)

instead of the original linear projection approach. These two ways of drawing Q are comparable in terms of both the resulting distribution of Q and computational cost. Second, we replace Step 3 of Algorithm 1 with Step 3′ of Algorithm 2 to approximate the lower and upper bounds of the prior robust posterior means, as well as those associated with the robust credible regions.

In Figures E.24, E.25, and E.26, the solid line shows the point-wise posterior medians, and the shaded area represents the 68% equal-tailed point-wise posterior probability bands. Their underlying data are from our baseline estimation outlined in Section 4. Alongside the posterior medians and probability bands, we plot the set of prior robust posterior means using dotted curves, and the corresponding 68% robust credible regions using dashed-dotted curves. Their underlying data are based on 1,000 independent draws of the reduced-form parameters and 100,000 orthogonal matrices draws for each reduced-form parameter.

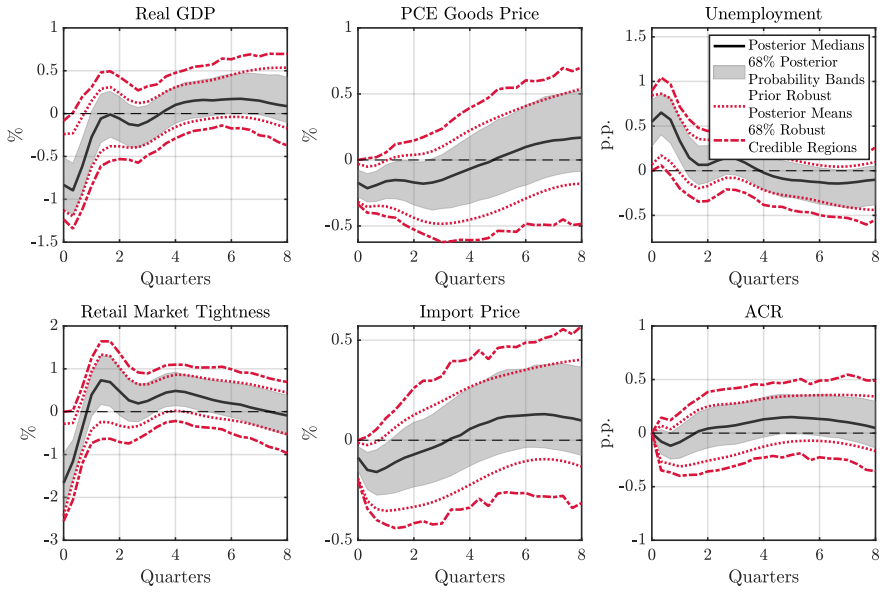


Figure E.24: IRFs to an Adverse Shock to Aggregate Demand Using the Prior Robust Approach in Giacomini & Kitagawa (2021)

Notes. The IRFs to a one standard deviation adverse shock to aggregate demand are estimated using the prior robust approach for the SVARs proposed by Giacomini & Kitagawa (2021). The solid line shows the point-wise posterior medians, and the shaded area represents the 68% equal-tailed point-wise posterior probability bands, which are based on the data from our baseline estimation outlined in Section 4. The dotted curves illustrate the set of prior robust posterior means, and the dashed-dotted curves depict the 68% robust credible regions. These curves are obtained from 1,000 independent draws of the reduced-form parameters and 100,000 orthogonal matrix draws for each reduced-form parameter.

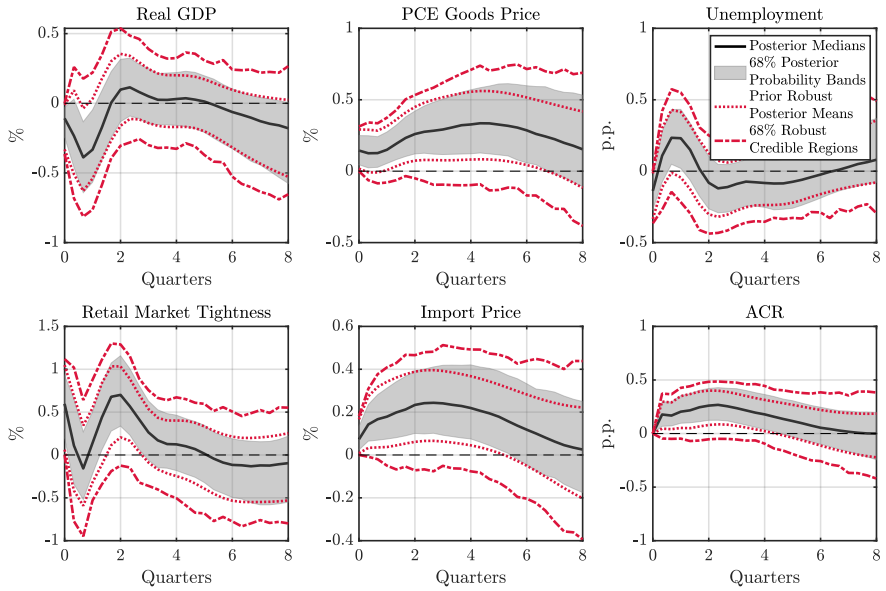


Figure E.25: IRFs to an Adverse Shock to Productive Capacity Using the Prior Robust Approach in Giacomini & Kitagawa (2021)

Notes. The IRFs to a one standard deviation adverse shock to productive capacity are estimated using the prior robust approach for the SVARs proposed by Giacomini & Kitagawa (2021). The solid line shows the point-wise posterior medians, and the shaded area represents the 68% equal-tailed point-wise posterior probability bands, which are based on the data from our baseline estimation outlined in Section 4. The dotted curves illustrate the set of prior robust posterior means, and the dashed-dotted curves depict the 68% robust credible regions. These curves are obtained from 1,000 independent draws of the reduced-form parameters and 100,000 orthogonal matrix draws for each reduced-form parameter.

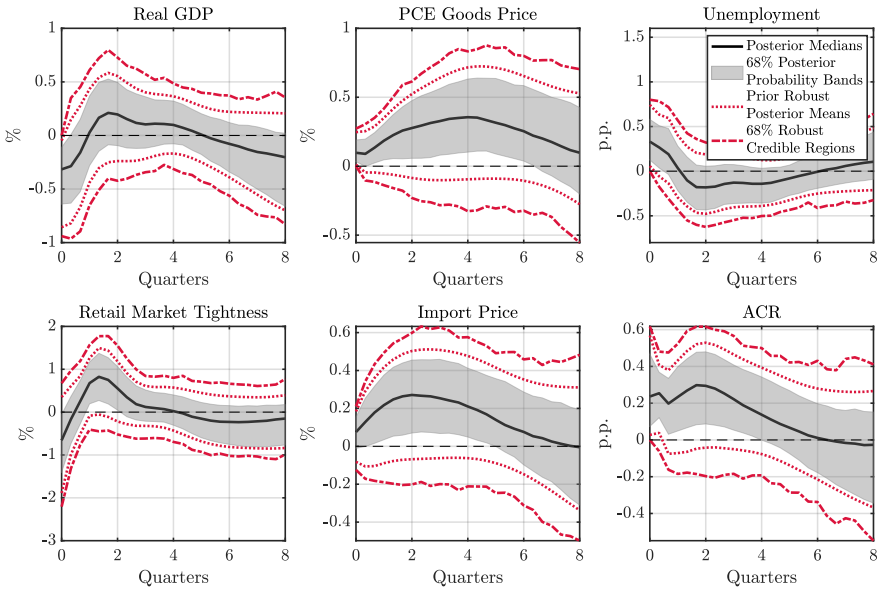


Figure E.26: IRFs to an Adverse Shock to Supply Chain Using the Prior Robust Approach in Giacomini & Kitagawa (2021)

Notes. The IRFs to a one standard deviation adverse shock to the supply chain are estimated using the prior robust approach for the SVARs proposed by Giacomini & Kitagawa (2021). The solid line shows the point-wise posterior medians, and the shaded area represents the 68% equal-tailed point-wise posterior probability bands, which are based on the data from our baseline estimation outlined in Section 4. The dotted curves illustrate the set of prior robust posterior means, and the dashed-dotted curves depict the 68% robust credible regions. These curves are obtained from 1,000 independent draws of the reduced-form parameters and 100,000 orthogonal matrix draws for each reduced-form parameter.

F. Alternative Indices of Supply Chain Disruptions

In this appendix, we compare our ACR index to other popular indices of supply chain disruptions from the existing literature: namely, the Harper Peterson Time Charter Rates Index (HARPEX), the Global Supply Chain Pressure Index (GSCPI) from the Federal Reserve Bank of New York (Benigno et al. 2022), and the Supply Disruptions Index (SDI) constructed by Smirnyagin & Tsyvinski (2022). Our analysis reveals significant disparities between these indices, which affect the impact of supply chain disruptions on key macroeconomic indicators.

F.1. HARPEX

Shipping costs are a natural proxy for supply chain disruptions, as supply chain issues can arise internationally due to a shortage of containers and port congestion (Klachkin 2021, Benigno et al. 2022). However, the responses of the transportation sector are also driven by both supply- and demand-side factors. An increase in the appetite for tradable goods fuels the derived demand for international shipping services, leading to a tighter transportation market and higher shipping costs.

Figure F.1 plots the ACR index against the Harper Peterson Time Charter Rates Index (HARPEX). The HARPEX is a widely-used composite indicator of container shipping rate changes in the time charter market for eight different classes of containerships (Attinasi et al. 2021, Benigno et al. 2022, Finck & Tillmann 2022) and is also used in the construction of the GSCPI as a measure of cross-border transportation costs. Not surprisingly, we observe that the two indices have moved similarly since the onset of the pandemic. As delays in container processing became more prevalent and port congestion escalated around the world, ships were tied up at ports. This led to a significant shortage in the supply of shipping services, resulting in surging shipping prices. However, it is also noteworthy that the two series did not align closely with each other before the onset of the pandemic and in its aftermath, because, as argued earlier, their fluctuations are influenced by both demand and supply-side factors.

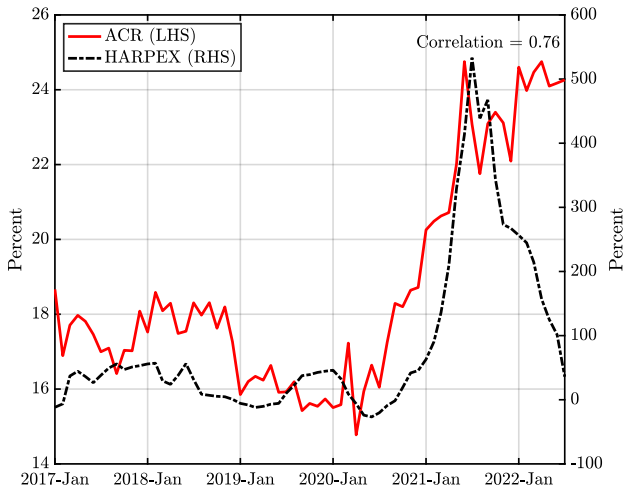


Figure F.1: ACR vs. HARPEX

Notes. Figure F.1 plots the ACR index (red solid line) against the HARPEX (black dashed-dotted line) for the sample period from January 2017 to July 2022. The ACR index is computed using the AIS data of containerships and our IMA-DBSCAN algorithm, as detailed in Appendix B. The original HARPEX series is published by Harper Peterson and is retrieved from the Refinitiv data platform. Following Attinasi et al. (2021), Benigno et al. (2022), we transform the original series by computing the year-on-year percentage changes. Both the ACR and HARPEX indices are measured in percent and have been seasonally adjusted.

Figures F.2, F.3, and F.4 plot the estimation results with the HARPEX included in the SVAR as a measure of supply chain disruptions. We also drop the zero restrictions while leaving the sign restrictions to discipline the IRFs. Compared to the IRFs obtained using the ACR index, the responses of the endogenous variables to a supply chain shock are less precisely estimated, and supply chain disturbances no longer explain the largest fraction of the unexpected fluctuations in the PCE goods and import prices. In terms of the historical decomposition of U.S. inflation, the HARPEX yields quantitatively similar results to those obtained using the ACR index. More specifically, the HARPEX attributes the initial fall in inflation at the onset of the pandemic to the collapse in demand and the subsequent, quick rise in inflation following the outbreak to both reduced capacity (e.g., labor shortage) and supply chain disruptions. Furthermore, it attributes the continuous surge in inflation since early 2021 to a combination of demand recovery, constrained capacity, and supply chain disturbances.

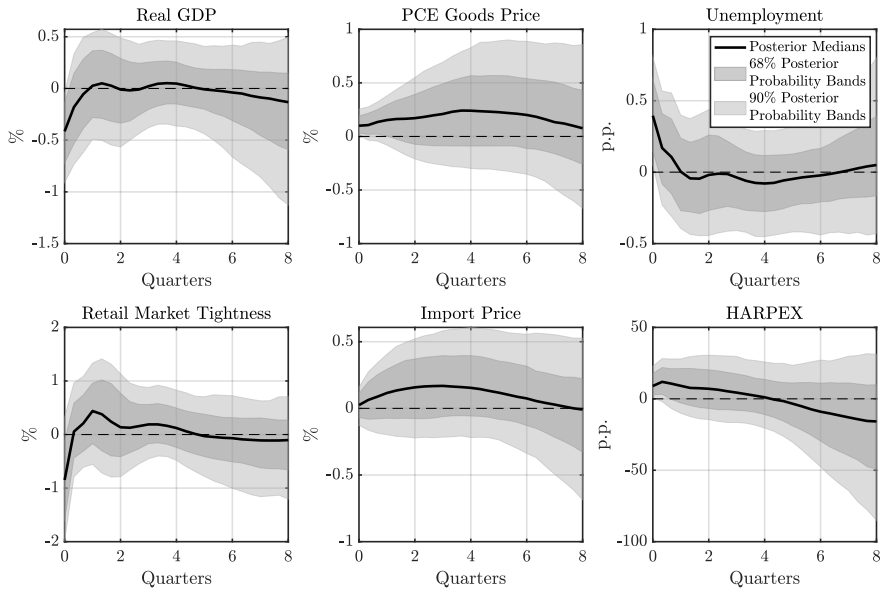


Figure F.2: IRFs to an Adverse Shock to Supply Chain: The HARPEX and Restrictions 1′, 2′, and 3′

Notes. The IRFs to a one standard deviation adverse shock to the supply chain are identified using the HARPEX and Restrictions 1′, 2′, and 3′. The solid line shows the point-wise posterior medians, and the shaded bands represent the 68% and 90% equal-tailed point-wise posterior probability bands. The figure is based on 100,000 independent draws.

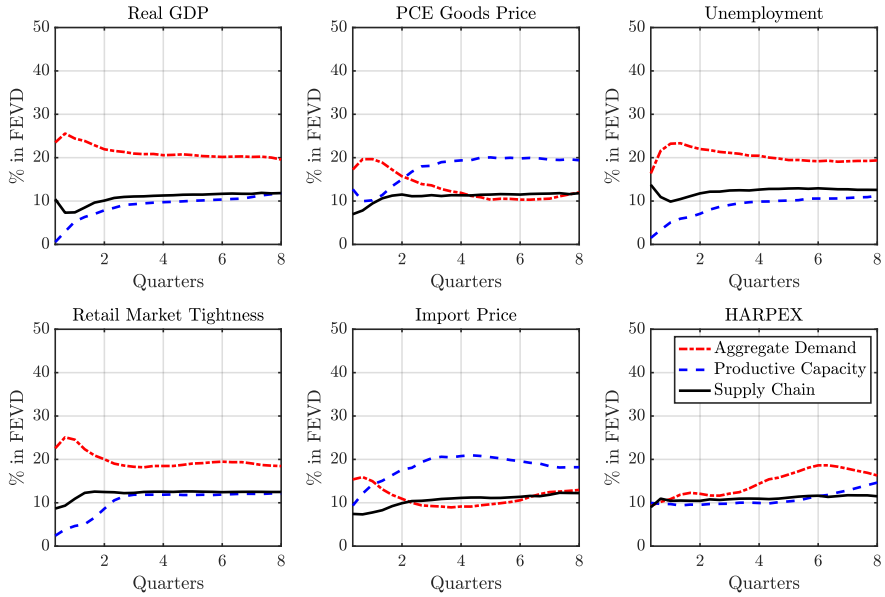


Figure F.3: FEVD from the SVAR: The HARPEX and Restrictions 1′, 2′, and 3′

Notes. Each line presents the median fraction of the forecast error variance for each endogenous variable, explained by each of the three identified structural shocks at various time horizons. The FEVD is estimated using the HARPEX and Restrictions 1′, 2′, and 3′, and based on 100,000 independent draws.

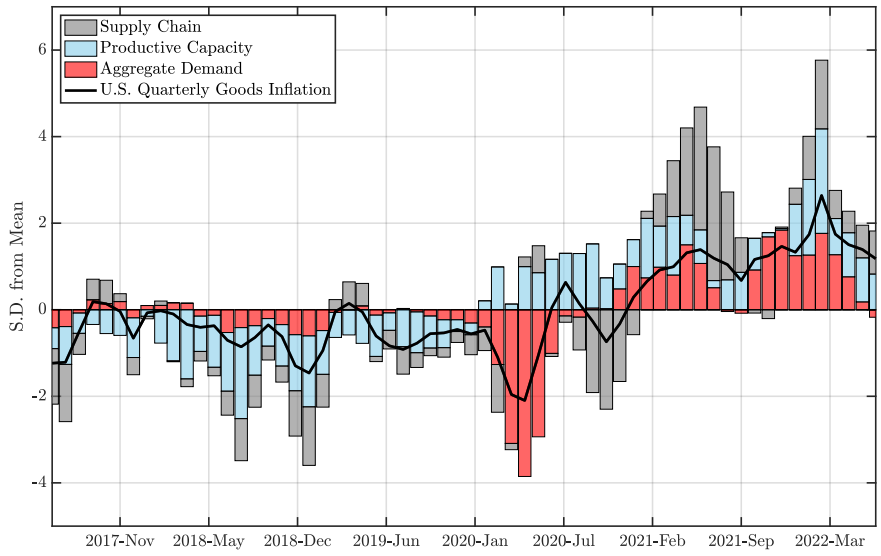


Figure F.4: HD of U.S. Goods Inflation: The HARPEX and Restrictions 1′, 2′, and 3′

Notes. The solid line represents the standardized quarterly goods inflation rate in the U.S., i.e., quarter-on-quarter growth of the PCE goods price index. The shaded bar represents the standardized cumulative historical contribution of each of the three structural shocks identified using the HARPEX and Restrictions 1′, 2′, and 3′ to U.S. goods inflation. The estimation results are based on all endogenous variables being measured as a percent change from the previous period, with the exceptions of unemployment and the HARPEX, which are measured as a change from the previous period. The figure is derived from 100,000 independent draws.

F.2. GSCPI

Next, we compare our ACR index with the GSCPI to highlight the differences in the measurement of supply chain disruptions. The GSCPI uses information on cross-border transportation costs and the sub-components of the country-specific manufacturing PMI (e.g., "delivery times" as in Kamali & Wang (2021), Benigno et al. (2022)) to infer supply chain disruptions.[14] As discussed in the introduction, the GSCPI is potentially problematic because it (i) relies on transportation costs that are subject to variations in both the supply of and demand for tradable goods, (ii) depends on information gathered from purchasing managers that might reflect subjective views rather than realized disturbances to the supply chain, and (iii) uses the PMI, which does not specify if an increase in delivery times results from a disruption to the supply chain or from issues with the actual production process.

[14]IHS Markit (Williamson 2021) calculates the suppliers' delivery times using the survey responses in the PMI. Specifically, participating purchasing managers are asked if it takes their suppliers more or less time to provide inputs to their factories on average. The percentages of companies reporting an improvement, deterioration, or no change in delivery times are then weighted to derive the index.

Table F.1: ACR, HARPEX, and Ship Visits

	(1) ACR	(2) HARPEX
# Ship Visits	-0.0018	-0.0286^{***}
	(0.00183)	(0.00614)
Port FE	Yes	N/A
Time FE	Yes	N/A
Obs	3,256	67
R^2	0.0355	0.2499

Notes. Column (1) shows the estimated coefficient when we regress the port-specific congestion rate on the number of ship visits to each port, controlling for both port and time fixed effects (FE). Column (2) presents the estimated coefficient when we regress the HARPEX on the total number of ship visits across the top 50 container ports worldwide. Both the congestion rates and the number of ship visits are computed using the AIS data of containerships and our IMA-DBSCAN algorithm, as detailed in Appendix B. The HARPEX is constructed by calculating the year-on-year percentage changes of the original series. *** indicates $p < 0.01$.

In contrast, our ACR index employs maritime satellite data to estimate congestion at seaports around the globe. Our approach sidesteps the main shortcomings of the GSCPI. As extensively documented in Stopford (2008), Song & Dong (2012), Wang et al. (2019), Brancaccio et al. (2020, 2023), containerships operate on fixed itineraries and predetermined routes.[15] Hence, our index is independent of variations in the demand for tradable goods and the derived demand for shipping services. Table F.1 shows that our ACR series is statistically uncorrelated with the number of ship visits at each port (Column 1), whereas the HARPEX, which captures shipping prices, is significantly correlated with the number of ship visits (Column 2).[16] Furthermore, any infrequent adjustments in shipping capacity across routes, and the resulting changes in congestion at different ports, are canceled out when we aggregate the congestion rates to construct the ACR index, thereby enhancing its

[15] Routes are rarely altered because diversions in shipping routes typically incur substantial transition costs. Moreover, changes in routes would severely affect the stability of shipping operations and the loyalty of customers (Wang et al. 2019).

[16] It should be noted that the correlation between the HARPEX and the number of ship visits is estimated at the global level, as there is no disaggregated data on shipping prices at the port level. We also check the robustness of our baseline results in Section 4 by applying a fitted ACR index in our estimation after regressing the port-specific congestion rate on the Oxford Stringency (OS) index (Mathieu et al. 2020) and port fixed effect. As shown in Appendix H, such results are quantitatively similar to those obtained using the ACR index directly.

exogeneity in measuring global supply chain disruptions. Finally, we avoid the issue of biased managerial perceptions by tracking the congestion at seaports in real-time. Collectively, our ACR index offers an exogenous and accurate measure of global supply chain disruptions.

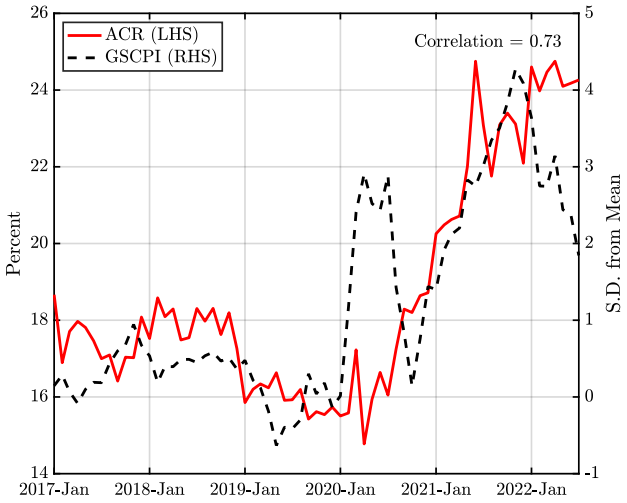


Figure F.5: ACR vs. GSCPI

Notes. Figure F.5 plots the ACR index (red solid line) against the GSCPI (black dashed line) for the sample period from January 2017 to July 2022. The ACR index is computed using AIS data of containerships and our IMA-DBSCAN algorithm detailed in Appendix B. The GSCPI is retrieved from the Federal Reserve Bank of New York's website (Source: `https://www.newyorkfed.org/research/policy/gscpi#/overview`, accessed August 10, 2022). The ACR index is measured in percent, while the GSCPI is in standard deviations from the mean. Both series are seasonally adjusted.

Figure F.5 displays the ACR and GSCPI indices over the sample period from January 2017 to July 2022. Before 2020, the dynamics of the two indices were similar, but the GSCPI substantially increased at the onset of the Covid-19 pandemic in early 2020 and remained elevated in the first half of the year. From late-2020 onwards, the two series rose similarly until January 2022. di Giovanni et al. (2022) attributes the jump in the GSCPI in early 2020 to the onset of the Chinese lockdown, and the sudden fall in the second half of 2020 to the partial reopening of China and Europe. Our index of port congestion suggests that the initial lockdown in China did not lead to congestion of a magnitude that would generate a global supply chain disruption, and equally, the reopening of China and Europe did not substantially ease port congestion. Thus, the changes in the GSCPI are likely driven by sudden shifts in demand and management's misperception of supply chain issues as recorded by the PMI surveys. We also note that the two series diverged again in early 2022, with the

ACR remaining elevated while the GSCPI began to plummet. We argue that the high ACR index can be largely attributed to the stringent containment measures still in place in China during the first half of 2022, which continuously exerted pressure on the global supply chain.

Now, we assess the implications of the differences between the ACR and GSCPI indices concerning the inferences the SVAR model makes about the causal effects of supply chain disruptions. Figure F.6 displays the IRFs following an adverse supply chain shock when using the GSCPI. While these responses are less precisely estimated, the reactions of real GDP, unemployment, and retail market tightness are similar to the baseline responses captured using the ACR index, as shown in Figure 11. However, the responses of the PCE goods and import prices hover around zero and are statistically insignificant. Moreover, the response of the GSCPI is positive initially but reverts to zero after one quarter.

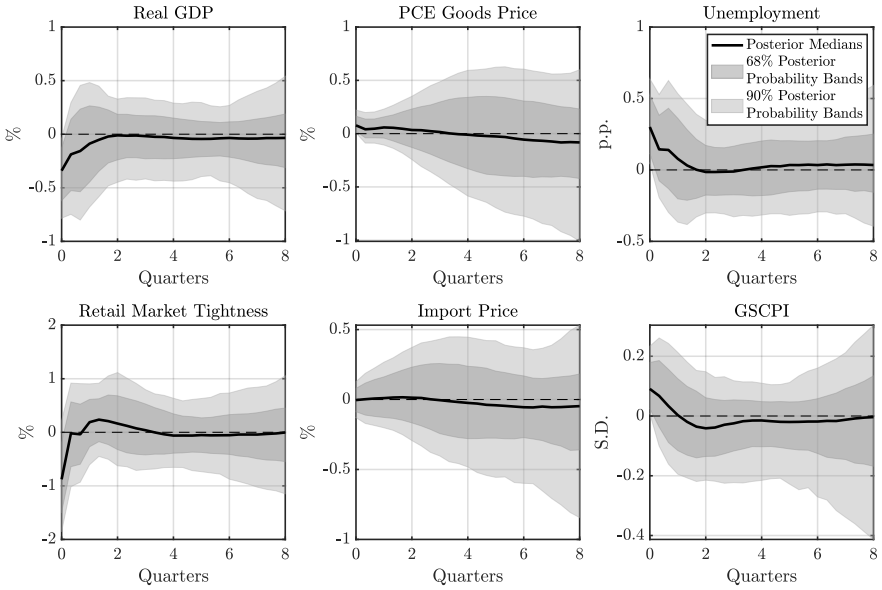


Figure F.6: IRFs to an Adverse Shock to Supply Chain: The GSCPI and Restrictions 1′, 2′, and 3′

Notes. The IRFs to a one standard deviation adverse shock to the supply chain are identified using the GSCPI and Restrictions 1′, 2′, and 3′. The solid line shows the point-wise posterior medians, and the shaded bands represent the 68% and 90% equal-tailed point-wise posterior probability bands. The figure is based on 100,000 independent draws.

Figure F.7 depicts the proportion of forecast error variance explained by each of the three structural shocks, identified using the GSCPI and Restrictions 1′, 2′, and 3′. In alignment with the decomposition achieved using the ACR index (as seen in Figure 12), aggregate

demand shocks remain the predominant source of unexpected fluctuations in real GDP, unemployment, and retail market tightness when the GSCPI is incorporated into the estimation. Nevertheless, while the supply chain shock explains a significant portion of the unanticipated variations in the PCE goods and import prices over extended periods using the ACR index, it accounts for only a minimal fraction with the GSCPI. This observation aligns with the zero and statistically insignificant responses of the PCE goods and import prices to the supply chain shock observed with the GSCPI index, as shown in Figure F.6.

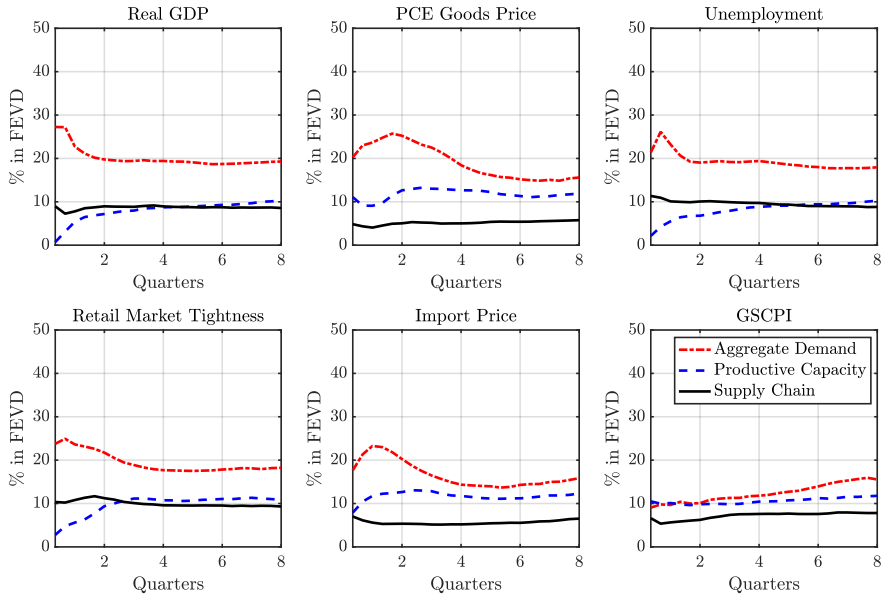


Figure F.7: FEVD from the SVAR: The GSCPI and Restrictions 1′, 2′, and 3′

Notes. Each line presents the median fraction of the forecast error variance for each endogenous variable, explained by each of the three identified structural shocks at various time horizons. The FEVD is estimated using the GSCPI and Restrictions 1′, 2′, and 3′, and based on 100,000 independent draws.

Finally, Figure F.8 shows the cumulative historical contribution of each of the three structural shocks to U.S. goods inflation when the GSCPI is included in the estimation. Unlike the results based on the ACR index, those using the GSCPI attribute the early falls in inflation following the Covid-19 pandemic to positive shocks to the supply chain. Meanwhile, the continuous rise in inflation from late 2020 onwards is principally explained by positive demand shocks.

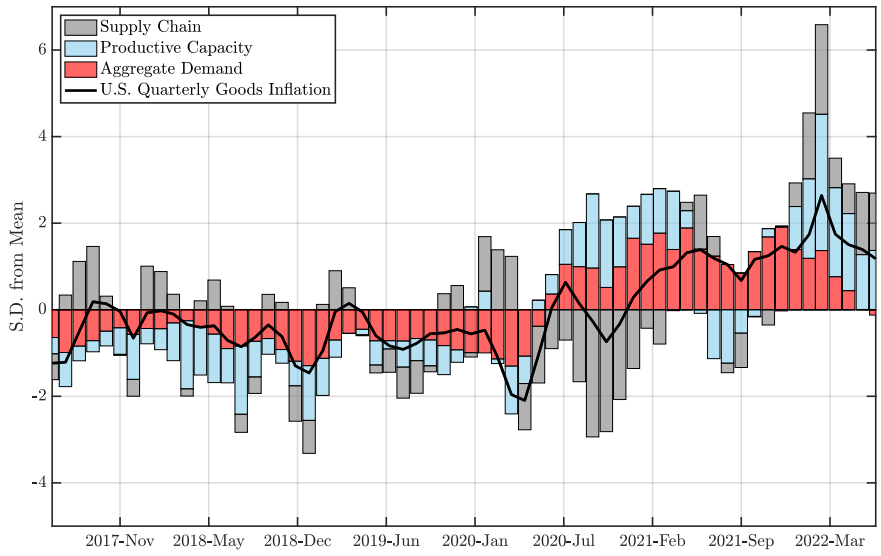


Figure F.8: HD of U.S. Goods Inflation: The GSCPI and Restrictions 1′, 2′, and 3′

Notes. The solid line represents the standardized quarterly goods inflation rate in the U.S., i.e., quarter-on-quarter growth of the PCE goods price index. The shaded bar represents the standardized cumulative historical contribution of each of the three structural shocks identified using the GSCPI and Restrictions 1′, 2′, and 3′ to U.S. goods inflation. The estimation results are based on all endogenous variables being measured as a percent change from the previous period, with the exception of unemployment, which is measured as a change from the previous period. The figure is derived from 100,000 independent draws.

F.3. SDI and Other Indices

In addition to the HARPEX and GSCPI, several other indices of supply chain disruptions utilize either more advanced techniques (e.g., machine learning) or more granular data (e.g., import transactions).[17] For instance, Smirnyagin & Tsyvinski (2022) leverage the S&P Global Panjiva dataset, a comprehensive repository of U.S. seaborne import records, to derive the U.S. Supply Disruptions Index (SDI). They identify supply chain disruptions by observing regular and active consignee-shipper relationships over quarterly periods; a disruption is marked when a consistently active relationship becomes inactive for a quarter before resuming. Although this identification strategy zeroes in on disruptions within established trading relationships, potential endogeneity concerns may surface. For example, a consignee might temporarily cease orders due to diminished demand rather than a genuine supply chain

[17] Another example is the text-based index of supply disruptions that Burriel et al. (2023) develop using newspaper data, following the methodology by Baker et al. (2016). Although this index sidesteps the endogeneity issue by selecting only supply-side events, it is not free from measurement errors inherent in word definitions. For instance, a disruption to "supply" differs from one to the "supply chain", as the former might arise from a labor supply shortage.

disruption. Parsing out these scenarios based solely on the activity of consignee-shipper relationships can be intricate. Furthermore, while the SDI provides invaluable insights into U.S. imports and excels in generating asset pricing predictions, the ACR, as a global index, is more aligned with our primary objective of pinpointing *global* supply chain disruptions.

Figure F.9 plots the ACR index against the SDI. The SDI is observed to fluctuate around the sample median before 2020, experience a massive but short-lived spike in 2020, and then undergo a prolonged yet muted increase in 2021-2022. Figures F.10, F.11, and F.12 plot the estimation results with the SDI included in the SVAR as a measure of supply chain disruptions. Similar to the results obtained using the GSCPI, the responses of the PCE goods and import prices to a supply chain shock are marginally above zero and statistically insignificant, and only a minimal fraction of the unexpected fluctuations in the PCE goods and import prices is explained by supply chain disturbances. In terms of the historical decomposition of U.S. inflation, the SDI attributes the initial fall in inflation at the onset of the pandemic to both the collapse in demand and favorable shocks to the supply chain, and it attributes the subsequent rise in inflation from late 2020 onwards to a combination of demand and supply shocks.

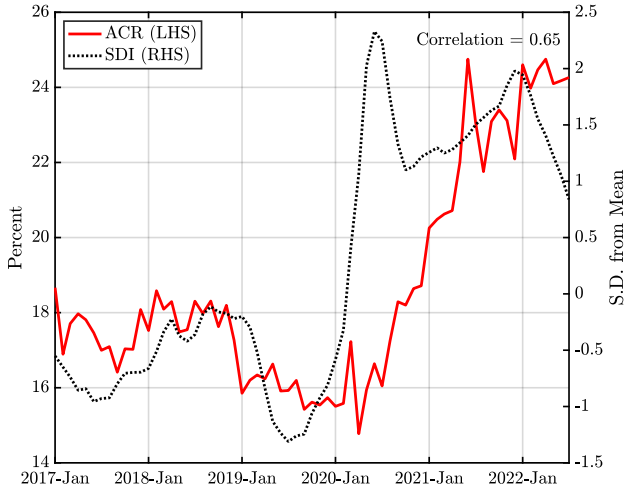


Figure F.9: ACR vs. SDI

Notes. Figure F.9 plots the ACR index (red solid line) against the SDI (black dotted line) for the sample period from January 2017 to July 2022. The ACR index is computed using the AIS data of containerships and our IMA-DBSCAN algorithm, as detailed in Appendix B. The SDI is retrieved from the author's website (Source: `https://www.disruptions.supply` (Accessed July 31, 2023)). The ACR index is measured in percent, while the SDI is measured in standard deviations from the mean. Both series are seasonally adjusted.

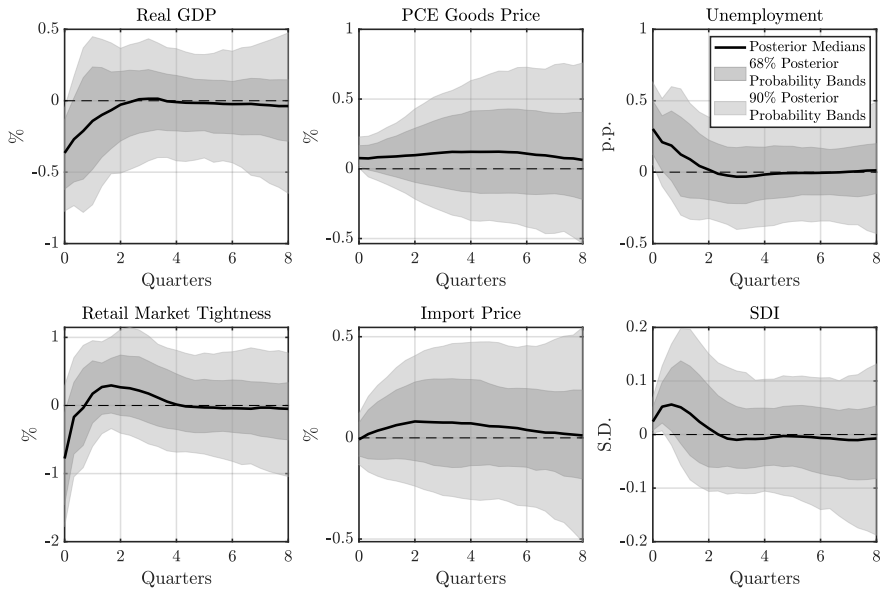


Figure F.10: IRFs to an Adverse Shock to Supply Chain: The SDI and Restrictions 1′, 2′, and 3′

Notes. The IRFs to a one standard deviation adverse shock to the supply chain are identified using the SDI and Restrictions 1′, 2′, and 3′. The solid line shows the point-wise posterior medians, and the shaded bands represent the 68% and 90% equal-tailed point-wise posterior probability bands. The figure is based on 100,000 independent draws.

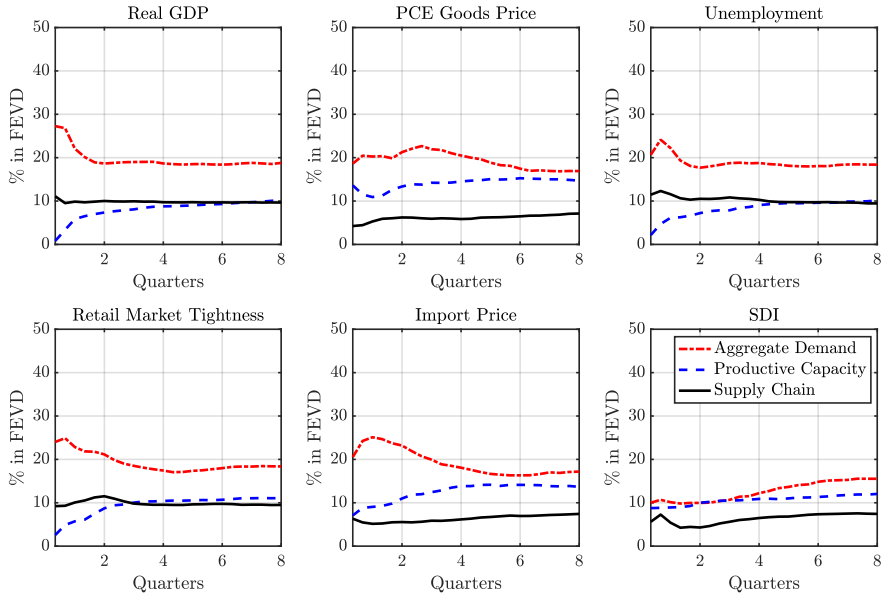


Figure F.11: FEVD from the SVAR: The SDI and Restrictions 1′, 2′, and 3′

Notes. Each line presents the median fraction of the forecast error variance for each endogenous variable, explained by each of the three identified structural shocks at various time horizons. The FEVD is estimated using the SDI and Restrictions 1′, 2′, and 3′, and based on 100,000 independent draws.

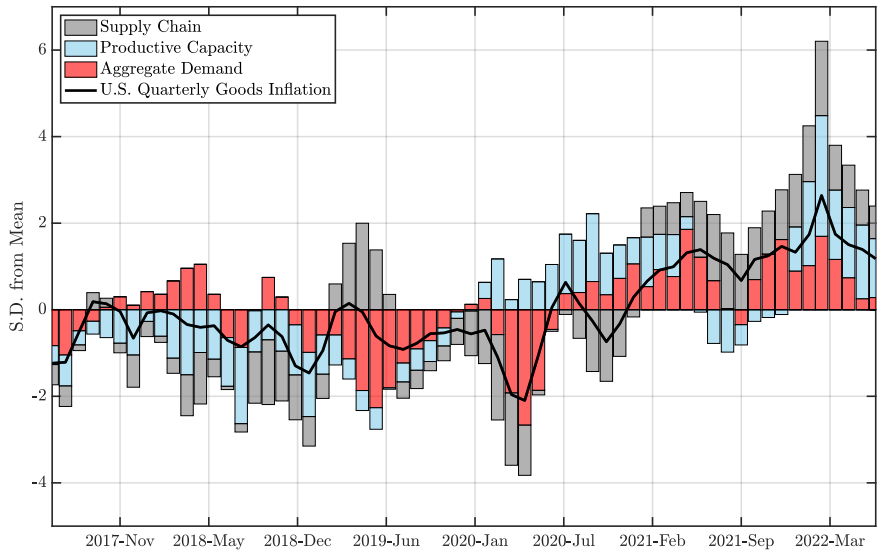


Figure F.12: HD of U.S. Goods Inflation: The SDI and Restrictions 1′, 2′, and 3′

Notes. The solid line represents the standardized quarterly goods inflation rate in the U.S., i.e., quarter-on-quarter growth of the PCE goods price index. The shaded bar represents the standardized cumulative historical contribution of each of the three structural shocks identified using the SDI and Restrictions 1′, 2′, and 3′ to U.S. goods inflation. The estimation results are based on all endogenous variables being measured as a percent change from the previous period, with the exception of unemployment, which is measured as a change from the previous period. The figure is derived from 100,000 independent draws.

Lastly, the Kiel trade indicator (Stamer 2021), which uses the same AIS data as ours, provides another angle to assess the widespread strain on the global supply chain from the estimate of imports and exports and the traffic of containerships at major ports as well as freight on stationary ships. However, this indicator entails several issues. First, the calculation of twenty-foot equivalent units (TEU) is problematic because the drought of a containership is not indicative of its loading status since loading and unloading operations could occur simultaneously. Second, variations in imports and exports are also subject to demand-side factors, leading to the same endogeneity issues of the indices based on transportation costs. Third, the calculation of cargo capacity tied up at ports does not differentiate mooring positions of containerships (berth vs. anchorage), which, as argued in Talley & Ng (2016), could result in an overestimation of port congestion.

G. Average Congestion Time

In this appendix, we introduce an alternative congestion metric for ports, the Average Congestion Time (ACT). This is again derived using the AIS data of containerships, coupled with our IMA-DBSCAN algorithm. Unlike the ACR index, the ACT index measures the average number of hours a containership waits in an anchorage area of a port before docking at a berth, weighted by the number of ship visits to the top 50 container ports worldwide:

$$ACT_t = \sum_{p \in \mathcal{P}} \left[\frac{Delayed_{pt} + Undelayed_{pt}}{\sum_{p \in \mathcal{P}} \left(Delayed_{pt} + Undelayed_{pt} \right)} \cdot \frac{DelayHours_{pt}}{Delayed_{pt} + Undelayed_{pt}} \right].$$

where $Delayed_{pt}$, $Undelayed_{pt}$, and $DelayHours_{pt}$ represent the number of delayed and undelayed ship visits, as well as the total number of hours that containerships spend in the anchorage areas of port p in month t, respectively.

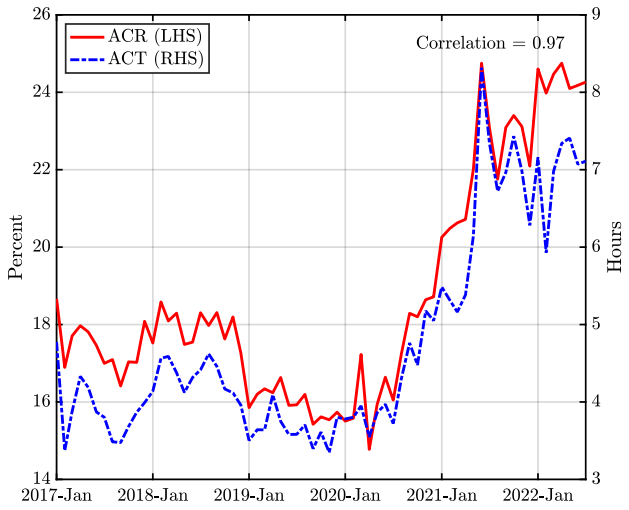


Figure G.1: ACR vs. ACT

Notes. Figure G.1 plots the ACR index (red solid line) against the ACT index (blue dashed-dotted line) for the sample period from January 2017 to July 2022. Both the ACR and ACT indices are computed using the AIS data of containerships and our IMA-DBSCAN algorithm, as detailed in Appendix B. The ACR index is measured in percent while the ACT index is measured in hours. Both series have been seasonally adjusted.

Figure G.1 plots the ACT index. As seen, it co-moves with the ACR index closely, with a correlation standing at 0.97. Not surprisingly, referring to Figures G.2, G.3, and G.4, using the ACT index in the causality assessment delivers quantitatively similar results to those obtained with the ACR index.

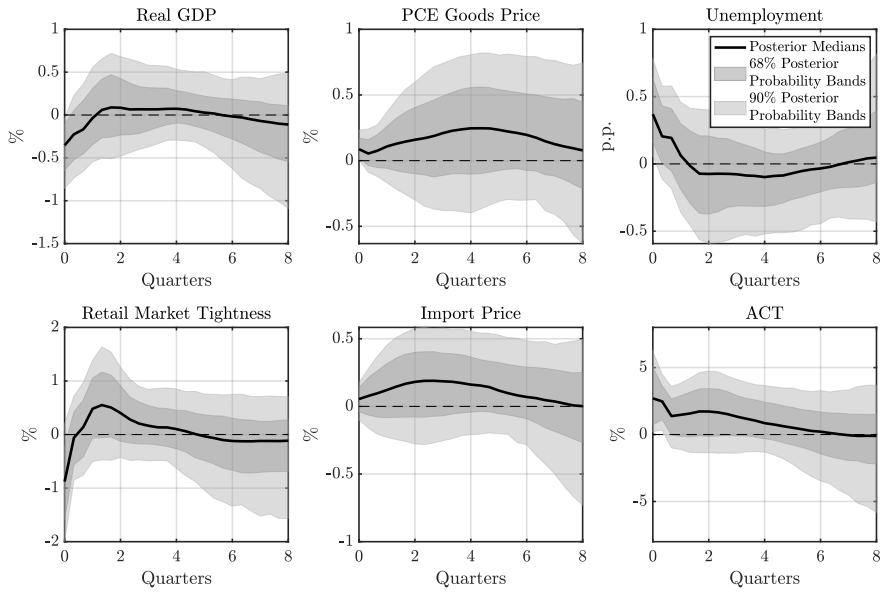


Figure G.2: IRFs to an Adverse Shock to Supply Chain: The ACT Index and Restrictions 1, 2, and 3

Notes. The IRFs to a one standard deviation adverse shock to the supply chain are identified using the ACT index and Restrictions 1, 2, and 3. The solid line shows the point-wise posterior medians, and the shaded bands represent the 68% and 90% equal-tailed point-wise posterior probability bands. The figure is based on 100,000 independent draws.

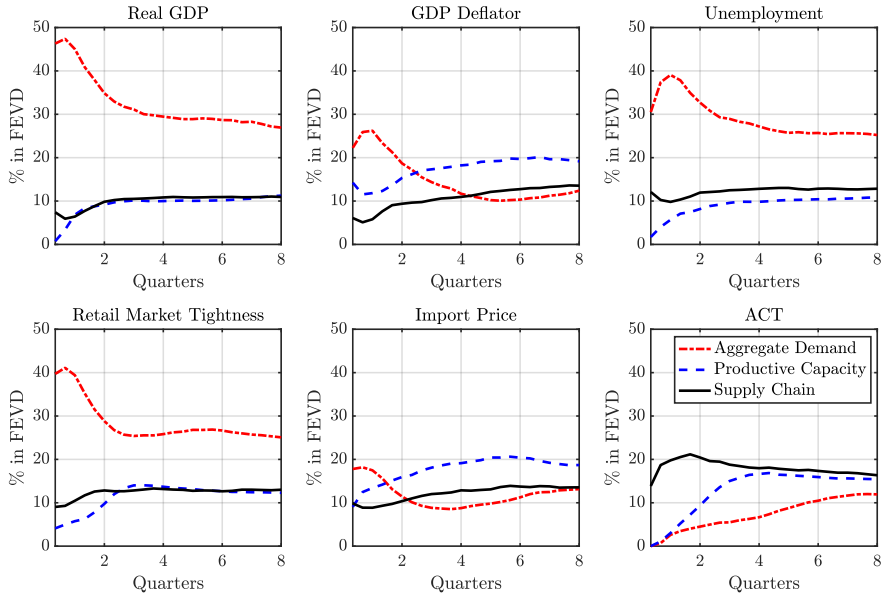


Figure G.3: FEVD from the SVAR: The ACT Index and Restrictions 1, 2, and 3

Notes. Each line presents the median fraction of the forecast error variance for each endogenous variable, explained by each of the three identified structural shocks at various time horizons. The FEVD is estimated using the ACT index and Restrictions 1, 2, and 3, and based on 100,000 independent draws.

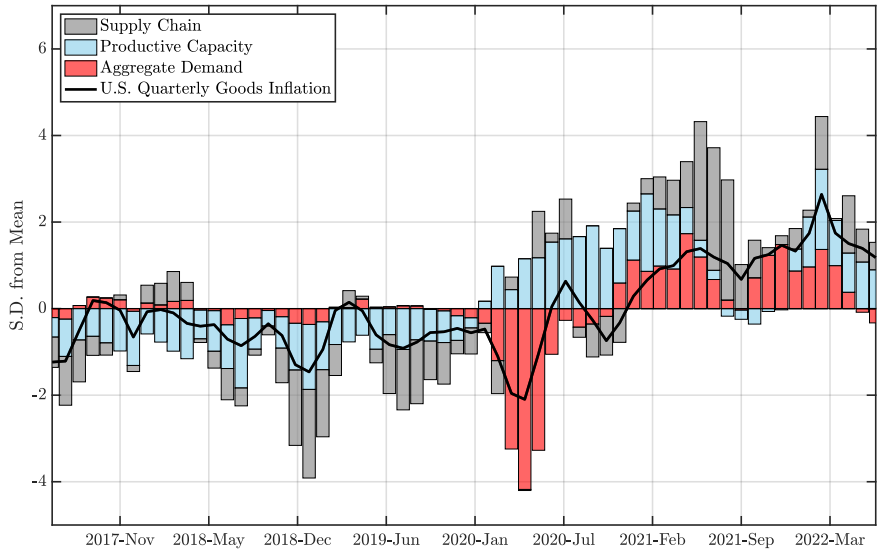


Figure G.4: HD of U.S. Goods Inflation: The ACT Index and Restrictions 1, 2, and 3

Notes. The solid line represents the standardized quarterly goods inflation rate in the U.S., i.e., quarter-on-quarter growth of the PCE goods price index. The shaded bar represents the standardized cumulative historical contribution of each of the three structural shocks identified using the ACT index and Restrictions 1, 2, and 3 to U.S. goods inflation. The estimation results are based on all endogenous variables being measured as a percent change from the previous period, with the exception of unemployment, which is measured as a change from the previous period. The figure is derived from 100,000 independent draws.

H. Fitted ACR

In this appendix, we conduct a robustness check of our baseline results by employing a fitted ACR index in our estimation after regressing the port-specific congestion rate on the Oxford Stringency (OS) index (Mathieu et al. 2020) and port fixed effect.[18] This robustness check is intended to mitigate the potential endogeneity concerns with the ACR index when significant changes in shipping capacity between routes, due to demand shifters, contribute to port congestion.

The OS index essentially measures the severity of mobility restriction policies. Specifically, it aggregates data on when and what actions governments take to mitigate the spread of COVID-19, averaging nine component indicators that reflect the intensity of school closures, workplace shutdowns, public event cancellations, restrictions on public gatherings, public transport closures, stay-at-home orders, public information campaigns, internal movement limitations, and international travel controls. Since the OS index is exclusively designed to capture the strictness of government policies, it is not influenced by demand-side factors. Notably, stringent government policies, as indicated by a high OS index, are presumed to significantly exacerbate port congestion globally, thereby playing a central role in the global supply chain disruptions. Therefore, the OS index serves as an instrument for the congestion rate, and the resulting fitted ACR index, $\widehat{\text{ACR}}$, is used to isolate the causal impact of global supply chain disruptions.

In practice, we compute the monthly average OS index for the country of each major container port, limiting our sample to start from January 2020, as the OS index data is only available from this point onwards. Next, we regress the port-specific congestion rate on the respective OS index and port fixed effect, extracting the fitted values and computing the weighted average, $\widehat{\text{ACR}}$, with weights still determined by the number of ship visits to each port. This fitted ACR index is then used in our estimation. Consistent with our earlier approach, we impose Restrictions 1, 2, and 3 on the IRFs, and the estimation follows the Bayesian methodology as outlined in Arias et al. (2018, 2019, 2023). Although we retain the same specifications as in the baseline, the reduced sample length necessitates including only

[18] We thank Kun Wang for suggesting this robustness check.

one lag in the estimation and calculating the IRFs for just one year post-impact to reduce parameter uncertainty.

The IRFs to each structural shock, as illustrated in Figures H.1 to H.3, are quantitatively akin to those depicted in Figures 9 to 11, confirming the robustness of our baseline results.

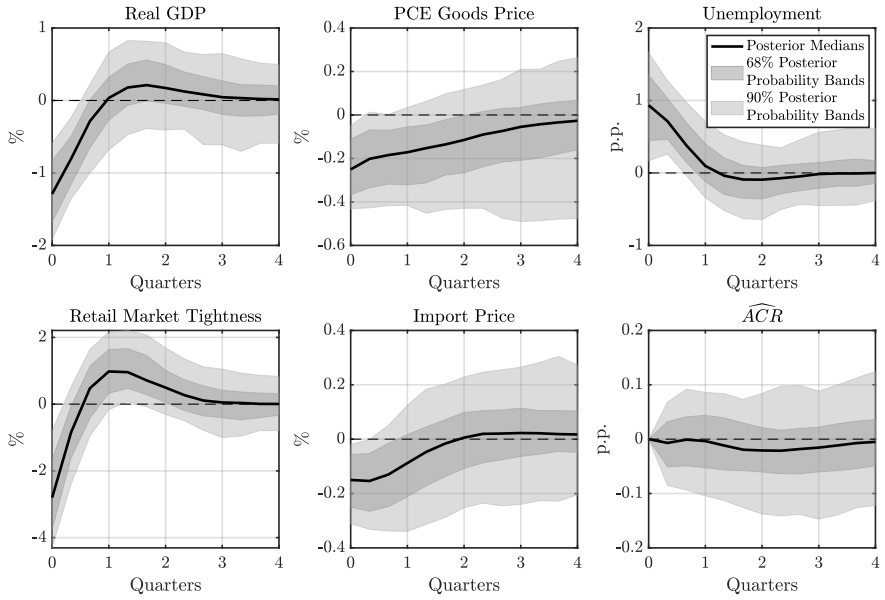


Figure H.1: IRFs to an Adverse Shock to Aggregate Demand: $\widehat{\text{ACR}}$

Notes. The IRFs to a one standard deviation adverse shock to aggregate demand are identified using $\widehat{\text{ACR}}$ and Restrictions 1, 2, and 3. The solid line shows the point-wise posterior medians, and the shaded bands show the 68% and 90% equal-tailed point-wise posterior probability bands. The figure is based on 100,000 independent draws.

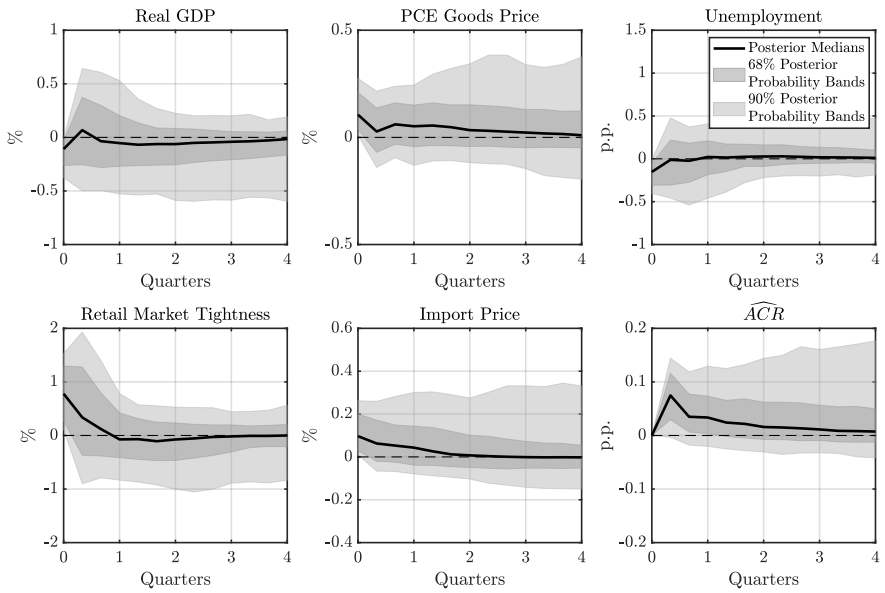


Figure H.2: IRFs to an Adverse Shock to Productive Capacity: $\widehat{\text{ACR}}$

Notes. The IRFs to a one standard deviation adverse shock to productive capacity are identified using $\widehat{\text{ACR}}$ and Restrictions 1, 2, and 3. The solid line shows the point-wise posterior medians, and the shaded bands show the 68% and 90% equal-tailed point-wise posterior probability bands. The figure is based on 100,000 independent draws.

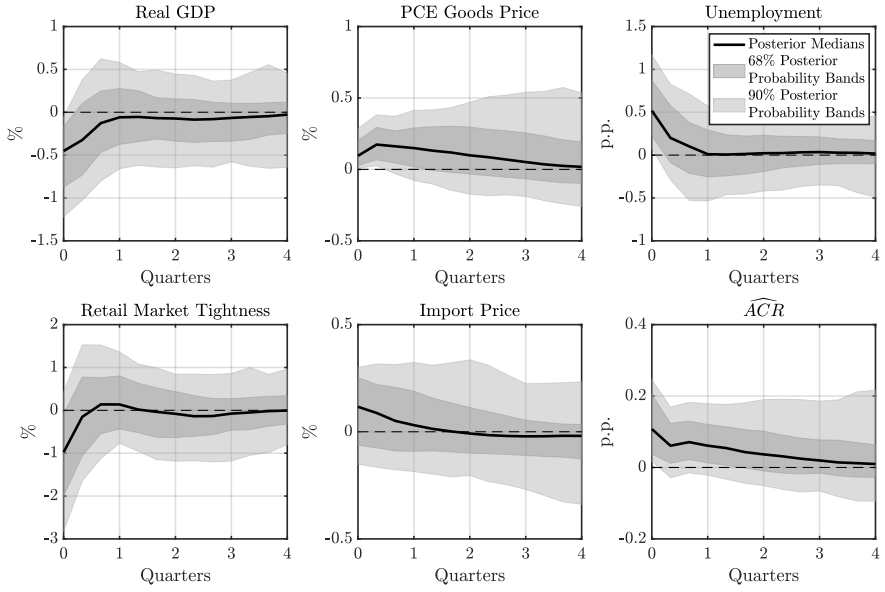


Figure H.3: IRFs to an Adverse Shock to Supply Chain: $\widehat{\text{ACR}}$

Notes. The IRFs to a one standard deviation adverse shock to the supply chain are identified using $\widehat{\text{ACR}}$ and Restrictions 1, 2, and 3. The solid line shows the point-wise posterior medians, and the shaded bands show the 68% and 90% equal-tailed point-wise posterior probability bands. The figure is based on 100,000 independent draws.

I. Priors and Identification in TVAR

I.1. Priors

Our formulation of the prior in the TVAR model follows Bańbura et al. (2010), Mumtaz & Zanetti (2012), Pizzinelli et al. (2020), and the same prior has been applied to the parameters in both the supply chain disrupted ($\mathbb{D}$) and undisrupted ($\mathbb{U}$) regimes. Specifically, we write the TVAR model in Equation (26) compactly as a system of multivariate regressions:

$$\boldsymbol{y} = (\boldsymbol{M}_{\mathbb{D}}\boldsymbol{x}_{\mathbb{D}} + \boldsymbol{u}_{\mathbb{D}})\boldsymbol{I} + (\boldsymbol{M}_{\mathbb{U}}\boldsymbol{x}_{\mathbb{U}} + \boldsymbol{u}_{\mathbb{U}})(\boldsymbol{1}_{T\times T} - \boldsymbol{I}), \tag{I.1}$$

where $\boldsymbol{y} = [\boldsymbol{y}_1 \ \dots \ \boldsymbol{y}_T]$ is an $n \times T$ matrix, $\boldsymbol{x}_{\mathbb{D}} = [\boldsymbol{x}_{\mathbb{D},1} \ \dots \ \boldsymbol{x}_{\mathbb{D},T}]$ is an $m \times T$ matrix with $\boldsymbol{x}_{\mathbb{D},t} = [\boldsymbol{y}'_{t-1} \ \dots \ \boldsymbol{y}'_{t-L} \ \boldsymbol{\omega}'_t]'$, $\boldsymbol{x}_{\mathbb{U}} = [\boldsymbol{x}_{\mathbb{U},1} \ \dots \ \boldsymbol{x}_{\mathbb{U},T}]$ is an $m \times T$ matrix with $\boldsymbol{x}_{\mathbb{U},t} = [\boldsymbol{y}'_{t-1} \ \dots \ \boldsymbol{y}'_{t-L} \ \boldsymbol{\omega}'_t]'$, $\boldsymbol{\omega}_t = [1, t]'$ is a 2×1 vector of a constant and a linear trend, $\boldsymbol{u}_{\mathbb{D}} = [\boldsymbol{\Sigma}_{\mathbb{D}}^{1/2}\boldsymbol{\epsilon}_1 \ \dots \ \boldsymbol{\Sigma}_{\mathbb{D}}^{1/2}\boldsymbol{\epsilon}_T]$ is an $n \times T$ matrix, $\boldsymbol{u}_{\mathbb{U}} = [\boldsymbol{\Sigma}_{\mathbb{U}}^{1/2}\boldsymbol{\epsilon}_1 \ \dots \ \boldsymbol{\Sigma}_{\mathbb{U}}^{1/2}\boldsymbol{\epsilon}_T]$ is an $n \times T$ matrix, $\boldsymbol{\Sigma}_{\mathbb{D}}$ and $\boldsymbol{\Sigma}_{\mathbb{U}}$ are the covariance matrices, $\boldsymbol{I} = diag[I_1 \ \dots \ I_T]$ is a $T \times T$ diagonal matrix, $\boldsymbol{M}_{\mathbb{D}} = [\boldsymbol{B}'_{\mathbb{D},1} \ \dots \ \boldsymbol{B}'_{\mathbb{D},L} \ \boldsymbol{C}'_{\mathbb{D}}]$ and $\boldsymbol{M}_{\mathbb{U}} = [\boldsymbol{B}'_{\mathbb{U},1} \ \dots \ \boldsymbol{B}'_{\mathbb{U},L} \ \boldsymbol{C}'_{\mathbb{U}}]$ are two $n \times m$ matrices containing the TVAR coefficients associated with each regime, and $m = nL + 2$. Given Equation (I.1), for each regime $r \in \{\mathbb{D}, \mathbb{U}\}$, we assume that the prior distribution of the parameter vector, $vec(\boldsymbol{M}_r)$, has a Normal-Inverse-Wishart conjugate form.[19] Such a form can be written as:

$$\begin{aligned} vec(\boldsymbol{M}_r)|\boldsymbol{\Sigma}_r &\sim N\Big(vec(\boldsymbol{M}_r^0), \boldsymbol{\Sigma}_r \otimes \boldsymbol{\Omega}_r^0\Big), \\ \boldsymbol{\Sigma}_r &\sim IW\Big(\boldsymbol{S}_r^0, \alpha_r^0\Big), \end{aligned} \tag{I.2}$$

where $vec(\boldsymbol{M}_r^0)$ is the prior mean of the parameter vector, $\boldsymbol{\Omega}_r^0$ controls the tightness around this prior, $\boldsymbol{S}_r^0$ is the prior scale matrix of the Inverse-Wishart (IW) distribution, and α_r^0 denotes the prior degrees of freedom. Essentially, the prior in Equation (I.2) is a generalization of the Minnesota prior discussed in Litterman (1986) and assumes that the endogenous variables follow a random walk or an AR(1) process. This is based on the idea that recent lags provide more reliable information on the dynamics of the system and therefore the estimation should assign them a higher weighting. Unlike the original formulation in Litterman

[19] $vec(\cdot)$ denotes the operator that stacks the columns of a matrix into a vector.

(1986) however, the prior in Equation (I.2) does not assume a diagonal, fixed, and known covariance matrix, making it more suitable for our structural analysis.

The Normal-Inverse-Wishart prior implies that, while the prior expectations and variances of the coefficient matrices for the constant and linear trend, $\boldsymbol{C}_r$, are diffuse, those associated with the autoregressive matrices, $\boldsymbol{B}_{r,l}$, can be written as:

$$\begin{aligned}\mathbb{E}[(\boldsymbol{B}_{r,l})_{i,j}] &= \begin{cases}\beta^0_{r,i}, & \text{if } i=j,\ l=1;\\ 0, & \text{otherwise;}\end{cases}\\ \mathbb{V}[(\boldsymbol{B}_{r,l})_{i,j}] &= \lambda\sigma_i^2/\sigma_j^2,\end{aligned} \tag{I.3}$$

where $\beta^0_{r,1},\ldots,\beta^0_{r,n}$ are the prior means of the autoregressive coefficients, $\sigma_1,\ldots,\sigma_n$ are the prior error standard deviations, and the hyper-parameter λ controls the overall tightness of the prior distribution such that a larger λ corresponds to a looser prior. As described in Bańbura et al. (2010) and commonly used in the literature of Bayesian SVARs, the prior moments in Equation (I.3) can be implemented by adding $T_{r,d}$ dummy observations $\boldsymbol{y}_{r,d}$ and $\boldsymbol{x}_{r,d}$ to the system of regressions in Equation (I.1) that correspond to each regime, with $\boldsymbol{y}_{r,d}$ and $\boldsymbol{x}_{r,d}$ satisfying:

$$\boldsymbol{y}_{r,d} = \begin{bmatrix} diag[\beta^0_{r,1}\sigma_1 & \ldots & \beta^0_{r,n}\sigma_n]/\lambda \\ \boldsymbol{0}_{n(L-1)\times n} \\ diag[\sigma_1 & \ldots & \sigma_n] \\ \boldsymbol{0}_{2\times n}\end{bmatrix},\ \boldsymbol{x}_{r,d} = \begin{bmatrix} J_L \otimes diag[\sigma_1 & \ldots & \sigma_n]/\lambda & \boldsymbol{0}_{nL\times 1} & \boldsymbol{0}_{nL\times 1} \\ \boldsymbol{0}_{n\times nL} & & \boldsymbol{0}_{n\times 1} & \boldsymbol{0}_{n\times 1} \\ \boldsymbol{0}_{1\times nL} & & \xi & 0 \\ \boldsymbol{0}_{1\times nL} & & 0 & \xi\end{bmatrix},$$

where $J_L = diag[1 \quad \ldots \quad L]$ and the hyper-parameter ξ controls the prior on the constant and the linear trend such that a small number makes the prior uninformative. Subsequently, the prior moments in Equation (I.2) are simply functions of $\boldsymbol{y}_{r,d}$ and $\boldsymbol{x}_{r,d}$, which are given by:

$$\begin{aligned}\boldsymbol{M}^0_r &= \boldsymbol{y}_{r,d}\boldsymbol{x}'_{r,d}(\boldsymbol{x}_{r,d}\boldsymbol{x}'_{r,d})^{-1},\\ \boldsymbol{\Omega}^0_r &= (\boldsymbol{x}_{r,d}\boldsymbol{x}'_{r,d})^{-1},\\ \boldsymbol{S}^0_r &= (\boldsymbol{y}_{r,d}-\boldsymbol{M}^0_r\boldsymbol{x}_{r,d})(\boldsymbol{y}_{r,d}-\boldsymbol{M}^0_r\boldsymbol{x}_{r,d})',\\ \alpha^0_r &= T_{r,d}-m.\end{aligned}$$

With the Normal-Inverse-Wishart prior being conjugate, the conditional posterior distri-

bution of the parameter vector is also Normal-Inverse-Wishart (Bańbura et al. 2010, Mumtaz & Zanetti 2012):

$$vec(\boldsymbol{M}_r)|\boldsymbol{\Sigma}_r, \boldsymbol{y} \sim N\Big(vec(\tilde{\boldsymbol{M}}_r), \boldsymbol{\Sigma}_r \otimes (\tilde{\boldsymbol{x}}_r \tilde{\boldsymbol{x}}_r')^{-1}\Big),$$
$$\boldsymbol{\Sigma}_r|\boldsymbol{y} \sim IW\Big(\tilde{\boldsymbol{S}}_r, T_{r,d} + 2 + T - m\Big),$$

where the parameters associated with the posterior are given by:

$$\tilde{\boldsymbol{M}}_r = \tilde{\boldsymbol{y}}_r \tilde{\boldsymbol{x}}_r' (\tilde{\boldsymbol{x}}_r \tilde{\boldsymbol{x}}_r')^{-1},$$
$$\tilde{\boldsymbol{S}}_r^0 = (\tilde{\boldsymbol{y}}_r - \tilde{\boldsymbol{M}}_r \tilde{\boldsymbol{x}}_r)(\tilde{\boldsymbol{y}}_r - \tilde{\boldsymbol{M}}_r \tilde{\boldsymbol{x}}_r)',$$

in which the terms $\tilde{\boldsymbol{y}}_r$ and $\tilde{\boldsymbol{x}}_r$ are the matrices of $\boldsymbol{y}_r$ and $\boldsymbol{x}_r$ augmented with the dummy observations $\boldsymbol{y}_{r,d}$ and $\boldsymbol{x}_{r,d}$ respectively.[20]

Following Mumtaz & Zanetti (2012), Pizzinelli et al. (2020), we obtain the values of the prior mean of each autoregressive coefficient, $\beta_{r,i}^0$, as well as the prior error standard deviation, σ_i, from the OLS estimation of a univariate AR(1) model for each endogenous variable. In addition, we set $\lambda = 0.25$ to ensure fast lag decay towards zero. Finally, in terms of the prior distribution of $\overline{ACR}$, we assume that it is normally distributed, with the mean set at the median of the ACR series and the standard deviation calibrated to deliver a Markov Chain Monte Carlo (MCMC) acceptance rate of approximately 70%.

I.2. Identification Using the PFA

Following Uhlig (2005), Mountford & Uhlig (2009), the identification scheme we employ in the study of the state-dependent effects of a contractionary monetary policy shock amounts to finding an impulse vector a that minimizes a given criterion function $f(\cdot)$ on the space of all impulse vectors. This function penalizes positive impulse responses of real GDP, GDP deflator, and import price as well as negative impulse responses of the Federal Funds Rate and unemployment at horizons $k = 1, \ldots, K$, while satisfying the zero restriction imposed on the impulse response of ACR at horizon $k = 1$. The scheme is applied separately for the observations in each regime. Hence, for simplicity, we drop the regime-specific notation $r \in \{\mathbb{D}, \mathbb{U}\}$ in the following description.

[20] $\boldsymbol{y}_r$ is the part of $\boldsymbol{y}$ that is associated with regime $r \in \{\mathbb{D}, \mathbb{U}\}$.

The PFA is implemented numerically as follows. Define the penalty function as:

$$f(x) = \begin{cases} x, & \text{if } x \leq 0; \\ 100x, & \text{if } x > 0, \end{cases} \tag{I.4}$$

which penalizes positive responses in linear proportion and rewards negative responses in linear proportion, albeit at a slope 100 times smaller than the slope for penalties on the positive side. For the true VAR coefficients, let $r_{j,a}(k),\ k = 1, \ldots, K$ be the impulse response of variable j and σ_j be the standard deviation of the series for variable j. Let $\iota_j = -1$ if j is the index of Federal Funds Rate or unemployment in the data vector, and $\iota_j = 1$ if j is the index of real GDP, PCE goods price, retail market tightness, or import price in the data vector. Define the contractionary monetary policy impulse vector as that impulse vector a, which minimizes the total penalty $\varphi(a)$ subject to the zero restriction imposed on the impulse response of the ACR index at horizon $k = 1$:

$$\varphi(a) = \sum_{j \in \left\{ \begin{array}{c} \text{“Federal Funds Rate”}, \\ \text{“real GDP”}, \\ \text{“PCE goods price”}, \\ \text{“unemployment”}, \\ \text{“retail market tightness”}, \\ \text{“import price”} \end{array} \right\}} \Big[\sum_{k=1}^{K} f\Big(\iota_j \frac{r_{j,a}(k)}{\sigma_j} \Big) \Big].$$

The re-scaling by σ_j is necessary to make the deviations across different impulse responses comparable to each other. Note that the sign of the penalty direction is flipped for the Federal Funds Rate and unemployment. Since the true VAR is unknown, we find the contractionary monetary policy vector for each draw from the posterior. Such a step involves numerical minimization, and we keep all the draws and accordingly calculate all the corresponding impulse vectors. As a result, the IRFs in the main text are calculated based on these.

I.3. Posterior and Identified Regimes

The posterior distribution of the threshold $\overline{ACR}$ is plotted in Figure I.1, while the time series of the identified regimes using the median of such a posterior is plotted in Figure I.2.

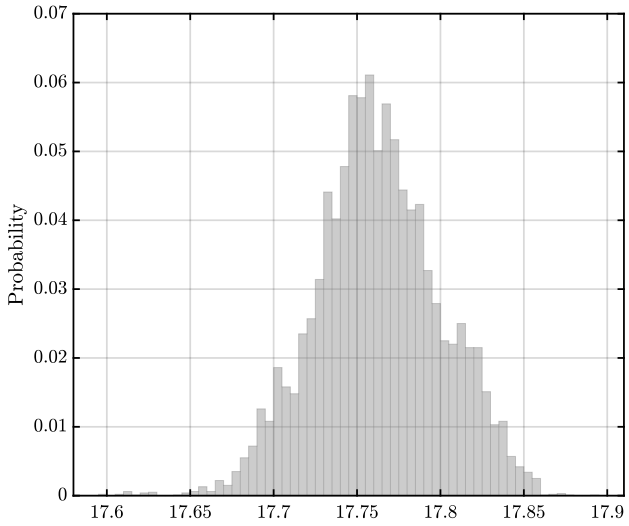


Figure I.1: Posterior Distribution of the Threshold $\overline{ACR}$

Notes. The figure plots the posterior distribution of the ACR threshold value, i.e., $\overline{ACR}$, based on 10,000 independent draws.

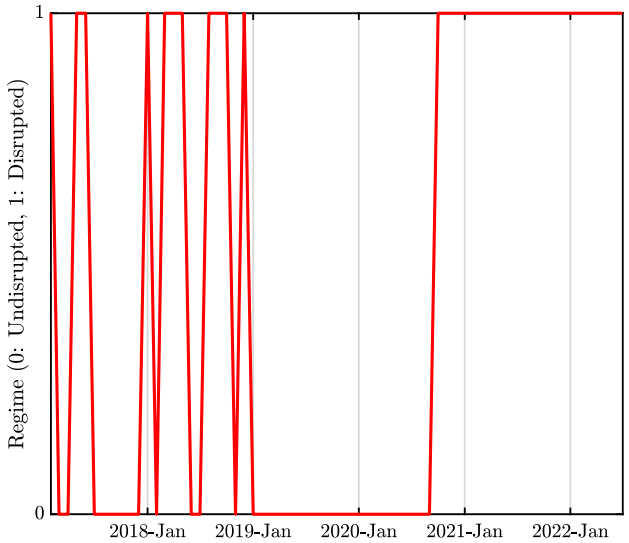


Figure I.2: Regimes Based on the Median of the Posterior $\overline{ACR}$

Notes. The solid line, switching from zero to one, represents the current regime as identified by the median of the posterior distribution of the ACR threshold, i.e., $median(\overline{ACR}) = 17.8\%$. The value of one corresponds to the supply chain disrupted ($\mathbb{D}$) regime, while the value of zero corresponds to the supply chain undisrupted ($\mathbb{U}$) regime.

J. Robustness of TVAR Results

In Figure J.1, we first show that our state-dependence results are robust to using the Wu-Xia Shadow Federal Funds Rate (Wu & Xia 2016) to reflect the stance of U.S. monetary policy. The Wu-Xia Shadow Federal Funds Rate provides an estimated Federal Funds Rate during periods when it is constrained by the Zero Lower Bound (ZLB), reflecting unconventional monetary policy effects and offering a nuanced gauge of economic conditions when traditional metrics are limited.

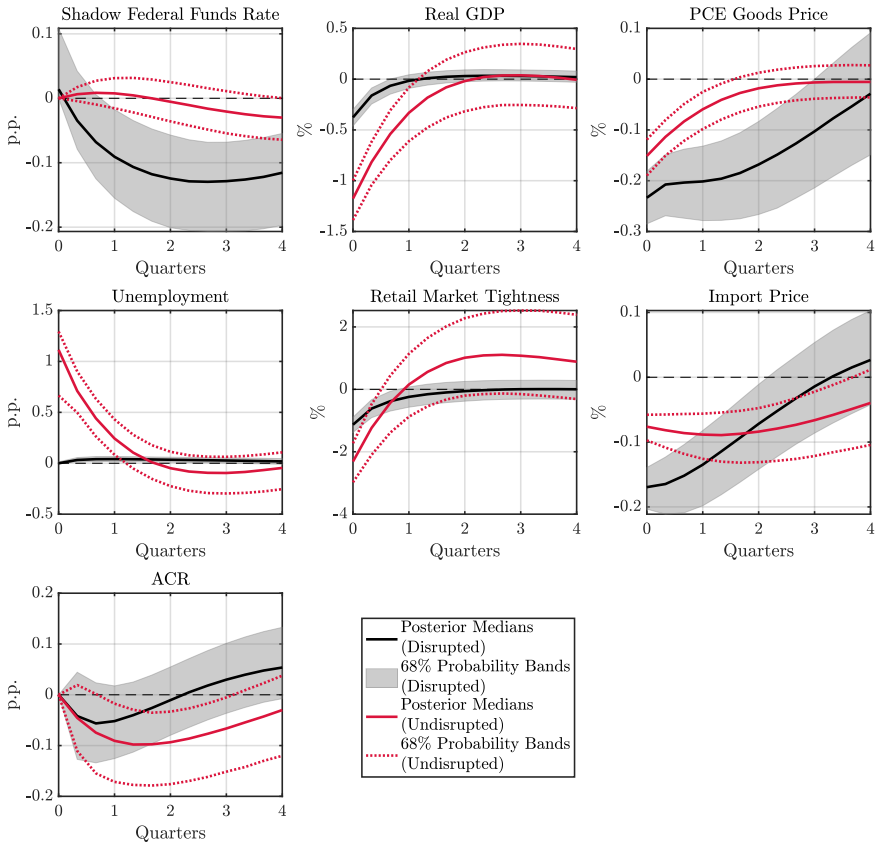


Figure J.1: State-Dependent Effects of a Contractionary Monetary Policy Shock: Wu-Xia Shadow Federal Funds Rate

Notes. The figure shows the IRFs to a one standard deviation contractionary monetary policy shock identified using a TVAR specification as in Equation (26), with the Wu-Xia Shadow Federal Funds Rate (Wu & Xia 2016) included to reflect the stance of U.S. monetary policy, as well as Restriction 4, for both the supply chain disrupted and undisrupted regimes. The black solid (red solid) line shows the point-wise posterior medians, and the black shaded area (red dotted lines) depicts the 68% equal-tailed point-wise posterior probability bands for the supply chain disrupted (undisrupted) regime. The figure is based on 10,000 independent draws from the posterior.

In Figure J.2, we show that our state-dependence results are robust to dropping the zero restriction imposed on the on-impact response of the ACR index to the contractionary monetary policy shock.

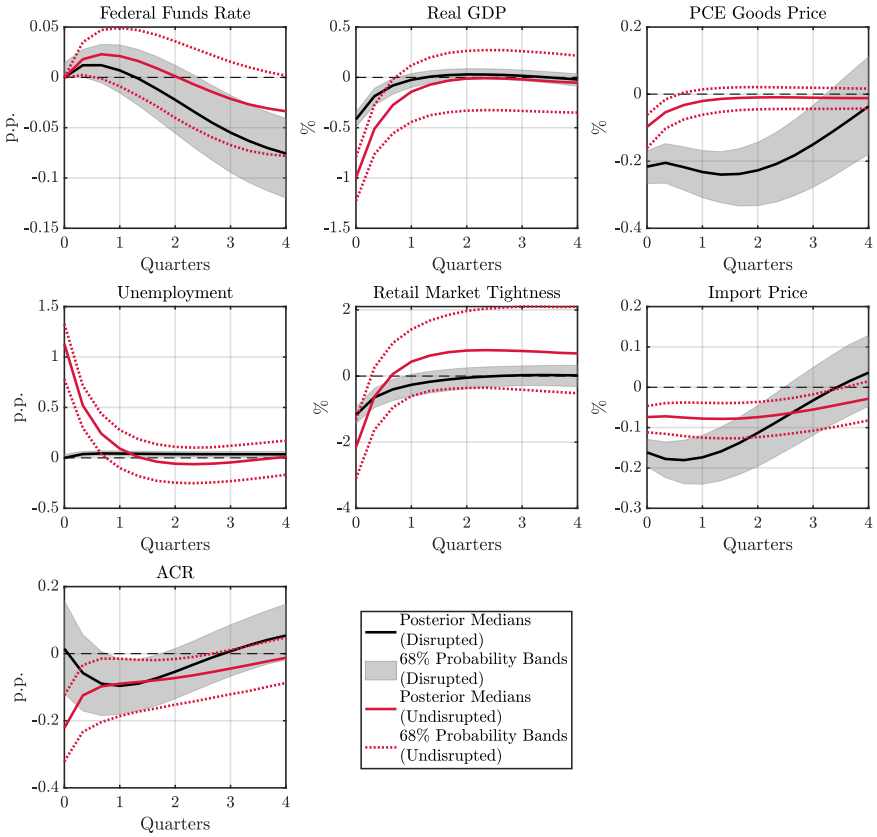


Figure J.2: State-Dependent Effects of a Contractionary Monetary Policy Shock: No Zero Restriction on the ACR Index

Notes. The figure shows the IRFs to a one standard deviation contractionary monetary policy shock, identified using a TVAR specification as in Equation (26), but without the zero restriction imposed on the on-impact response of the ACR index, for both the supply chain disrupted and undisrupted regimes. The black solid (red solid) line shows the point-wise posterior medians, and the black shaded area (red dotted lines) depicts the 68% equal-tailed point-wise posterior probability bands for the supply chain disrupted (undisrupted) regime. The figure is based on 10,000 independent draws from the posterior.

Furthermore, in Figures J.3 and J.4, we show that our state-dependence results are robust to considering different lag structures, i.e., two or three lags. We do not consider four lags or beyond due to parameter uncertainty resulting from our limited sample length. We also show in Figure J.5 that the results are robust when a looser prior is undertaken in the estimation, i.e., $\lambda = 0.5$.

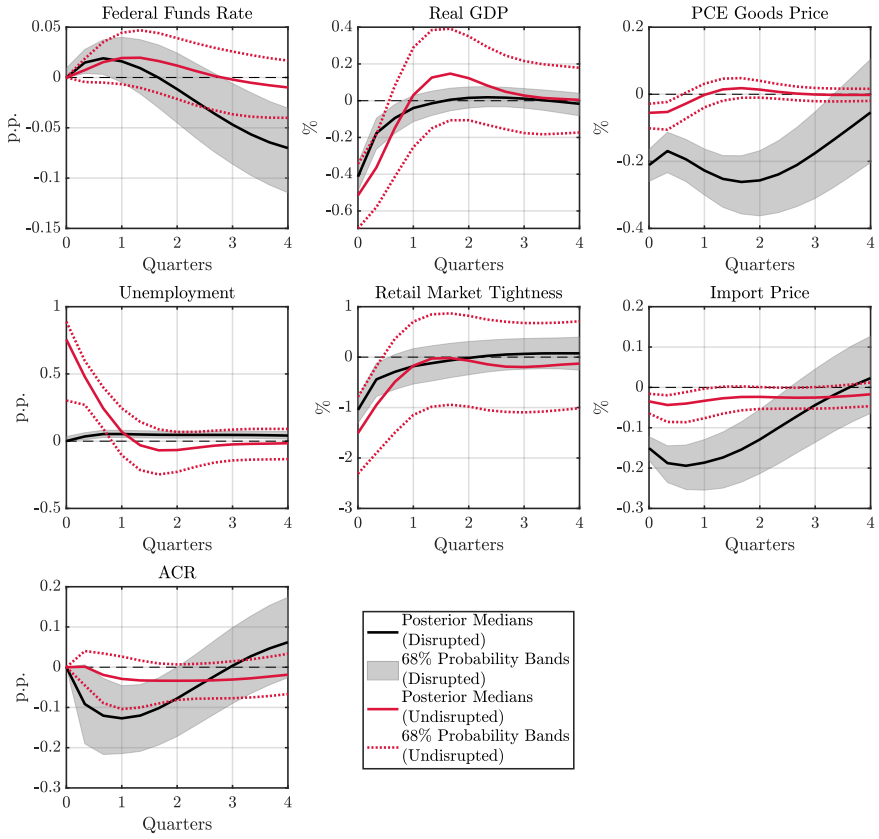


Figure J.3: State-Dependent Effects of a Contractionary Monetary Policy Shock: Two Lags

Notes. The figure shows the IRFs to a one standard deviation contractionary monetary policy shock identified using a TVAR specification as in Equation (26) with two lags, as well as Restriction 4, for both the supply chain disrupted and undisrupted regimes. The black solid (red solid) line shows the point-wise posterior medians, and the black shaded area (red dotted lines) depicts the 68% equal-tailed point-wise posterior probability bands for the supply chain disrupted (undisrupted) regime. The figure is based on 10,000 independent draws from the posterior.

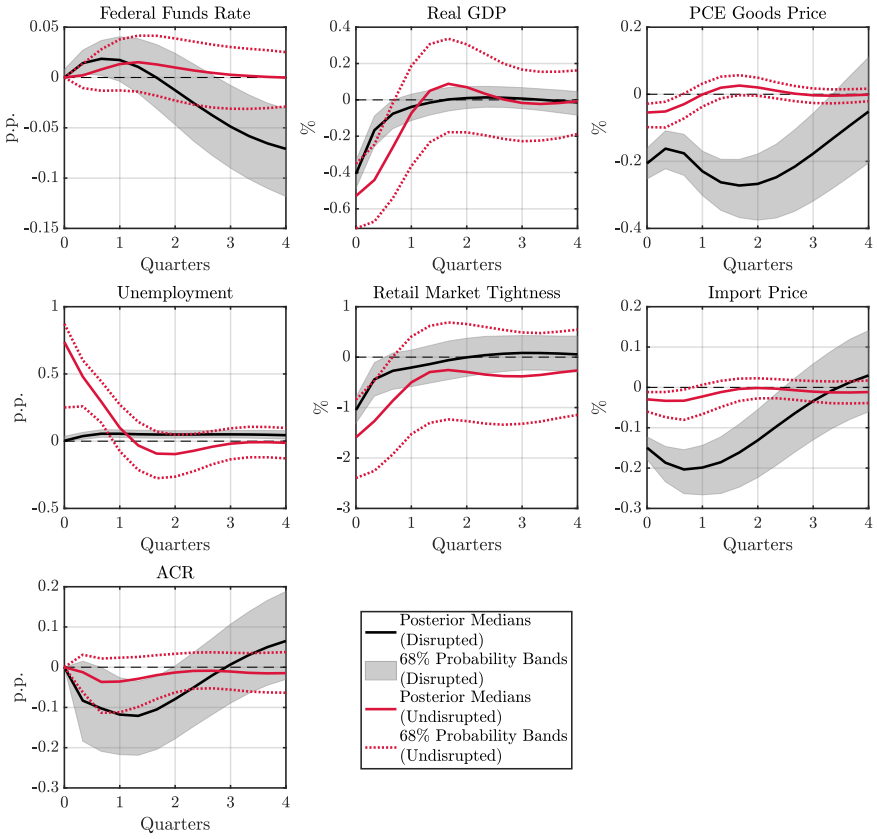


Figure J.4: State-Dependent Effects of a Contractionary Monetary Policy Shock: Three Lags

Notes. The figure shows the IRFs to a one standard deviation contractionary monetary policy shock identified using a TVAR specification as in Equation (26) with three lags, as well as Restriction 4, for both the supply chain disrupted and undisrupted regimes. The black solid (red solid) line shows the point-wise posterior medians, and the black shaded area (red dotted lines) depicts the 68% equal-tailed point-wise posterior probability bands for the supply chain disrupted (undisrupted) regime. The figure is based on 10,000 independent draws from the posterior.

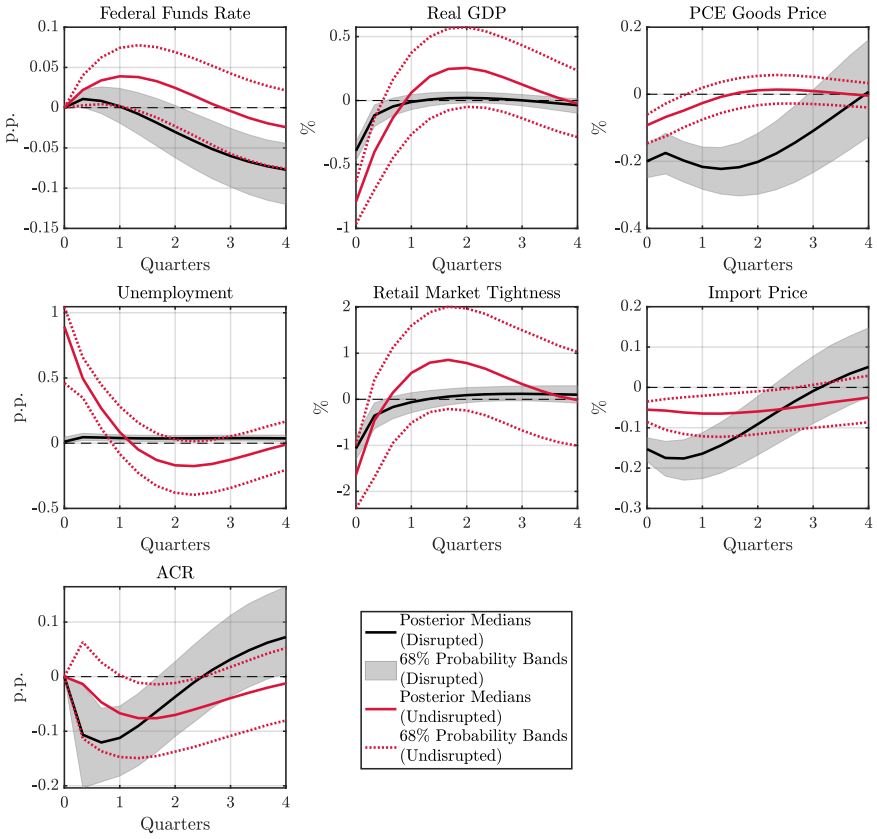


Figure J.5: State-Dependent Effects of a Contractionary Monetary Policy Shock: Loose Prior

Notes. The figure shows the IRFs to a one standard deviation contractionary monetary policy shock identified using a TVAR specification as in Equation (26) with $\lambda = 0.5$, as well as Restriction 4, for both the supply chain disrupted and undisrupted regimes. The black solid (red solid) line shows the point-wise posterior medians, and the black shaded area (red dotted lines) depicts the 68% equal-tailed point-wise posterior probability bands for the supply chain disrupted (undisrupted) regime. The figure is based on 10,000 independent draws from the posterior.

K. State-Dependence Results Using Local Projections

In this appendix, as a robustness check to our state-dependence results obtained using the TVAR model, we work with the local projections (LPs) to identify a contractionary monetary policy shock and analyze how it affects the macro aggregates for the U.S. economy depending on the level of global supply chain disruptions. LPs are a flexible approach that allows us to address the state-dependence of monetary policy without making strong parametric assumptions. Specifically, we use the LPs with interaction terms as in Ramey & Zubairy (2018), Ghassibe & Zanetti (2022), Arias et al. (2023), and our identification scheme consists of sign restrictions implemented as described in Plagborg-Møller & Wolf (2021). Consider the following $n \times (K+1)$ projections:

$$\begin{aligned} y_{i,t+k} =& I_t \left[\boldsymbol{\beta}'_{\mathbb{D},i,k,0} \boldsymbol{y}_t + \sum_{l=1}^{L} \boldsymbol{\beta}'_{\mathbb{D},i,k,l} \boldsymbol{y}_{t-l} + \boldsymbol{C}'_{\mathbb{D},i,k} \boldsymbol{\omega}_t \right] \\ &+ (1 - I_t) \left[\boldsymbol{\beta}'_{\mathbb{U},i,k,0} \boldsymbol{y}_t + \sum_{l=1}^{L} \boldsymbol{\beta}'_{\mathbb{U},i,k,l} \boldsymbol{y}_{t-l} + \boldsymbol{C}'_{\mathbb{U},i,k} \boldsymbol{\omega}_t \right] + u_{i,k,t}, \end{aligned} \tag{K.1}$$

where $1 \leq i \leq n$, $0 \leq k \leq K$, $\boldsymbol{y}_t$ is an $n \times 1$ vector of the same endogenous variables as in Section 5.2 save for the ACR index (since it is the variable we use to split the sample), $y_{i,t+k}$ is the value of the i-th variable in $\boldsymbol{y}_{t+k}$, $\boldsymbol{\omega}_t = [1, t]'$ is a 2×1 vector of a constant and a linear trend, and $u_{i,k,t}$ is the reduced-form error corresponding to the i-th variable. The vector of the reduced-form errors for $k = 1$, $\boldsymbol{u}_{1,t} = [u_{1,1,t} \ \ \dots \ \ u_{n,1,t}]'$, is assumed to have mean zero and covariance matrix equal to $\mathbb{E}(\boldsymbol{u}_{1,t} \boldsymbol{u}'_{1,t}) = \boldsymbol{\Sigma}$.

Similar to the setup in the TVAR model, I_t is a dummy variable that indicates whether the supply chain is disrupted. The supply chain disrupted regime is determined based on whether the one-month lag of the ACR index is above its median level over the sample. Figure K.1 shows the times series of the ACR index along with its 50th and 60th percentiles. As seen, there were frequent switches between the supply chain disrupted and undisrupted regimes before 2019. Subsequently, from early-2019 to mid-2020, the ACR index was constantly below its sample median. Such a pattern was reversed from mid-2020 onwards, as the ACR index started to climb up and the U.S. economy stepped into the disrupted regime. Note

that the switches between the two regimes shown in Figure K.1 are almost identical to those illustrated in Figure I.2 when the threshold $\overline{ACR}$ is determined endogenously in the TVAR estimation.

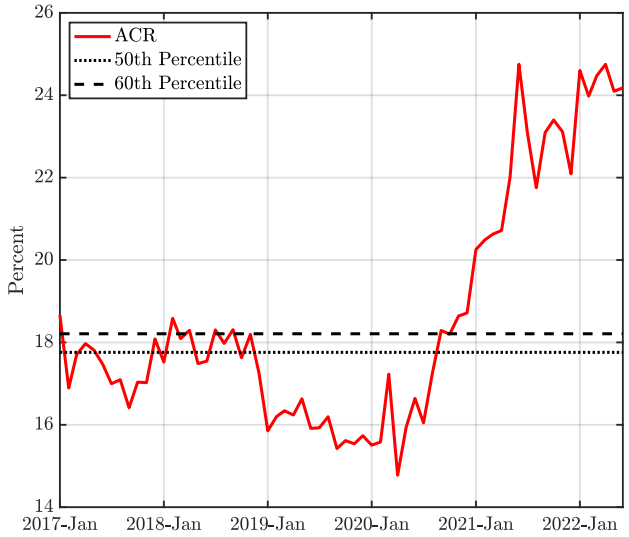


Figure K.1: ACR and Its 50th and 60th Percentiles

Notes. The figure plots the ACR index as well as its 50th and 60th percentiles during the sampling period from January 2017 to July 2022. The ACR index is computed using the AIS data of containerships and the IMA-DBSCAN algorithm developed in Appendix B. The ACR index is measured in percent and has been seasonally adjusted.

With the two regimes defined, the parameters $\boldsymbol{\beta}_{\mathbb{D},i,k,0}$, $\boldsymbol{\beta}_{\mathbb{D},i,k,l}$, and $\boldsymbol{C}_{\mathbb{D},i,k}$ correspond to the supply chain disrupted regime ($\mathbb{D}$), while the parameters $\boldsymbol{\beta}_{\mathbb{U},i,k,0}$, $\boldsymbol{\beta}_{\mathbb{U},i,k,l}$, and $\boldsymbol{C}_{\mathbb{U},i,k}$ correspond to the supply chain undisrupted regime ($\mathbb{U}$). Same as our choice of the lag structure in the TVAR model, we include only one lag in the estimation of the LPs so as to reduce parameter uncertainty.

In order to identify a contractionary monetary policy shock, we follow our theoretical prediction in Proposition 6 and come up with an identification scheme similar to that in Section 5.2. Yet, since the ACR is not included in the estimation, we drop the zero restriction in Restriction 4 and re-write it as the following:

Restriction 4′. ***A contractionary monetary policy shock*** *leads to a negative response of real GDP, PCE goods price, retail market tightness, and import price, as well as to a positive response of unemployment and the Federal Funds Rate at* $k = 1, 2, 3$. *In addition,*

the on-impact response of the PCE goods price in percent is bounded to be smaller than that of the Federal Funds Rate in p.p.

Note that Restriction 4′ is similar to Restriction 4, except that we impose restrictions on the subsequent horizons to sharpen our identification, and an elasticity bound is imposed to discipline the identified set of IRFs corresponding to the PCE goods price. The latter variation is critical to ensure that our estimation is plausible, as in the absence of such a bound, the identified set would include a decline in the PCE goods price of one hundred percent as being equally likely as a decline in the PCE goods price of one percent following an unexpected increase in the Federal Funds Rate of 0.05 percentage point. Hence, we use a bound to rule out dubious IRFs following Kilian & Murphy (2012), Arias et al. (2019, 2023).

With Restriction 4′, we compute the identified set of IRFs in each regime by numerically solving the quadratic program described in the supplement to Plagborg-Møller & Wolf (2021) using Algorithm 2 of Giacomini & Kitagawa (2021). Without loss of generality, we normalize the first shock to be the shock of interest. Let $\boldsymbol{S}$ denote a $18 \times n$ matrix that selects the IRFs which we restrict to be either positive or negative (there are in total eighteen sign restrictions in Restriction 4′). Then, for each regime, we draw $D = 100,000$ orthogonal matrices $\boldsymbol{Q}_{r,d}$ (i.e., $\boldsymbol{Q}_{r,d}'\boldsymbol{Q}_{r,d} = \boldsymbol{Q}_{r,d}\boldsymbol{Q}_{r,d}' = \mathbf{1}_{n\times n}$) that satisfy the following:

$$\begin{aligned} \boldsymbol{S}\hat{\boldsymbol{B}}_{r,0:2}\hat{\boldsymbol{\Omega}}\boldsymbol{Q}_{r,d}\boldsymbol{e}_1 &\geq 0, \\ \frac{\boldsymbol{e}_3'\hat{\boldsymbol{B}}_{r,0}\hat{\boldsymbol{\Omega}}\boldsymbol{Q}_{r,d}\boldsymbol{e}_1}{\boldsymbol{e}_1'\hat{\boldsymbol{B}}_{r,0}\hat{\boldsymbol{\Omega}}\boldsymbol{Q}_{r,d}\boldsymbol{e}_1} + 1 &\geq 0, \end{aligned} \tag{K.2}$$

where $r \in \{\mathbb{D}, \mathbb{U}\}$, $1 \leq d \leq D$, $\hat{\boldsymbol{B}}_{r,0:2} = [\hat{\boldsymbol{B}}_{r,0}' \ \hat{\boldsymbol{B}}_{r,1}' \ \hat{\boldsymbol{B}}_{r,2}']'$, $\hat{\boldsymbol{B}}_{r,k} = [\hat{\boldsymbol{\beta}}_{r,1,k,0} \ \ldots \ \hat{\boldsymbol{\beta}}_{r,n,k,0}]'$, $\hat{\boldsymbol{\beta}}_{r,i,k,0}$ is the OLS estimate of $\boldsymbol{\beta}_{r,i,k,0}$, $\hat{\boldsymbol{\Omega}} = chol(\hat{\boldsymbol{\Sigma}})'$, $chol$ is the upper triangular Cholesky decomposition of $\hat{\boldsymbol{\Sigma}}$, and $\hat{\boldsymbol{\Sigma}}$ is the OLS estimate of $\boldsymbol{\Sigma}$.[21] Given that the entry (i, j) in $\hat{\boldsymbol{B}}_{r,k}\hat{\boldsymbol{\Omega}}\boldsymbol{Q}_{r,d}$ gives the response of the i-th variable to the j-th shock at horizon k, the first inequality condition in Equation (K.2) summarizes all the sign restrictions imposed on IRFs, while the second inequality condition contains the elasticity bound, as $(\boldsymbol{e}_3'\hat{\boldsymbol{B}}_{r,0}\hat{\boldsymbol{\Omega}}\boldsymbol{Q}_{r,d}\boldsymbol{e}_1)/(\boldsymbol{e}_1'\hat{\boldsymbol{B}}_{r,0}\hat{\boldsymbol{\Omega}}\boldsymbol{Q}_{r,d}\boldsymbol{e}_1)$ denotes the ratio between the on-impact responses of the PCE goods price and the Federal Funds Rate, where e_i is the i-th column of the n-dimensional identity matrix.

[21] Vector inequalities are to be understood element-wise.

Given $\hat{\boldsymbol{B}}_{r,k}$ and $\hat{\boldsymbol{\Omega}}$, let $\{\boldsymbol{Q}_{r,d}\}_{d=1,\dots,D}$ be the draws that satisfy the restrictions in Equation (K.2). The identified set of IRFs of the i-th variable at horizon k is thus given by:

$$\left[\min_d \left\{0.05\frac{\boldsymbol{e}_i'\hat{\boldsymbol{B}}_{r,k}\hat{\boldsymbol{\Omega}}\boldsymbol{Q}_{r,d}\boldsymbol{e}_1}{\boldsymbol{e}_1'\hat{\boldsymbol{B}}_{r,0}\hat{\boldsymbol{\Omega}}\boldsymbol{Q}_{r,d}\boldsymbol{e}_1}\right\}_{d=1,\dots,D}, \max_d \left\{0.05\frac{\boldsymbol{e}_i'\hat{\boldsymbol{B}}_{r,k}\hat{\boldsymbol{\Omega}}\boldsymbol{Q}_{r,d}\boldsymbol{e}_1}{\boldsymbol{e}_1'\hat{\boldsymbol{B}}_{r,0}\hat{\boldsymbol{\Omega}}\boldsymbol{Q}_{r,d}\boldsymbol{e}_1}\right\}_{d=1,\dots,D}\right], \tag{K.3}$$

where the factor $0.05/(\boldsymbol{e}_1'\hat{\boldsymbol{B}}_{r,0}\hat{\boldsymbol{\Omega}}\boldsymbol{Q}_{r,d}\boldsymbol{e}_1)$ is a normalization so that in both regimes, the contractionary monetary policy shock raises the Federal Funds Rate by 0.05 percentage point on impact.

Figure K.2 plots the point-wise medians and 68% equal-tailed point-wise probability bands associated with the identified set of IRFs in each regime following a contractionary monetary policy shock. We show the IRFs from horizon $k = 0$ up to horizon $k = 6$. The shorter horizon relative to the horizon of the IRFs shown in the TVAR model (Figure 15) is due to parameter uncertainty associated with the LPs. Nevertheless, as clearly seen in Figure K.2, the state-dependent effects of a contractionary monetary policy shock are still observable, as the responses of real GDP and unemployment are weaker while those of the PCE goods price and import price are stronger when the global supply chain is disrupted (i.e., $ACR_{t-1} > 17.8\%$, which is the sample median of the ACR index). The responses of the retail market tightness between the two regimes, once again, cannot be disentangled from each other.

We also consider a threshold at the 60th percentile of the ACR index (i.e., 18.2%) to distinguish between the supply chain disrupted and undisrupted regimes. As shown in Figure K.3, the main results are robust. We do not consider thresholds higher than the 60th percentile because, as shown in Figure K.1, they would imply a sharp division of our sample at around mid-2020, which may lead to a biased result.

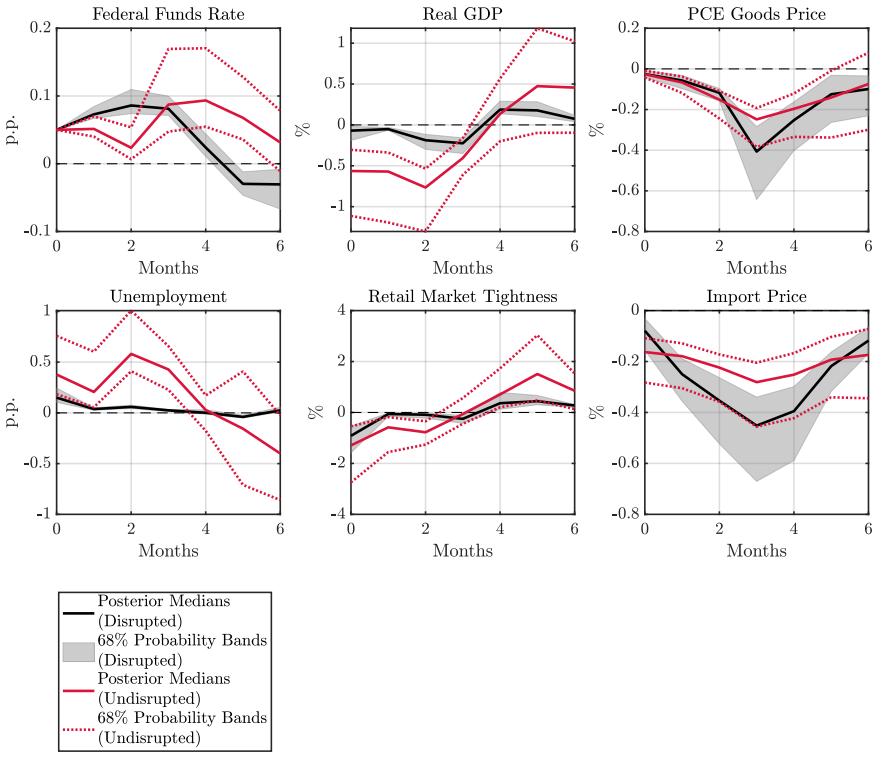


Figure K.2: State-Dependent Effects of a Contractionary Monetary Policy Shock: Using the LPs With Interaction Terms and a Threshold at the Median of the ACR Index

Notes. The figure shows the IRFs to a contractionary monetary policy shock identified using the LPs with interaction terms, as in Ramey & Zubairy (2018), Ghassibe & Zanetti (2022), Arias et al. (2023), along with Restriction 4′, for both the supply chain disrupted and undisrupted regimes. A threshold at the sample median of the ACR index (i.e., 17.8%) is applied to distinguish between the two regimes. The black solid (red solid) line shows the point-wise medians, and the black shaded area (red dotted lines) shows the 68% equal-tailed point-wise probability bands for the supply chain disrupted (undisrupted) regime. The figure is based on 100,000 draws of orthogonal matrices.

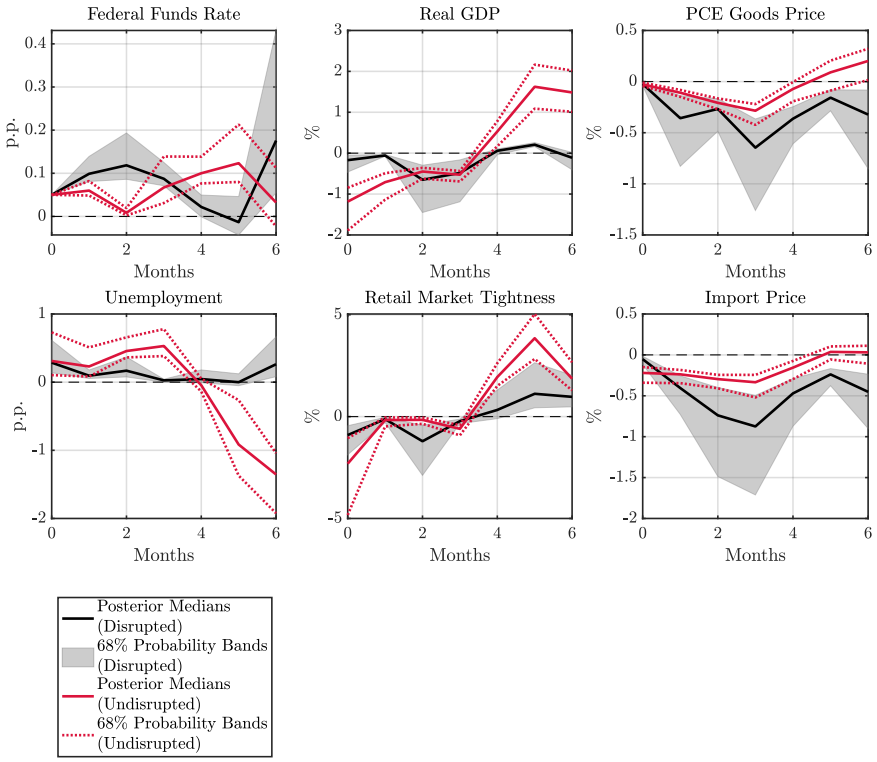


Figure K.3: State-Dependent Effects of a Contractionary Monetary Policy Shock: Using the LPs With Interaction Terms and a Threshold at the 60th Percentile of the ACR Index

Notes. The figure shows the IRFs to a contractionary monetary policy shock identified using the LPs with interaction terms, as in Ramey & Zubairy (2018), Ghassibe & Zanetti (2022), Arias et al. (2023), along with Restriction 4′, for both the supply chain disrupted and undisrupted regimes. A threshold at the 60th percentile of the ACR index (i.e., 18.2%) is applied to distinguish between the two regimes. The black solid (red solid) line shows the point-wise medians, and the black shaded area (red dotted lines) shows the 68% equal-tailed point-wise probability bands for the supply chain disrupted (undisrupted) regime. The figure is based on 100,000 draws of orthogonal matrices.